TECHNICAL REPORT N-70-7

AN EXPERIMENTAL INVESTIGATION OF SOIL-STRUCTURE INTERACTION IN A COHESIVE SOIL

Volume I

by

G. E. Jester

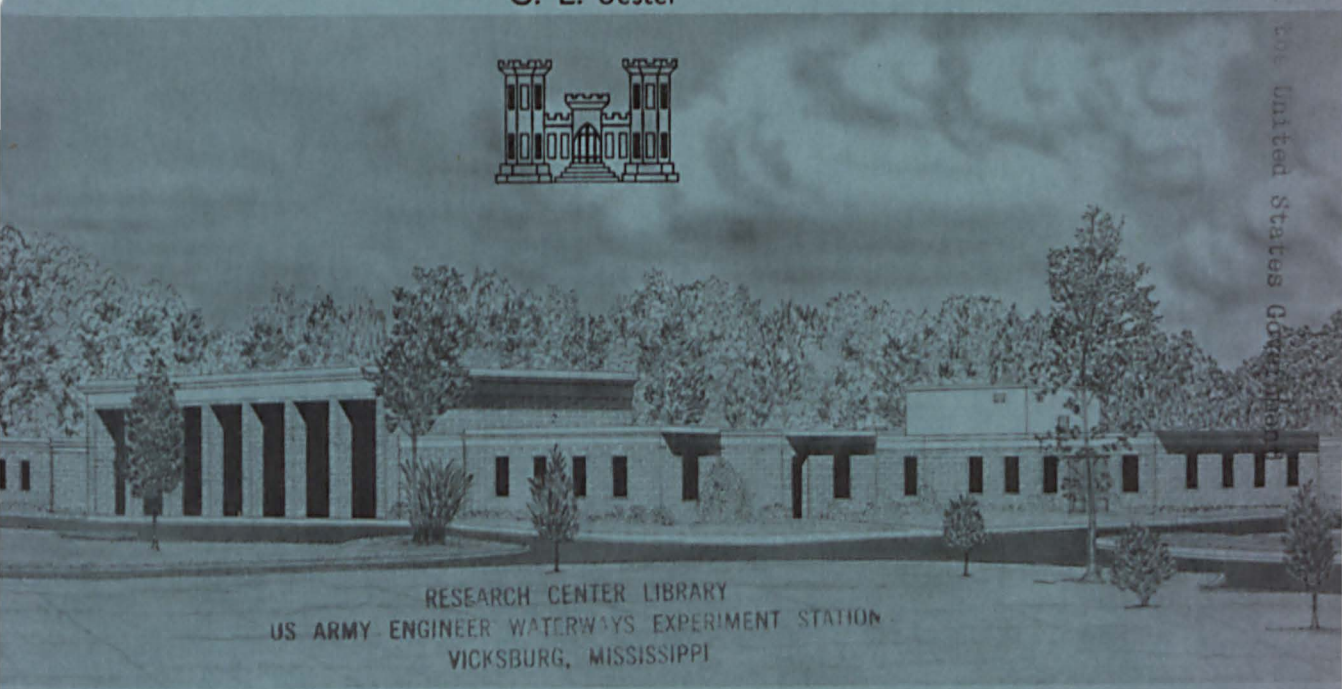

March 1970

Sponsored by Defense Atomic Support Agency

Conducted by U. S. Army Engineer Waterways Experiment Station, Vicksburg, Mississippi

TECHNICAL REPORT N-70-7

AN EXPERIMENTAL INVESTIGATION OF SOIL-STRUCTURE INTERACTION IN A COHESIVE SOIL

Volume I

by

G. E. Jester

March 1970

Sponsored by Defense Atomic Support Agency
NWER Subtask SC210

Conducted by U. S. Army Engineer Waterways Experiment Station, Vicksburg, Mississippi

ARMY-MRC VICKSBURG, MISS.

FOREWORD

This report, published in two volumes, was prepared in the Nuclear Weapons Effects Division, U. S. Army Engineer Waterways Experiment Station, under the sponsorship of the Defense Atomic Support Agency as part of Nuclear Weapons Effects Research Subtask SC210 (formerly Subtasks R13B010 and RSS3210010), "Response of Buried Structures to Ground Shock." The work was accomplished during the period November 1966 through January 1969. During this time, Mr. G. L. Arbuthnot, Jr., was Chief of the Nuclear Weapons Effects Division, and Mr. W. J. Flathau was Chief of the Protective Structures Branch.

This report was prepared by COL Guy E. Jester, CE, and is essentially a thesis submitted in partial fulfillment of the requirements for the degree of Doctor of Philosophy in Civil Engineering to the University of Illinois, Urbana, Illinois.

Directors of the Waterways Experiment Station during the preparation and publication of this report were COL John R. Oswalt, Jr., CE, and COL Levi A. Brown, CE. Technical Directors were Mr. J. B. Tiffany and Mr. F. R. Brown.

AN EXPERIMENTAL INVESTIGATION OF SOIL-STRUCTURE INTERACTION IN A COHESIVE SOIL

Guy Earlscort Jester, Ph. D.
Department of Civil Engineering
University of Illinois, 1968

ABSTRACT

This study was an experimental investigation of the behavior of an idealized structure buried at various depths in a compacted cohesive soil (buckshot clay, water content = 26%). Eight static and 20 dynamic plane-wave loadings up to 310 psi were conducted.

The cylindrical test devices (5 inches high and 6 inches in diameter) were oriented vertically and their stiffness relative to the soil was varied. In addition a device whose top could be extended and contracted hydraulically was buried at various depths and the relation between load and deformation changes was studied at static overpressures of 37.5 and 75 psi.

At low static and dynamically applied surface pressures (P_S = 37.5 psi) and a depth of burial of one structure diameter ($H/B = 1$), the amount of active arching depended upon the stiffness of the structure relative to that of the soil. Under these conditions, it was possible to relieve practically all the overpressure on the test structure just by decreasing its stiffness. At $H/B = 1$, the structure behaved as if it were fully buried under dynamic and static pressures less than 40 psi.

As the surface pressure was increased, the amount of arching at $H/B \geq 1$ became more dependent upon the shear strength of the soil.

When the scaled depth of burial was increased to $H/B = 3$ at surface pressures in the 150- to 250-psi range, the differential pressure, as calculated by subtracting the average pressure acting on the top of the device from the surface pressure at the same time interval, increased but it did not increase as much as the load on the structure. At $P_s = 150$ psi under dynamic conditions the differential pressure was 32 psi or 2.5 times the shear strength of the soil as determined by unconfined compression tests ($q_u/2$) as compared to 25 psi or 1.4 times the shear strength of the soil at $H/B = 1$. When the surface pressure was increased to 240 psi under dynamic conditions at $H/B = 3$, the differential pressure was only 35 psi. Under static conditions, the differential pressure was 37 psi at $P_s = 150$ psi and 54 psi at $P_s = 175$ psi. When the static surface pressure was increased to 240 psi, the differential pressure only increased to 58 psi or 5.2 times the shear strength of the soil. Once the strength of the soil at a particular depth had been fully developed, increasing the surface pressure had very little effect on the amount of arching.

There was a transition zone between those surface pressures at which the amount of arching was determined by relative structure flexibility and the pressure at which it was more dependent upon soil strength. The pressures which limited the transition zone depended

upon depth of burial and the time in which the load was applied. Within the transition zone, the role played by the relative stiffness changed gradually.

Based on the very limited amount of data developed in this test program ($P_s < 65$ psi and $H/B = 1$), passive arching does not appear to be sensitive to structure stiffness. Once the relative structure stiffness (K_T/K_S) exceeded a value of approximately 4, there was no increase in the amount of arching with an increase in the structure stiffness. The maximum scaled differential pressure ($2\Delta P/q_u$) never exceeded a value of 1.1.

Regardless of the stiffness of the structure or the state of arching considered, static arching curves produced by lowering or raising the top of the structure by internal means could not be used to estimate the amount of arching that a similar spring test device would induce under static or dynamic external loads. In addition it was found that static arching data produced with the spring device could not be used to predict the design loads on a comparable structure at dynamically applied surface pressures in excess of 40-70 psi, depending on the depth of burial.

AN EXPERIMENTAL INVESTIGATION OF SOIL-STRUCTURE INTERACTION IN A COHESIVE SOIL

BY

GUY EARLSCORT JESTER
B.S., United States Military Academy, 1951
M.S., University of Illinois, 1958

THESIS

Submitted in partial fulfillment of the requirements
for the degree of Doctor of Philosophy in Civil Engineering
in the Graduate College of the
University of Illinois, 1968

Urbana, Illinois

ACKNOWLEDGEMENT

This thesis is based upon experimental studies conducted at the U. S. Army Engineer Waterways Experiment Station (WES) under the sponsorship of the Defense Atomic Support Agency.

These studies were conducted under the general direction of Dr. N. M. Newmark, Professor and Head of the Department of Civil Engineering, University of Illinois, and under the direct supervision of Professor A. J. Hendron, Jr., of the Department of Civil Engineering. Their invaluable assistance, guidance, and encouragement are gratefully acknowledged.

The writer wishes to express his gratitude to COL John R. Oswalt, Director of WES, and COL C. H. Schilling, Head of the Department of Military Art and Engineering at the U. S. Military Academy, who encouraged him to further his education and allowed him the time necessary to complete his studies.

It would not be possible to acknowledge individually all the advice and assistance the writer received from the staff at WES without which this study would not have been possible. The writer wishes to particularly thank Mr. George Downing, Mr. Leo Steen, and Mr. Billy Benson who assisted in all phases of the study, and Miss Katharine Jones and her staff at the Reproduction and Reports Branch, whose experienced and tireless efforts enabled the writer to complete the report in the shortest possible time.

Acknowledgement is made to Mr. G. L. Arbuthnot, Chief of the Nuclear Weapons Effects Division, WES, and his staff for their assistance and invaluable suggestions throughout the experimental program.

The writer is particularly indebted to his wife, Roberta, and children for their patience and encouragement during the trying period of this study.

TABLE OF CONTENTS*

* The bibliography, tables 1 through 7, figures 1 through 99, and Appendixes A, B, and C and their associated tables and figures are bound in Volume II.

TABLE OF CONTENTS (CONT'D)

TABLE OF CONTENTS (CONT'D)

NOTATION

a	Cavity radius
A	A constant
ACC	Accelerometer; when followed by a number it signifies a particular accelerometer
AF	Amplification factor
b	Width of tunnel
B	Trapdoor diameter; or diameter of test device
BLH	Baldwin-Lima-Hamilton
c	Coefficient of damping
C	Cohesion; or damping; or propagation velocity of the peak soil stress between any two points of interest
C_c	Critical damping
CEC	Consolidated Electrodynamics Corporation
CIC	Computer Instruments Corporation
d_b	Deflection of base of test device
d_t	Deflection of top of test device or trapdoor
D	Gage diameter; or when followed by a number, a deflection gage for which the number identifies its location and instrumentation channel
DASA	Defense Atomic Support Agency
D_S	Soil deflection at 35-in. level
D_T	Total deflection of test device ($d_b + d_t$)

E Modulus of elasticity, Young's modulus

E_g Modulus of gage

E_s Modulus of solid

E.M.F. Electromotive force

f Frequency

F Force acting on top of the test device at any time; or an instrumentation channel recording the force acting on the top of the test device

$F_{(t)}$ Force acting on top of test device at time t

g Acceleration of gravity

G_s Specific gravity

h Depth of burial to top of an arch cavity

H Depth of burial from soil surface to top of structure; or a horizontal pressure gage

$2H$ Gage thickness

IP Pressure inside the test device under dynamic test conditions

k Any spring constant

K Ratio of horizontal to vertical soil pressure; or any spring constant

K_n Spring constant of any individual spring or spring segment

K_p Spring constant of two or more springs in parallel

KH	Kilohertz
K_S	Soil stiffness
K_T	Test device or cylinder stiffness
K_1, K_2, K_3	Spring constant of a particular spring segment
LL	Liquid limit of soil
LVDT	Linear variable differential transformer
m	Mass
M_c	Constrained modulus
M_S	Soil modulus
M_T	Modulus of test device
MIT	Massachusetts Institute of Technology
n	Number of springs
p	Vertical or internal stress
p_o	Stress acting on structure roof
P	Pressure
P_s	Soil pressure at 35-in. level
$\bar{P}_s$	Approximate soil pressure at 35-in. level
P_B	Pressure acting on the test chamber base
P_C	Pressure acting on inside of test device
P_I	Pressure inside test device
P_S	Surface pressure; or bonnet pressure gage
P_T	Average force per unit area acting on top of test device

PE Bonnet pressure measured by Norwood gage on east side of bonnet

PI Plasticity index

PN Bonnet pressure measured by Norwood gage located on north side of bonnet

PW Bonnet pressure measured by Norwood gage located on west side of bonnet

q Horizontal stress; or amount of stress in excess of free-field stress acting on a gage

q_u Unconfined compressive strength of soil

Q Field stress

r Distance from center of gage; radius

R_2,R_3 Radius of particular interest

S Symbol signifying an accelerometer, usually followed by a number identifying its location and instrumentation channel

SBLG Small Blast Load Generator

SDF Single degree of freedom

SE Soil stress gage; when followed by a number, it signifies a particular soil stress gage

t Time

t_f Time of soil failure

t_o Rise time to first pressure peak (steep part of pressure trace)

t_r Rise time to maximum pressure (no reflection)

t_s Rise time at surface

T Period of structure; or specific thrust

TOA Time of arrival

u Deflection of soil at any depth

u_o Deflection of roof

v Vertical pressure exerted on arch

WC Water content of soil (in percent of dry weight)

WES U. S. Army Engineer Waterways Experiment Station

x,y Coordinates

$x_{(t)}$ Deflection of top of test device at time t

$\dot{x}_{(t)}$ Velocity of top of test device at time t

$\ddot{x}_{(t)}$ Absolute acceleration of top of test device at time t

X A symbol signifying an accelerometer, usually followed by a number identifying its location and instrumentation channel

α A constant; or angle between plane of maximum shear and vertical axis

β A constant determined by the ratio of the loaded area to its perimeter

γ Specific weight of soil

γ_d Dry density of soil

ΔD Differential deflection ($D_T - D_S$)

ΔP Differential pressure ($P_T - P_S$)

ε Axial strain; or an instrumentation channel recording strain

$\dot{\varepsilon}$ Strain rate

θ Angle between direction of maximum normal stress and vertical axis

ν Poisson's ratio

ρ Wet density of soil

σ Stress

σ_h Horizontal stress

σ_{max} Maximum stress

σ_o Radial stress

σ_v Vertical stress

σ_x Stress acting parallel to the x axis

σ_y Stress acting parallel to the y axis

σ_1 Vertical stress

σ_3 All-around confining stress

σ_θ Circumferential stress

τ Shearing stress

τ_{hv} Shearing stress acting on the hv plane

τ_{max} Maximum shear stress

τ_{xy} Shearing stress acting on the xy plane

ϕ Angle of internal friction

Ψ Tangent angle to a soil arch

1-D One-dimensional compression test device

LIST OF TABLES

LIST OF FIGURES

LIST OF FIGURES (CONT'D)

LIST OF FIGURES (CONT'D)

LIST OF FIGURES (CONT'D)

LIST OF FIGURES (CONT'D)

LIST OF FIGURES (CONT'D)

LIST OF FIGURES (CONT'D)

LIST OF FIGURES (CONT'D)

LIST OF FIGURES (CONT'D)

LIST OF FIGURES (CONT'D)

LIST OF FIGURES (CONT'D)

LIST OF FIGURES (CONT'D)

LIST OF FIGURES (CONT'D)

LIST OF FIGURES (CONT'D)

LIST OF FIGURES (CONT'D)

VITA

Guy Earlscort Jester was born in Dyersburg, Tennessee, on October 20, 1929. Following graduation from Gulf Coast Military Academy, Gulfport, Mississippi, he entered the United States Military Academy. He received the Bachelor of Science degree in February 1951. Upon graduation he was commissioned as a regular officer in the United States Army Corps of Engineers. He attended the Engineer Officers' Basic Course at Fort Belvoir, Virginia, and served a short orientation tour as a Company Commander in the 27th Engineer Battalion, en route to assignment with the 7th Infantry Division in Korea. From March 1952 through December 1953 he was with the 13th Engineer Battalion in Korea as a platoon leader, Company Commander, and Assistant Division Engineer. From January 1954 to June 1955, he served as an Instructor with the Department of Engineering, the Engineer School, Fort Belvoir, Virginia. In June 1965, he reported to the Fort Worth District, Corps of Engineers, where he served as a Project Engineer and as a Deputy Area Engineer. In June 1956 he entered graduate training in civil engineering at the University of Illinois. He received his Master of Science degree from Illinois in February 1958. This was followed by graduation from the Engineer Officers' Advance Course at Fort Belvoir in July 1958. From July 1958 to June 1961 he served with Northern Area Command, Europe, as a Post Engineer and Chief of

the Engineering Division. In August 1961 he entered the Command and General Staff College, Fort Leavenworth, Kansas, and graduated in June 1962. From July 1962 to July 1965, he was assigned to the Department of Military Art and Engineering, U. S. Military Academy, where he served as an Instructor and Assistant Professor of Civil Engineering. During this period he continued his graduate education at Columbia University, New York City, in the evenings and at the University of Illinois in the summers. In August 1965, he was assigned to the U. S. Army Engineer Waterways Experiment Station, Vicksburg, Mississippi, as Deputy Director. Following his tour with WES, he attended the U. S. Army War College, graduating in June 1968. He currently holds the rank of Lieutenant Colonel in the Corps of Engineers, and is a member of the American Society of Civil Engineers and an Associate Member of the Society of Sigma Xi. He is a Registered Professional Engineer in the State of Texas.

CHAPTER 1

INTRODUCTION

1.1 BACKGROUND

The art and science of designing underground structures to resist the effects of nuclear detonations is plagued by many unknowns. It is therefore inherently difficult to design economic, hardened missile complexes, command and control facilities, logistics installations, and other strategic structures with an assured degree of protection. In addition, it is practically impossible to determine the degree of hardness of existing facilities without testing them or modeled facilities to destruction. Furthermore, the design of fortifications and protective structures to resist the effects of even conventional explosives is not well formulated.

One of the major facets of the design problem which has caused difficulty is the determination of the loads which act upon a buried structure. There are many elements involved, not the least of which is the determination of means to estimate or predict the free-field stresses and ground motions transmitted through the soil to the vicinity of the structure.

Once the free-field stresses and/or strains reach the area where they begin to be influenced by the presence of the structure, the designer must determine how the loads which act on the buried

structure are influenced by the interaction between the structure and the surrounding soil.

Unlike the load systems generally assumed in the design of surface structures, the loading and response of buried structures must not be treated as independent phenomena. There is considerable evidence (Voellmy; Terzaghi, 1943; Taylor; Spangler, 1956; etc.)[1] to indicate that a structure stiffer than the medium that it is buried in will tend to attract load. On the other hand, stress will be diverted around or away from a structure which is less stiff than the surrounding medium. This transfer of load to or away from a structure is one of several phenomena which are normally termed "soil arching." It generally is called "passive arching" when the structure is loaded above the free-field stress and "active arching" when the structure is acted on by stresses below the free-field stress. The load system causes the structure to deform which changes the deformation pattern in the soil and this, in turn, changes the loads which reach the structure. The transfer of load from the surrounding soil to the structure may be thought of as a cyclic or iteration process, i.e., the applied load causes structural deformations, the deformations alter the form of the load, etc. Also involved in the determination of the design load is the

[1] Authors and dates refer to bibliography in Volume II.

length of time the load impinges on the structure and the area of the structure involved, and thus the total energy transfer involved. This is especially true under dynamic loading conditions. Not only the magnitude of the load, but also the distribution of this load are affected by soil-structure interaction. Thus, the load system acting on a buried structure can be greatly affected by the deformations of the structure itself.

1.2 STATEMENT OF THE PROBLEM

Neither soil arching nor the interaction of an undergound structure and its surrounding medium is well understood at present. These are not new problems, but only within the past several years have such problems associated with protective structures been well defined (Newmark and Haltiwanger). However, engineers (Engesser; Janssen; Terzaghi, 1936c) have recognized their existence in various forms for almost a hundred years. Arching in silos and grain bins has received extensive study (Airy; Jamieson; Jaky; Jenike). The stability of tunnels and the design of subsurface structures have always been influenced to some extent by soil arching and the interaction phenomena (Engesser; Terzaghi, 1919). Much of the early research was accomplished using the deadweight of the material and/or very low surface pressures (Engesser; Terzaghi, 1936b). Consequently, the deformations were

small and only static forces were considered.

With the advent of nuclear weapons and the need for providing hardened facilities or determining the degree of hardness of existing structures, an analysis procedure was needed which could deal with large structural and medium deformations as well as the additional effects of dynamic forces. There was also a need for procedures to predict the environment to which structures and their contents might be subjected by either air-induced or direct ground shock or some combination thereof. Much work, as cited in Chapter 2, has been accomplished in this field since World War II, but there are still a multitude of unknowns in the state-of-the-art (Merritt and Newmark).

Authors of design manuals and procedures often comment on the lack of well-documented experimental and field data with which to compare current procedures and analytical theories (Newmark and Haltiwanger). In the latter category are a number of intricate and complex theoretical codes and analytical procedures for determining loads on buried facilities (Aggarwal, et al.; Baron and Parnes; Costantino, et al., 1964). The codes require a medium-structure interaction mechanism and the input of various idealized medium and structure parameters. To date authors of the various codes and analytical techniques have had difficulty constructing a mechanism which realistically describes the problem and which

incorporates real soil and structure parameters.

Economies can be realized in the design of hardened structures through a better understanding of soil-structure interaction. The structure as well as its contents will be involved, since the capability will exist to define more adequately the shock environment inside the structure. Savings could amount to 10 to 20 percent of the total cost of a single hardened complex.

1.3 PURPOSE OF THE INVESTIGATION

The purpose of this investigation was to study in detail the arching mechanism in cohesive soils and to determine how it is influenced by structure stiffness, depth of burial, and surface pressure.

Several corollary objectives were established:

1. Determine if soil arching can exist in cohesive soils under dynamic conditions.

2. If soil arching exists, determine the mechanism of load transfer involved.

3. Determine the applicability of static trapdoor and similar experiments to the dynamic arching problem.

4. Produce well-documented experimental data on the soil-structure interaction problem under dynamic conditions to include: the relative deformations involved; the size of the soil zone

involved in stress transfer; the influence of burial depth, surface pressure, and structure stiffness on the extent of arching; the amount of load transfer possible in a clay soil; and how structural loading is influenced by the medium and depth of burial as well as surface pressure.

5. Produce a means by which the experimental results will be of immediate use to planners, designers, and analysts of strategic structures.

1.4 DEFINITION OF SOIL ARCHING

In any study concerning soil arching and/or soil-structure interaction, it is important for the author to define soil arching as he uses the term and the role this arching plays in the loads an underground structure experiences. For example, Wiehle has stated that the interplay between the soil and structure, i.e. the loading and response of structure and soil, as the stress wave in the soil propagates past the structure is called structure-medium or soil-structure interaction.

As previously discussed, soil-structure interaction may involve not only soil arching but also reflections and diffractions of the stress wave by the structure, the gross transfer of momentum between the soil and structure and vice versa, the redistribution of the load from one portion of the structure to another, and the complete

loading and unloading of portions of the structure as they move away from and into the soil boundary.

Soil arching, as it is defined for this study, is a physical phenomenon in which differential soil deformations of sufficient magnitude transfer loads from, to, or around one portion of the medium to another portion of the medium. This transfer of load causes the stresses in the affected portions of the medium to be different from those which would have been present had no differential deformations taken place.

Prior to the onset of the differential deformation, the soil behaves like a mass possessing the properties of a continuous medium. The most commonly discussed type of disturbance supporting soil arching is that in which a differential deformation occurs at a point in the medium at which either the proportional or ultimate limit of the material's shear strength is exceeded. This is a plastic type action. Of course, the amount of soil area involved in this action has an effect on the amount of arching. The elastic solution to the trapdoor problem shows that load transfer can take place without the development of a general or gross yield condition over a large area. Localized slippage planes or merely relative deformations within the elastic range of the materials are entirely possible.

It is also possible for the transfer of load to be accomplished

without exceeding the ultimate strength and/or the proportional limit of the medium over a large area. This arching may be thought of as "quasi-elastic" although the soil particles may or may not return to their same relative positions.

The amount and type of arching depend upon the amount of relative deformation within the soil, the stress-strain curves for the soil under the condition in which it is being strained, the boundary conditions, and the total area of soil involved. Although the shear strength of the soil is normally involved in most arching calculations, yielding may be more complicated than just simple shear. Notice the definition as developed does not include the processes which induce or support the differential deformations within the soil.

1.5 SCOPE OF THE INVESTIGATION

This study is an experimental investigation of the behavior of an idealized structure buried at various depths in a compacted cohesive soil (buckshot clay, water content = 26 percent). Eight static and 20 dynamic plane wave loadings up to 310 psi were conducted. The cylindrical test device (5 inches high and 6 inches in diameter) was oriented vertically and its stiffness relative to the soil was varied. This report does not purport to be a design manual; however, the conclusions developed should be important to those

who prepare design manuals and design protective structures.

The basic idea of the experiments in this investigation follows that used by K. Kienzl to study arching in the laboratory of K. Terzaghi in the 1930's. His experimental device consisted of a container with a trapdoor in the bottom. He placed sand at different depths over the trapdoor and then determined the load on the trapdoor as it was lowered. A somewhat similar device has been used by A. J. Hendron (1968) and J. W. McNulty to study static arching in clay and sand, respectively.

Since this investigation proposed to study arching under dynamic conditions, it was necessary to move the controlled trapdoor, used in previous experiments of this nature, away from a fixed boundary. At the same time it was desirable to proceed to a configuration closer to that of a real structure.

The basic scheme was a trapdoor device built on the order of a pressure cell. Essentially it was a 6-inch-diameter cylinder with two end plates mounted on a spring assembly. Means for measuring the deflection of the top cylinder and varying the stiffness of the springing system were provided. The 6-inch diameter was chosen to enable a comparison to be made with previous studies and to limit the possibility of the area involved in arching being disturbed by friction between the soil specimen and the sidewalls of the test chamber.

The device was placed inside a 47-inch dynamic test chamber, the Small Blast Load Generator (SBLG), located at the Waterways Experiment Station (WES). Five preliminary dynamic tests were conducted to determine the best soil water content and test configuration to use. In addition the range of the instrumentation and the gross effects were determined. Next, eight static tests were conducted using two device configurations, one with hydraulic controls external to the test chamber and one made up of a spring system which responded to the soil pressures acting on it (Section 3.2.2). Then twenty dynamic tests were performed with the device using a variable spring system to complete the experimental program.

The parameters selected for study were:

1. To determine the effects of the method of inducing arching, two test configurations were used.

2. To examine the effect of depth of burial, four depths, ranging from a depth of burial-to-trapdoor diameter ratio (H/B) of 1/3 to 7, were used.

3. To examine overpressure effects and compare results with previous static tests, essentially four levels of overpressure were used: 37.5, 75, 150, and 240 psi.

4. To examine the effects of the relative stiffness of the soil-structure mechanism, the structure stiffness was varied through eight stiffnesses from very flexible to very stiff.

In the static portion of this test program, soil arching was studied with very little concern for other elements of soil-structure interaction, except for the interaction of the base of the test device with the soil in contact with it. In the dynamic portion of the test program, it was not possible to separate the arching from the other parts of the soil-structure interaction phenomenon. An extensive discussion of what constitutes soil-structure interaction under dynamic conditions has been prepared by Wiehle.

A review of significant experimental and analytical work in arching and soil-structure interaction is presented in Chapter 2.

The test device, soils, and instrumentation used in the experiments, their placement in the test chamber, and the test procedures used are discussed in Chapter 3.

A detailed summary of the experimental results is presented in Chapter 4. Trends are examined and discussed.

In Chapter 5, a compilation and comparison of results as well as pertinent conclusions are presented. Each of the test variables is examined in detail in an attempt to analyze its effect on arching.

Chapter 6 contains the summary of results, conclusions, and some recommendations for future research which appeared warranted by this study.

CHAPTER 2

SUMMARY OF PREVIOUS RESEARCH

2.1 GENERAL

In this chapter some of the significant experimental and analytical work in soil arching and soil-structure interaction directly related to this study is reviewed. In addition, certain pertinent studies concerning pressure cells, silos, underground cylinders, and conduits are reviewed.

At least three annotated bibliographies have been published in this field. One prepared by Van Horn (1963b) is an excellent review of the early studies of loads on underground structures. The bibliography prepared at the Royal Military College of Canada by Hughes, Locker, and Stewart is probably the most complete listing of work in the field of soil dynamics and soil-structure interaction. The report prepared by Wiehle for the Defense Atomic Support Agency (DASA) is undoubtedly the most comprehensive review and analysis of the theoretical and experimental information relative to the interaction of structures with soils under dynamic loading. The annotated bibliography in Part II of this report contains 160 entries. Although the author's opinions concerning some of the work reviewed may be questioned, this report should be read by anyone working in this field.

2.2 EARLY THEORETICAL AND EXPERIMENTAL INVESTIGATIONS

Study of soil arching is not new; in fact, some of the most famous early investigators in the art and science of soil mechanics dealt with this problem extensively. One of the earliest pertinent analytical and experimental investigations was made by Engesser, and was a study of soil pressure on tunnel walls. Engesser had found that these pressures were considerably smaller than those predicted by the theory of soil pressures used in his day which assumed that the load on a buried structure was equal to the entire weight of the soil above it. He stated that the vertical pressure on a horizontal strip of width, b , and at a depth, h , beneath the surface could assume any one of an infinite number of values which lie between two limits, Figure 1. Engesser was interested in the lower of the two limits.

A summary of Engesser's analysis is presented below. Considering the initial equilibrium of a homogeneous mass of soil, the total weight of the body ABCD in Figure 1a will rest on the strip AB. If the supporting strip AB sinks, some motion will occur in the soil mass and a new equilibrium with lower vertical pressures on the strip will be established. Part of the total weight of the body ABCD will be transmitted to the firm ground on both sides. Based on his observations, Engesser assumed that a parabolic arch formed in the soil through the arching action of the individual soil particles. In considering a halfspace made up of a cohesionless

soil, Engesser stated that if the soil mass consisted of individual rigid blocks, the entire weight of mass ABCD would be transferred to the abutments and no pressure would be exerted on the lower surface of the arch AGB, Figure 1b. Since the idealized blocks were actually cohesionless soil, the vertical pressure would cause a downward flow of material unless it was prevented by a vertical force acting up on the lower surface of the arch. Engesser stated that these forces corresponded to the minimum soil pressure that would be exerted on the lower surface of the arch AGB. By the use of the friction angle, ϕ , and specific weight, γ , of the material, plus the tangent angle to the arch at A and B, ψ , he developed formulas for the specific thrust, T , at A and B of the lowest soil arch and the vertical pressure, v , exerted on the arch. He next assumed that the smallest vertical force and thrust would result when the lowest soil arch supported only its own weight and obtained the following formulas:

$$T = \frac{b}{2 \tan \psi}\left(\gamma - \frac{v}{h}\right) \tag{1}$$

$$v = T \tan^2\left(\frac{90 - \phi}{2}\right) \tag{2}$$

By substituting the value of T in the formula for v and setting $\psi = \phi$, Engesser obtained what he termed the minimum value for vertical pressure

$$v = \frac{hb\gamma \tan^2\left(\frac{90 - \phi}{2}\right)}{2h \tan \phi + b \tan^2\left(\frac{90 - \phi}{2}\right)} \tag{3}$$

In order to "check his theory," Engesser performed experiments to determine the minimum pressure acting on a horizontal strip in a box 40 cm high and 20 cm wide mounted on legs as shown in Figure 1c. The opening in the bottom could be controlled by means of a slide located above the bottom of the box. The box was filled with sand and one pan of a laboratory balance was placed under the opening and pressed against the bottom of the box by the weight on the other pan. After the slide was opened, the right tray was gradually unloaded until the lower limit of equilibrium was reached. This was indicated by a sudden downward motion of the tray under the box. For large depths of sand, Engesser found that his theory gave reasonably accurate estimates of the load. For a sand height of 40 cm, the pressure measured was 140 to 144 grams. His theory yielded a weight of 140 grams. The values observed with the box filled to a height of 15 cm were almost the same. With the box filled to a height of 6 cm the observed minimum pressure increased to 180 grams, whereas his theory yielded a value of 133 grams. Thus it was obvious that the assumptions of the theory were not completely satisfied at small heights. The observed minimum pressure was considerably closer to the amount computed by his theory than it was to the customary theory used in that day, which assumed that the entire weight of the soil above the door would be exerted on the door. The author also developed the stresses that would act

against the walls of the tunnel, considering the weight of the material above the tunnel, the thrust exerted by the arch above the tunnel, and the lateral pressure of the soil at the level of the tunnel.

Terzaghi wrote about arching from several points of view. One of his early papers (1919) discussed earth pressure phenomena in locally stressed fills. Terzaghi considered Engesser's work as a correct explanation of the occurrence of wedging in a fill between rough walls of a container or inside a locally unloaded fill. But he considered the analysis using a "fill-vault," his word for Engesser's arches, to be of questionable value since it was not related to earth pressure theory. From the results of his investigations, Terzaghi concluded that the first equilibrium disturbance occurs where the stress in the soil first reaches a limit of the upper active or lower passive earth pressures. Within the limiting stresses the relation between stress and deformation is similar to that in an elastic mass.

To explain his theory, Terzaghi used the analogy of a concrete block whose dimensions were so large that the stresses produced by its deadweight almost lead to its failure. This block was placed on a base cut between A and B as shown in Figure 2a. Terzaghi stated that tensile stresses as indicated by the minus signs would occur directly above the cut base. Compressive stresses indicated by the plus sign would occur above the tensile stresses. Terzaghi

stated that since the tensile stress of concrete was very low, the block would fail by tension and form a load-bearing vault above the cut. He considered the term "vault" not to mean a new formation resulting from a rearrangement of soil particles, but as a designation for a part of the soil in which only compression and shear stresses occur prior to the onset of the first soil disturbance. The major principal stresses would be oriented horizontally.

Terzaghi (1936b) stated that arching per se had been known and studied for at least 100 years at the time he wrote his articles. Terzaghi (1936a) expressed an opinion that the contradiction between retaining wall theory and reality was due to the arching of the material between the wall and the zone of soil which was not moving. He explained this arching by stating that the lateral expansion of the soil must be associated with a vertical shortening of the expanding material regardless of the boundary conditions between the soil and the retaining wall. The body of material located above the expanding zone moved downward.

Terzaghi's (1936b, c) study of arching in sand, which he conducted with a trapdoor arrangement fitted to the bottom of the box filled with sand, is the classic experimental study in the field. In these trapdoor studies, he found that small downward movements of the trapdoor reduced the vertical pressure on the door to a small fraction of what it had been before. As long as the movement of the

trapdoor remained small, it produced a vertical expansion and a lateral contraction of the lower part of the body of sand which was located above the trapdoor. Because of this deformation, the sand located on both sides of the deforming body expanded laterally like the backfill of a retaining wall. Since the lateral expansion was associated with a vertical contraction, shear stresses developed along two inclined planes and transferred part of the weight of the body onto the undisturbed part of the medium. Terzaghi stated that the arching phenomenon also could be expected to occur in tunnels, well shafts, and grain bins.

In his textbook, Theoretical Soil Mechanics, Terzaghi (1943) discussed arching from the point of view of a shear failure in an ideal soil. He developed relations for the load on a yielding horizontal strip using the concept of the vertical shear planes as explained in the previous paragraph. These relations were derived by considering the pressure on the yielding strip equal to the difference between the weight of the material and any superimposed loads located above the strip and the full frictional resistance developed along the vertical surfaces.

All modern theories of soil arching appear to be derived from some combination of the basic theories postulated by Engesser and Terzaghi.

One of the most comprehensive investigations of the static

forces acting on embedded structures such as pipes, conduits, tunnels, etc., was accomplished by Voellmy. He first investigated the pressures on buried structures without allowing them to deform. He then investigated the problem allowing the structure to deform while the bedding material under the structure material around the structure settled. Most of his investigations dealt with circular structures. Voellmy included a detailed survey of the literature dealing with earth pressures and reactions as they applied to the problem of determining pressures acting on the buried structure through 1934. He compared the results of these investigations with those of his own and a series of experiments that he performed on pipe structures.

In his analytical approach to the problem, Voellmy considered the magnitude and distribution of the earth load as well as its limiting value considering the elastic behavior of the structure and the soil. He chose inclined plane surfaces as his failure planes. Voellmy's study showed that the loads on an embedded structure were dependent upon the manner of installation and the relative deformation between the structure and the soil around it.

Tschebotarioff has written considerable material on arching and the transfer of stress. Much of his material is concerned with earth pressures against retaining walls and vertical arching behind a bulkhead. In his book, Soil Mechanics, Foundations, and Earth Structures, 1951, he summarized some of the work in the field and work

that he had performed and reported. In addition, Tschebotarioff discussed the pressures in silos and bins and the arching involved which he calls "bin arching."

Tschebotarioff considered the term "arching" to be ambiguous since he did not believe arching was involved when shearing stresses were developed between soil elements which transferred pressures from one part of a bulkhead to another. In fact, he stated that the terms "arching" and "transfer of pressure by shear stresses" were not synonymous. He agreed that arching may involve some transfer of pressure by shear but stated that pressure could be transferred by shear without any arching being involved. Tschebotarioff limited the term "arching" to the transfer of either vertical or horizontal pressures toward two or more rigid boundaries since an arch must have rigid abutments. He developed what he termed a true parabolic arch and used it to illustrate the reasons for the distribution of pressure behind a bulkhead. He appeared to believe that arching could not exist in clay since the formation of an arch requires a tightly packed wedge against two unyielding abutments (Tschebotarioff, 1951).

2.3 CONDUIT AND CYLINDER STUDIES

Experimental and analytical work in the area of conduit and tunnel design has been going on for some time; design of underground cylinders

as protective structures is a similar problem of more recent origin. Work in the design of buried conduits and cylinders is related to the study of arching and soil-structure interaction. Dorris provided an excellent summary of the work in both conduits and cylinders.

The work by Marston and Spangler should be noted particularly. This work was summarized in 1948 by Spangler and extended by him in 1956. Their basic approach was to consider the equilibrium of the soil above the conduit between two vertical planes of shear. The summation of the friction forces along these planes and the weights of the differential elements made it possible to determine a pressure or force acting on the conduit. Both rigid and flexible conduits were considered. Some of the analysis is similar to that of Voellmy.

An important concept in the work of Marston and Spangler was the use of a plane of equal settlement separating the soil which experiences a deformation from that which was merely furnishing a load. This plane could be located above the soil surface or within the soil medium; its location was determined by the use of an empirically derived curve.

In the analysis of flexible conduits, the use of a horizontal modulus was required. The use of this modulus provided the means for calculating the horizontal support of the soil which resisted the lateral deflection of the conduit. This modulus of passive

soil resistance is difficult to determine. The basis for their failure criteria was either a maximum allowable change in diameter or a maximum allowable stress in the conduit wall.

Watkins (1964, 1966) has extended the work of Spangler and Marston based on the assumption that the conduit ring is just one component of a soil-structure interaction system. He also has attempted to correlate the modulus of soil reaction with properties that are easily measured. Watkins considers that the soil not only exerts a pressure on the conduit but it also contributes to structural strength as determined by the relative stiffness of soil and conduit. He assumes small displacements in order to justify elastic analysis. His structural design is based on conduit deformations which fall into two areas of consideration: wall-crippling and ring deflection. He compares his approach to the classical theory of column design which is based on an allowable stress which is governed by buckling, crushing, or a transition between these two types of failures.

The soil is assumed to be homogeneous and of great extent in all directions. Cohesion is not specifically included since soil modulus is assumed to be much more important than soil strength.

2.4 PRESSURE CELL RESEARCH

The development of pressure cells seems to be particularly

applicable to the static investigations of this study. Considerable work has been expended in trying to design a pressure cell which would correctly record the pressures in soils and concrete. Without such a cell it is not possible to check some of the theories, especially in the field of soil mechanics.

Kogler and Scheidig pointed out that a gage more rigid than the surrounding soil would indicate pressures greater than those existing in the soil before the gage was introduced. A gage less rigid than the soil would indicate a pressure below that actually occurring in the material. In other words, to be free of error the gage should have the same modulus as the soil.

As explained in the next chapter, the structure used in this test program is somewhat similar to a gage. Information developed in the investigation of pressure cells was used in the design of the test device. The soil pressure cell investigation published by the U. S. Army Engineer Waterways Experiment Station (WES) (1944) concluded that, among other things, diameter to thickness ratio of a pressure cell should exceed 5, and the ratio of the diameter to the deflection of the gage diaphragm should exceed 2,000.

Taylor, using the concepts of soil mechanics and previous developments by Carlson (1936), developed a relation between cell error and dimension. Taylor derived an expression relating the dimension of a pressure cell to its accuracy. He used a proportionality factor which

he called the "cell action factor," a function of the modulus of the gage in relation to the modulus of the soil. He found that provided the "cell action factor" was greater than 10, the error factor was approximately constant. Thus, he concluded that overregistration would be a known constant and would not vary with the relative stiffness of the soil provided the gage was very stiff in relation to the soil.

Whiffen and Morris described a gage which was developed for the Road Research Laboratory in Great Britain. This gage possessed an elastic modulus higher than that of any soil. They demonstrated that the ratio of the change in error to change in the modulus ratio became negligible when the modulus of the gage greatly exceeded that of the soil. In their case it was 10 percent irrespective of the soil properties.

Monfore investigated the distribution of pressure on the face of a gage embedded in a homogeneous, elastic mass. The analysis was more rigorous than Taylor's investigation of the influence of the cell on pressure distribution in or near the cell. Boussinesque equations were used to set up a system of simultaneous equations for several cases of interest. The solution of these systems of equations gave the stress distribution on and near the gage. The gage was a small disk-shaped device 1/2 inch thick and 2-1/2 inches in diameter.

The stress distribution and the variation in the stress

distribution with the ratio of the thickness to the diameter of the gage are shown in Figure 3a. From this figure, it can be seen that the thicker the gage, the higher the overregistration. Similar results were derived by Taylor.

The effect of the ratio of elastic moduli on gage errors is shown in Figure 3b. According to Monfore's calculations the stress gage will have positive errors when the gage modulus is greater than the modulus of the soil and negative errors for the reverse. The errors are numerically smaller when the gage modulus is larger than that of the soil. Monfore concluded that the modulus of the gage should be the same as the soil or other medium used, when possible; if this is not possible, it should be larger than the modulus of the medium.

The significance of the pressure cell work will become apparent upon examination of the experimental results from this test program and those of Mason, Criner, Waissar, and Wallace. The effects of the ratio of the length to diameter of the test structure as well as the effects of relative structural stiffness were similar to those predicted by the pressure cell studies.

2.5 SILO AND GRAIN ELEVATOR STUDIES

One type of arching which has received extensive study is that which exists in silos and grain elevators. As noted in

Section 2.2, Tschebotarioff (1951) believed that the only condition under which arching could take place was when two rigid walls were available. Whether a soil mass is moving with respect to a fixed wall or whether there is relative movement within the medium is not important in the consideration of whether arches form or not. Therefore, the study of soil arching should take into consideration what has been learned from the design and testing of silos and grain bins. Although the method of applying pressure to the material in a silo may be considerably different from that of applying pressure to the surface of a soil, there is some relation between these two problems. There is pressure relief in one part of the medium while packing or compression takes place in other parts in both cases.

Jamieson gave evidence that late in the 19th century it was realized that the pressure on the walls of silos and grain bins was not uniform and that the pressure on the base was not the total weight of the material in the container. Early work in this area originated from the necessity to design stable silos and bins. Analytical approaches were presented by Airy and Janssen. Formulas derived by Janssen can be found throughout the literature.

Airy made tests to obtain the coefficient of friction between the grain and the construction materials normally used. From these data and the weight of the grain, he formulated a means for calculating the pressures in a bin of any depth or breadth. From his

formulas, Airy found that the maximum weight on the bottom of a bin occurred when the depth of the grain was equal to 3-1/2 times the width of the bin. As more grain was added to the bin, the load on the bottom decreased until the grain ultimately reached a depth when the only remaining load on the bottom of the bin would be that of a cone of grain whose sides were at the greatest angle of repose of the material and whose base was equal to the horizontal cross-sectional area of the bin. The rest of the weight would be carried by the bin walls.

Caquot (1934, 1949, and 1957) derived expressions for the pressures in a yielding mass. He assumed the entire mass to be a system of parabolic arches which he termed "conjugate surfaces." In the case of silos filled with grain, the arches were supported by the friction acting at the walls of the silo.

Extensive studies of the flow of bulk solids have been performed by Jenike and others (1958 and 1964) at the University of Utah. They have derived a mathematical concept for the flow of bulk solids. The concept was adapted to a modified rigid plastic Coulomb solid.

In this type of problem, the author was interested in the flow pattern and the fact that the material would continue to flow; therefore, Jenike was trying to determine a factor which depicted the condition he calls "no doming" and "no piping" within the container.

He found that when a bin was opened the material that fell out formed an arch or dome in the vicinity of the opening if pressures in the arch of material did not exceed its strength. If the pressure applied to the material exceeded the strength, then the dome or arch disintegrated. Jenike's work is directed toward the design of bins, bin outlets, sides or openings, flow channels, and items of this nature. His limiting case is a self-supporting arch of unit height with the mass of the material above this arch exerting no force on it.

Richmond in his paper on gravity hopper design considered the arch formed at the exit to have a semi-infinite extent of material above it. He considered bins with both smooth and rough walls. Richmond stated that if the cross section of the hopper was too small at any location or if the slope of the wall was too small, the material would form an arch or dome which would prevent the material from moving. He considered the best design to be one in which the material was everywhere on the verge of arching. His analysis appears to be nothing more than an equilibrium approach in which arbitrary horizontal sections are used and the forces in a vertical direction are summed. In other words, he has made a force balance of the force acting on his horizontal slice of material.

All the arching studies seem to consider the formation of an actual arch or arches within the material. Some are at the outlet,

while some are up in the medium. All authors perform a summation of the forces acting on the arch while considering the strength of the material itself and the friction acting at the walls. The major difference seems to be the shape of the container and manner in which the forces are applied to the arch.

An interesting paper by Kallstenius shows pictures of flow patterns observed during the emptying of a container of sand, which had vertical lucite walls, 500 mm high. The trapdoor at the bottom had three possible openings, 8, 25, and 50 mm. The author filled the container with alternate layers of two colors of normal sand. The photographs enabled him to study the zones of disturbance. He found that the diameter-to-height ratio of the disturbed material increased with time as more material flowed out of the container. Before the disturbance reached the surface of the medium, the flow pattern changed so that the disturbed zone sloped out from the edges of the door and formed more of an inverted triangle. Kvapil performed similar experiments on a much larger scale with similar results.

All the literature found considers arching to occur in grain elevators, tanks, bins, etc., used for storing compressible materials unless the height of the material is small compared to the radius of the container. If the depth of material is small, most of the weight is transferred directly to the floor. As the depth of material increases, a larger percentage of the weight is supported by friction at the walls. At some given height, all of the weight of any added

material may be transferred by friction to the walls. This friction between the material and walls seems to induce formation of an arch, according to most investigators. Unfortunately, most of the analyses are directed toward finding reasonable values for the hole size necessary to maintain or support flow out of the container. The significant facts are: arches have been observed in cohesive and frictional material, and most of the analyses are supported by actual measurements or experiments.

2.6 RECENT THEORETICAL AND EXPERIMENTAL STUDIES

2.6.1 General. A rather large number of theoretical and experimental studies recently have become available in the fields of arching and soil-structure interaction. Most of this information has been generated by the needs of Defense Department agencies that are seeking methods to design protective structures for command centers, weapons enclosures, or logistic installations which are reasonably economical to construct but which give assured protection to the contents. Much of the problem centers around methods for determining the loads on and the environment within underground structures. In addition, means of analyzing the structures as well as means of analyzing the method by which loads are applied to the structure are of interest. Of current interest is the old but unsolved problem of designing protective structures against conventional weapons.

In the area of fundamental research concerning the arching phenomenon, there have been at least two static studies which involved

the trapdoor approach. One study used dry sand, while the other was in clay. There have been several other studies in which a trapdoor arrangement was used to study the deformation of sand in a container with deflection of the trapdoor. There are at least three studies in which a configuration other than a trapdoor was used at the base of a test chamber. One was a dome. Another group of reports is concerned with a square structure and still another group covers work with a vertical cylinder. The base of the test chamber seems to apply an unrealistic boundary condition to the close examination of the soil-structure interaction problem.

Several experimental studies have been accomplished with various structural shapes located in the medium away from the base. The majority of these were concerned with cylinders and arches. All except two of these reports deal with structures buried in sand. Two of the reports contained a small number of tests in clay. Only one of these test series was made with dynamic overpressures. All of these fundamental arching studies are summarized briefly in Section 2.6.3.

In addition to the experimental programs, there have been a considerable number of theoretical studies either to support experimental programs and interpret the data or in an effort to determine means whereby structures can be designed without resort to tests. Several of these programs are summarized in the section below.

2.6.2 Theoretical Studies. A majority of the theoretical studies deal with ideal materials. Mathematical models are

formulated that can be solved or an attempt can be made to solve by classical mathematical techniques. One example of these theoretical studies is that by Finn in which he presents a general solution for the stresses anywhere in a soil mass with a yielding base. In his analysis, Finn used what he terms the linear theory of elasticity, i.e., he assumes that the stress-strain curve for the material is linear and that the theory of small deformations holds. The author points out that elastic theory may be applied to nonelastic soil if a constant ratio exists between the stresses and strains. He criticizes Terzaghi's solution to the problem since it gave the distribution of pressures vertically above the trapdoor only.

Evidently the author had not seen the article by Terzaghi and Richart. Finn defines arching as "the transfer of pressure from a yielding soil mass to a stationary soil mass." The author believes arching can take place with only relative motion. He further states that while instantaneous arching may occur in plastic clays, creep can be expected to eliminate this condition over a period of time. He considers the theories which utilize the development of slip surfaces to be based on a "radical assumption" and a state of plastic equilibrium.

Finn presents a two-dimensional solution of the trapdoor problem with small displacements. The author's results show that the stresses in the vertical direction dissipate rapidly with distance above the yielding base. At a distance of 2-1/2 B above the trapdoor this

stress is only 4 percent less than that on the base itself. For small displacement, Finn's analytical expressions show that stress is proportional to the displacement of the door. The pressure distribution at the level of the trapdoor due to the displacements only is shown in Figure 4. The tension above the door would be relieved by the amount of compressive stress contributed by the weight of the material above the door.

Chelapati modifies Finn's solution to take into consideration the depth of the soil and an imposed load on the surface of the soil. Chelapati had trouble with this problem in that at the edges of the yielding strip the arching stress becomes unbounded so that the interval cannot be evaluated. He assumes that tensile forces cannot be transmitted to the soil and discards that portion of the stress distribution where the tensile force exceeds the compressive force. This may not be a particular drawback when large surface pressures are imposed. The major limitation seems to be the fact that he has dealt with an elastic, homogeneous medium.

From the results of this test program it will be seen that the strains experienced by a clay material usually exceed what could be termed linear deformations.

Bedesem (1964) presents a somewhat different approach to the problem of the trapdoor deflecting away from a medium. His model is based on the two-dimensional plain-strain, plastic solution for a material satisfying the Mohr-Coulomb failure criteria. The

equations of dynamic motion for this material are developed and they include the possibility of inertia. Fully plastic solutions to the equations developed for the motion of the medium are attempted only for a plastic material which is incompressible. It is necessary for the author to increase the angle of internal friction as a function of the cover-to-span ratio in order to obtain agreement between his results and experimental data.

Sirieys presents an elastoplastic solution for the stress around a tunnel located in rock which satisfies the Mohr-Coulomb failure criteria. The distribution of circumferential stresses along a radial line, Figure 5, should be consulted when checking the pressure profiles in Chapter 4. McNulty discusses Sirieys' distribution and compares his test results with it. The stress distribution includes both a plastic and an elastic region, which seems to be reasonable in the light of the results found in this test program.

Sylwestrowicz presents the results of an experimental investigation of the punch of a footing into sand and clay. The experiments were conducted under conditions of plane strain. He compares the behavior of the footing with the Drucker-Prager theory of plastic behavior of materials. His displacement distributions in the modeling clay look very similar to a passive arching stress distribution.

A theoretical study by Gravesen may offer some possibility of correlating the trapdoor studies. Gravesen presents a solution for

the problem of a piston moving perpendicular to a stiff plate which has been placed on an elastic halfspace. He allows the piston to deflect away from the elastic halfspace while the halfspace is restrained by the stiff plate. Gravesen finds a relation between the deflection of the piston and the force on the piston using a series of circular areas and the superposition of a load on each area similar to the work done by Monfore. The author assumes a stress distribution on the piston and then approximates this stress distribution with a series of steps. In a referenced report, the author has applied a uniform load to the piston and computed the deflections which would occur in a similar series of circular areas. He computed the deflection of a point at various radii from the center of the picture due to a unit load. The results of this previous work are presented in tabular form in his 1959 paper. Step loading can then be visualized as the difference between a uniformly distributed load over the hole and the sum of uniformly distributed loads within the various circles of increasing radius. The greater the number of circles, the more accurate the results. Since the piston must remain horizontal, the displacements of all points on the piston must be the same. Using this boundary condition, the author presents a set of equations involving the pressures acting on the piston within the various circular areas. The results show that the load on the piston decreases very rapidly with a small deflection.

Hendron (1968) has studied Gravesen's work in detail and compares his solution with the static trapdoor study conducted in sand by McNulty and Hendron's similar work in clay. The significant finding was that Gravesen's elastic solution comes close to the trapdoor experimental results in the region where most of the load on the trapdoor is lost and yet, the deflections involved are quite large in terms of those normally associated with elastic problems.

There are several groups working on the theoretical analysis of the problem of the dynamic interaction of a medium and some inclusion within the medium. The inclusion used is normally a circular cylinder of infinite extent or a shell. One such group is that at Paul Weidlinger and Associates. An example of this work is contained in the report by Baron and Parnes. An elastic medium is used. The problem is solved initially with an unlined cavity and later extended to a lined circular cavity. As in all such analyses a considerable number of approximations have to be made in analysis. In addition, the liner must be glued to the medium. The authors assume a plane wave moves through the surrounding medium such that the front is parallel to the axis of the cylinder. This essentially reduces the problem to one of plane strain.

The authors consider a set of generalized coordinates and develop relations between the radial and tangential displacements in terms of these generalized coordinates. Generalized forces are

obtained by the application of virtual work.

Yoshiharo, Robinson, and Merritt investigated the interaction of plane elastic waves with a thin, hollow, cylindrical shell placed in an elastic medium. The shell is considered to be thin, elastic, isotropic, homogeneous, and of infinite extent. The approach is similar to that used by Baron.

Such analyses furnish guidelines to consider in interpreting the results of properly designed experiments with similar boundary conditions.

The efforts of another group which has attempted a theoretical solution of the interaction problem are represented by the report by Aggarwal, Soldate, and Hook. This report extended some earlier elastic studies that they made. The model exhibits a bilinear compressional stress-strain curve in the conventional uniaxial test. This model exhibits elastic behavior up to a certain stress and then linear work hardening above this stress. The structure used as an inclusion is a rigid, infinitely dense cylinder. No solutions were obtained.

Mow has written several reports in this area. One of his reports presents a review of some of the recent developments in the stress wave-cavity interaction problem as it is pertinent to the design of underground openings for protective construction. In addition to the spherical cavity problem, he also discusses the cylindrical cavity in this report. Mow presents dynamic stress concentration

factors around lined and unlined cylindrical openings as well as those unlined spherical openings in an elastic medium under various dynamic loadings. This report also contains an interesting discussion of failure mechanisms.

Costantino (1964 and 1966) attempts a closed-form solution to the interaction problem. He uses a hypothesized stress-time history at the level of the inclusion as a driving function. A numerical approach is used to solve his equation which included the free-field stress, the foundation modulus times the relative displacement between the inclusion and the free field and a damping function times the relative velocity between the free field and the inclusion. The foundation modulus is dependent upon the free-field stress. This function changes as the stress changes, based on the slope of the one-dimensional compression test curve. Costantino's formulation of the problem seems to offer more promise than most analytical solutions since it is at least an approach toward using the real properties of the medium.

Richart presents the classical arching theories relating to the silo and trapdoor problems. He considers the "arching" phenomenon to be a process of stress transfer whereby loads are carried around an ineffective zone of support. This transfer of load is accomplished by the development of shear stresses within a sufficient zone of material until the load is transferred to an adequate support.

Richart states that "the shearing stresses developed in the arching process are as permanent as those developed in other methods of transferring loads into granular materials.... The quantities which determine the magnitude of the shear stresses that can be developed in the material govern the effectiveness of an arch which can be developed. Thus the arch formation is a function of the material used, the stress state applied to this material, and the geometry of the boundaries. Consequently, in view of the numerous variables involved, any theory developed for the study of the arching process must necessarily include several assumptions and approximations."

In addition to his explanation of classical arching theories, Richart also presents an analytical treatment of the stress distribution caused by arching in a continuous elastic medium. Richart reviews the previous work he did with Terzaghi (1952) in which they studied the stress developed around elliptical tunnels and spheroidal cavities in an elastic medium. The 1959 report contains a more complete determination of the stresses above a flat, elliptical tunnel located in an extended homogeneous, isotropic, elastic medium and subjected to a homogeneous stress field. The equations used are available in the Terzaghi and Richart paper or a book by Neuber. The 1959 report shows the distribution and direction of the principal stresses at points around the tunnel. Assuming that the material could withstand no tensile stresses, Richart shows the amount of

material that must be supported in a tunnel roof. His calculations and figures show that the stress lines go around the cavity in a manner analogous to fluid flow in hydrodynamics.

2.6.3 Experimental Studies. Two of the more comprehensive experimental studies were conducted by McNulty and Hendron (1968), respectively, to study the effect of active and passive arching under static load conditions. Both studies were made with the same test apparatus, a 4-foot-diameter cylindrical test chamber whose height could be varied and whose lower base contained a flush-mounted trapdoor which could be raised or lowered under controlled conditions.

McNulty made his study with two types of granular material, a smooth and an angular sand. The surface was subjected to static surcharges of approximately 40, 75, and 110 psi. Six- and three-inch trapdoor sizes were used. Distribution of vertical stress on the base of the test chamber was measured by pressure cells located at various distances from the trapdoor. The major experimental results are a series of dimensionless load-deflection curves which were obtained by moving the trapdoor either into or away from the sand. These load-deflection curves show that extremely small deflections can have a drastic effect on the load that the trapdoor experiences and that the trapdoor size is not important if the ratio of the depth of the soil above the door (H) to the diameter of the device (B) is held constant. McNulty's results also show that the depth of burial was important to

the shape of the load-deflection curve at small values of H/B . For values of depth-to-diameter ratios larger than two, the shape of the load-deflection curve does not show much change.

Hendron (1968) used the same apparatus with a cohesive soil called buckshot clay. The variables investigated were depth of cover, overpressure, and strength of the clay. Active arching tests at overpressures of 37 and 75 psi and at depths of cover ranging from 1/3 to 3 times the trapdoor diameter were performed. Passive tests were conducted at 37 and 75 psi for depths of cover 1/3, 1, and 2 times the diameter of the trapdoor. Hendron found that the test data seemed to collapse more readily when the differential pressure between the surface and door scaled by the unconfined compressive strength of the soil was plotted versus the scaled deflection rather than using the pressure on the door scaled by the surface pressure. Some of Hendron's data are presented later in this report for comparison purposes.

One of the more interesting small-scale structure test series was that conducted by Whitman, Getzler, and Höeg. They used domes buried at the bottom of a sand-filled test chamber and supported on a load cell. There was no sand underneath the dome, but it was possible to support the dome on a more flexible foundation and thus give the structure an overall change in flexibility in relation to the soil. A uniform static pressure was applied to the top of the mass. This is one of the few test series found in which the movement

of the medium of burial was measured. The deflection of the dome crown and the vertical force on the dome were also measured.

The authors found that the stiffer the structure in relation to the sand, the larger the difference between the deflection of the crown and the deflection of the sand. In addition, they found that there were sharp decreases in the pressure applied to the dome as it moved away from the soil and that a sand arch seemed to form. As the crown of the dome yielded, the sand arch assumed some of the pressure which had been acting on the dome, thus preventing buckling or total collapse of the structure. For the more flexible structures, the authors found that beneficial arching was developed prior to crown yield even for depths of burial as small as one-half the dome span. Another important result was that there was little tendency toward a large amount of passive arching when the sand was very loose.

Depth of burial seemed to have little effect on the arching action once the structure was buried at a scaled depth of approximately one-half the span. The domes did not develop the typical snap-through buckling under average vertical pressures which were almost three times the pressures that buckled the domes in an unburied configuration. The failure was normally a bending near the support.

The next series of tests which seemed to have a bearing on the problem were those performed by Triandafilidis, Hampton, and Spanovich. Right circular cylinders were buried in three densities of

sand and with four depths of cover. The vertically oriented cylinders were 1-1/2 inches in diameter and were placed to project from a rigid base in three different lengths. Two cylinder configurations were used. One structure was constructed so that the sidewalls were connected to its upper end plate. The structure was designed to measure the contributions from the free-field stress, the arching stress, and the sidewall friction stress. The other configuration was a disk contained within a cylinder of the same shape and size as that previously described. The disk was separated from the sidewall so that its flexibility could be varied by its support. By varying the density of the sand from a loose condition to a dense condition, it was hoped that both active and passive arching could be induced.

The loads which the fixed-end structure experienced were always larger than the surface pressure. This is understandable since it was rigidly fixed to the base of the test chamber and had no ability to deflect. With the disk structure, the authors found that the depth of cover increased the arching whether it was active or passive if the other parameters were held constant. The length of structure embedded in the material also had an effect on the arching.

Static surcharges of 14.5 to 72.5 psi were applied to the sand surface. It was found that overpressure did not have a significant influence on the normalized arching stress. In fact, the effects of overpressure on the arching and friction stresses appear to be

insignificant in comparison to the effects of flexibility, soil cover, or the amount of embedment. The authors found that the soil density affected the normalized arching stresses more than any other soil parameter studied. This indicates that it was the relative compressibility of soil and structure which was the most significant parameter in these studies.

The test series by Triandafilidis was a pilot study for a much more comprehensive test program conducted and reported by Abbott. This research was both experimental and theoretical. In the theoretical portion, Abbott divided the static arching problem into three parts which he termed the no failure condition, the complete failure condition, and the local failure condition. When speaking of the no failure condition, Abbott assumed that the maximum shear stress is not reached anywhere in the material and that no surface of sliding develops. The author also made assumptions relative to the coefficient of friction between structures and soil, the weight of the material, and the bending of the structure. He treated the structure as if it was up in the medium. This he calls a "floating structure." He made the structure placed on the bottom of the test chamber a special case which he calls the "rigid base structure." All loads were static.

Abbott started his development with the relative deflection of the structure in the soil due to an overpressure applied at the surface

of the soil. He considered the modulus of the soil and the structure to be defined by their tangent moduli. The author obtained an expression for the arching stress on the structure in terms of the stress applied at the surface of the medium. Next the author introduced additional assumptions concerning the cross section of the structure; these assumptions are functions of the structure's shape and depth of burial. Abbott determined his burial function experimentally but derived his shape factor.

Abbott secondly considered the problem of complete failure of the medium. His solution was based on an equilibrium approach of an element of soil mass between two vertical failure planes. He points out that the limit of the active and passive arching is measured by the shear strength of the medium. His failure surfaces extended from the top of the structure to the surface of the medium. The direction in which the shear stresses act on the element determines whether passive or active arching is taking place. He assumed a constant value for the ratio of the horizontal to the vertical stress in order to derive the friction acting on his soil disk. Abbott used Mohr's circle to obtain a relation between horizontal and vertical pressure for the limiting passive and limiting active arching conditions.

For his third case, local failure condition in the vicinity of the structure, Abbott was not able to provide a solution. He does

discuss the difficulty of obtaining a solution to this problem. Unfortunately, this case appears to be the most prevalent for actual buried structures.

Static tests were performed on a right circular cylinder structure buried in 20-30 Ottawa sand. The author included a rigid base test, a floating test, and a qualitative test to determine or to observe the residual deformation pattern of the sand in the vicinity of the structure. Most of the structural flexibility experiments were performed with the rigid base test. The floating tests contained a very rigid structure and a very flexible structure.

Most of the data obtained from the experimental program seem to indicate or infer that the complete failure and the no failure solutions represent bounds to the passive arching problem for a structure with a given height-to-diameter ratio and stiffness relative to the medium. At small depths of burial, the complete failure theory gives an upper bound to the loads on the structure which is lower than that given by the no failure theory.

From the floating structure test in sand, the results seem to indicate that the arching factor is independent of the overpressure level. For the stiff structure, the arching factor reaches a maximum somewhere between 1 and 2 and remains constant for the remaining depths of burial. The author's theoretical

prediction is reasonably close to the data. His best comparison is obtained with a Poisson's ratio of 0.64, which seems to be rather high.

With his flexible structure analysis, Abbott used the tangent to the stress-strain curve derived from tests made in a confined tank as a measure of the stiffness of the soil. He plots the ratio of the stiffness of the soil to the stiffness of the structure for the various overpressures to which the flexible structures were subjected. The curves seem to increase with overpressure at a decreasing rate. Test results show excellent agreement with his no failure theory at scaled depths of burial greater than 0.5. This is the reason Gravesen's elastic theory worked so well for Hendron (1968).

The next group of reports discussed concern a different theoretical technique for the determination of the loads on underground structures and the experiments performed to check these techniques. The work was performed at the Illinois Institute of Technology. Some of the reports covering this work are those of Selig (1960), Selig (1961a), Selig, McKee, and Vey (1961b). Their approach was based upon the concept of slip planes that extend vertically from the edges of the structure to the surface of the medium of burial. The mathematical expressions were derived by an equilibrium approach similar to that used by Terzaghi, except for the dynamic case. For

this case they assumed sufficiently high pressures existed so that the mass of soil between the roof and the surface moved down onto the roof. In addition to the assumption relative to the extent of the failure planes, it was assumed that the magnitude of deformations would be sufficient to develop the full shear strength of the soil. An equilibrium equation for the soil mass was developed just as was done in several of the static theories, except that an inertia term was added.

A rapid increase in failure overpressures with increasing depth of burial is inherent in the development of the full failure planes to the soil surface. Such an assumption may not be reasonable except for shallow depths of burial.

The theory also predicts that the effects of the dynamic surface load would be to significantly reduce the forces felt by the structure because of the inertia forces of the soil plug and the sliding resistance within the adjacent soil masses. Results of this nature appear to be questionable.

The test program consisted of placing two types of structures in the bottom of a glass-sided box filled with sand and subjecting them to static overpressure applied at the surface. One type of structure was such that the top could be lowered after the surface pressure had been obtained. Large displacements took place and slip planes did form in the soil as predicted. These slip planes seem

to have been affected in large measure by the rigid supports on both sides of the yielding top and the very large displacements. Some of the slip planes propagated vertically directly over the supports projecting into the sand. Some of the slip planes showed evidence of curving to the inside and thus emerging at the soil surface closer together than the dimension of the structure.

The second type of structure was one in which the roof was made flexible enough so that it would yield under pressure. Again the deformations seemed rather large. The nearness of the boundary to the base of the structure appear to have affected the test results.

Havers performed additional tests with this apparatus using both sand and clay materials. The structures were restricted to the flexible panel type. Dynamic loadings were simulated by the use of an air-actuated shock tube. The friction material was a dry Ottawa sand. The cohesion material was 95 percent by weight kaolinite and 5 percent bentonite. The Atterberg limits of the soil were: plastic limit, 28 percent; and liquid limit, 68 percent. Its moisture content was between 36 and 39 percent.

The test results show that the load applied at the surface, either static or dynamic, was considerably larger than the load experienced by the structure. The load reduction was larger for the Ottawa sand.

In the clay tests, there was evidence that the soil had a limiting strength for a particular depth of burial. This strength was essentially independent of the applied surface load. Although it appears that the loads from the static tests were larger than those from the dynamic tests, it is difficult to interpret the data since the static test data were based on a particular scaled deflection of the structure in relation to what the deflection was at zero depth of burial.

Van Horn (1963a) takes some of the previous work in the field and presents a static and dynamic method of analysis. The first part of his study is devoted to the development of a method for evaluating a load on a buried structure due to static overpressures. He has extended the work of Marston and Spangler previously discussed in this chapter. He assumes vertical surfaces of sliding and computes the shear forces and the weight of the material above the structure. He considers the relative compressibility of the soil and structure and computes the loads based upon the equilibrium of forces on a soil plug above the structure. One of the items that he considers is the plane of equal settlement; i.e., that point at which the soil over the structure and that adjacent in the free field settle the same amount. This is the point above the structure at which the soil is no longer disturbed by the presence of the structure.

In the second part of his analysis, Van Horn extends the work

previously accomplished on the effects of time-dependent overpressures. The method retains the static pressure theory that is presented in the first part of the paper. Using the methods and assumptions introduced by Selig, the pressures on the structure produced by time-dependent overpressure and the weight of the soil are determined. From these mathematical expressions, it was possible to determine the equivalent load or the static load which is equivalent to the dynamic load; i.e., the static load that would have to be applied to the surface of the soil in order to give the same pressure effects on the structure as the dynamic load.

Van Horn found that there was very little difference between the loads determined with a sand and with a clay for the particular type of materials he chose to use. The strength of the clay was expressed in terms of a ϕ of 10 degrees and a C equal to 400 psf, while the sand had a ϕ of 35 degrees and a C of zero. For all the cases he examined, which included two values of soil deflection, two durations of the pressure pulse, two types of soil, and four scaled depths of burial, he found that the equivalent static overpressure which could be used for design ranged between 76 and 93 percent of the peak dynamic overpressure. The equivalent static overpressure changed very little for pronounced changes in the scaled depth of burial. The results seem to indicate

that duration of load is the most predominant effect, and that if a structure is designed for a particular static overpressure it will withstand a dynamic overpressure of the same magnitude.

In spite of the lack of definite information from which to determine the soil-structure mechanism and a method by which the loads acting on a buried structure can be properly determined, it has been necessary to design underground structures for the last several years. Design manuals which furnish criteria summarize the state-of-the-art at the time at which they were written and include the best judgment of the writers concerning the information available. The best example of such a manual is the Air Force Design Manual by Newmark and Haltiwanger. The method of approach to soil arching used in this manual was adopted from the treatment given this subject by Terzaghi (1943) as a result of his earlier trapdoor studies. The analysis assumes vertical surfaces of sliding as shown in Figure 6a. The assumed variations of shearing stress versus displacement and the assumed variations of displacement and shearing stress with depth are shown in Figures 6b and c, respectively. This approach does not have the disadvantage of those methods which do not take into consideration the so-called "elastic" action in the soil as well as plastic action. The shear planes do not have to be fully developed nor does the deformation zone have

to extend to the surface but the extent of the shear planes must be decided. This method also takes into consideration the deformation of the structure which induces the deformation of the soil. The soil deformation dissipates along an exponential curve. The authors consider this analysis primarily a static analysis or one for very slow dynamic input. The shearing stresses developed along the deformation planes are the primary factor in determining the load imposed on the structure.

Merritt and Newmark give a comprehensive review of static and dynamic arching and soil-structure interaction in Part V Nuclear Geoplosics. The state-of-the-art at that time is summarized in this report.

Adine and Dai adapted the system explained above to the dynamic case by adding an acceleration term to the equilibrium of the soil disk shown in Figure 6a. The terms in the equation are the vertical pressure, the shear acting on the element, and the inertia of the element. The assumed shearing stress-deformation relation is the same as previously noted, Figure 6b. The authors consider that at some critical deformation the entire shear strength of the material will be developed. Any deformation less than this critical deformation will develop a proportion of the entire shear strength of the material. The displacement term considered is the relative displacement between two points on each side of the shear point. A

second stress deformation relation is developed considering the material as being elastic. This relation expresses the compressibility of the soil element. Using this expression it is possible for the authors to derive two expressions for the stress along the vertical axis X . One equation is for the case when the deformation is in the "elastic" region, and the other when it is in the plastic region.

The authors have written a program to solve their equations numerically for the static case, where the inertia terms go to zero. The program is capable of computing the displacement and stresses along the X axis.

The authors state that arching is a function of three groups of parameters; geometrical, structural, and soil. The dimensions of the region above the structure are termed the geometrical parameters of the system. From their analysis, Adine and Dai found that the height of this region has minor effects on the arching since 70 percent of the arching developed within a height equal to the width of the structure. The only structural parameter examined was structural flexibility. For this parameter they note that high flexibility produced larger relative displacements and thereby enabled the soil to develop its maximum shearing capacity.

Allgood and Seabold adopted some of the assumptions and techniques developed by both Selig and Newmark from the Terzaghi approach to the analysis of small buried arches. Their equations are based upon vertical shear planes and the development of an arching force as a result of the total motion of the structure and the soil above it. They consider the effect of the stress wave traversing the structure as an impulse which imparts translation and velocity to the structure. The movement of the footing is considered to be the primary rigid body motion which induces arching. The soil is considered as an elastic, homogeneous halfspace and the properties are considered from the point of view of a foundation modulus. Equations of motion are used to derive expressions for the vertical motion of the structure considering the mass of the soil above the structure, the mass of the structure, and the mass of the soil that moves with the footings. The authors state that their method should be applicable to the initial estimate of the loads that the structure will experience.

With assumptions similar to those previously discussed, Allgood developed equations for the load on a horizontally oriented, buried cylinder.

In the work by Bedesem, Das, and Robinson, the effects of arching in granular soils on the pressures transmitted to a buried structure were examined. In this analysis the overpressure was assumed

to vary slowly with time and to be uniformly distributed over an infinitely large area as compared to the structure. The soil was assumed to be a homogeneous, isotropic, granular material satisfying the Mohr-Coulomb failure criteria. A plasticity approach with deformations assumed large enough to mobilize failure planes to the surface was used. The length ratio of the structure was considered to be large enough to permit a two-dimensional plane-strain formulation of the problem.

Mosborg and Talda reported on an experimental investigation conducted to verify the analytical results obtained from the theoretical analysis introduced in the previous paragraph. Two dry sands were used, one with angular grains and one with smooth grains. Static and dynamic tests up to a peak overpressure of 500 psi were conducted in a 2-foot-diameter cylindrical tank. The tank bottom contained a long rectangular rigid plate supported by springs which allowed the plate to deflect vertically under load. Two stiffnesses of springs and two widths of trapdoors, 3 and 6 inches, were used.

In the theoretical analysis, the authors state that the angle of internal friction was increased as a function of the depth-to-span ratio in order to account for the additional lateral restraint which the soil mass provides at deeper depths. This was pointed out by Bedesem et al. This increase in ϕ improves the agreement between the theoretical and experimental results. The authors assume that

slip lines develop when the shear stress at a point on some plane exceeds the allowable for the material. The region bounded by the limiting slip lines may be in a state of plastic equilibrium or it may contain areas that remain essentially elastic.

The results of the test program indicate that the theory has some limitation in its ability to predict the loads of a configuration similar to that used in this test.

Mason, Criner, Waissar, and Wallace describe an experimental and theoretical study of the soil-structure interaction characteristics of a granular soil. The theoretical portion of the report develops equations for the static, passive, and active arching phases of soil-structure interaction. These equations were developed by assuming vertical surfaces of sliding at the extremities of the structure and summing the forces acting on a differential soil element. Friction forces along the surface of sliding were determined by the Mohr-Coulomb failure criteria. The equations representing the static behavior are presented for active and passive arching and compared with experimental data.

The experimental program was conducted using structures consisting of small, vertically oriented cylinders varying in diameter from 1/2 to 6 inches. The cylinders were of three different length-to-span ratios, four different uniform compressibilities, three different diameters, and three different lengths. The soil used was a

dry, 20-30 Ottawa sand. Dynamic loads from 49 to 115 psi were used. Rise times were 1 to 1-1/2 msec. The test data show that during the passive arching phase the structures experience stresses two times the free-field stress. The test data also show that the overstress is dependent upon depth, stress level, density of the soil, length-to-span ratio, and the compressibility of the structure.

The authors conclude that static arching behavior is basically dependent upon the relative compressibility of the soil and structure, and that dynamic arching behavior is generally similar to the static arching behavior but with larger loads acting on the structure.

In a later report, Mason (1965) continues this study of soil-structure interaction and the effects of compressibility as well as structural length on the arching phenomena. His mathematical model still involves vertical shear planes in the soil and the equilibrium of the forces on a soil element. In this derivation, he also considers the zone of influence in the soil that is affected by the structure. The length and width of the structure are used to determine the zone of influence. These structural parameters are also used to determine the effects of the relative compressibility of the structure.

Since there were no experimental data to compare with his equations, the author performed a limited test program with a structure whose flexibility he could vary. This cylindrical structure was

6 inches in diameter and 6 inches in length, and was buried in a 20-30 Ottawa sand. After the effects of the sidewall friction on the test structure had been taken into consideration, the results showed reasonably good correlation with the theoretical developments.

In order to further verify his equations, Mason modified them to take into consideration the trapdoor type configuration. He then checked the equations against McNulty's test results. He obtained a reasonably good correlation. Because Mason had assumed fully developed shear planes, the agreement was not good at small displacements or shallow depths, but improved for larger displacements at greater depths.

The report by Whipple on the dynamic response of arches subjected to blast loading is primarily a study of the effectiveness of soil in restraining the lateral movement of arches, but it contains an interesting formulation of the soil-structure interaction problem. The arches were considered to be buried near the surface of a semi-infinite soil mass. The depth was sufficient so that reflected pressures and dynamic pressures were not considered in the loading of the structure. Whipple limited the depth of cover over the top of the structure to one-half the arch span. The structure studied was a two-hinged arch which the author modeled by use of four rigid bars connected by moment resisting joints. The resistance of the soil-structure arch was formulated considering the bending

resistance of the arch as it deforms, the frictional and shearing resistance developed within the soil as the arch moves into or away from it, and the mass effects of the arch and the soil. Whipple developed the forces involved and then formulated an equation of motion for the entire system.

Whipple divided the soil surrounding the two sides and top of the arch into three soil blocks, one on each side which acted on the interior or exterior haunch and one acting on the top. He also divided the soil resistance into two parts: the inertia resistance or that due to the mass of the soil which moves with the arch, and the deformation resistance which is due to the presence of fully developed shear and frictional forces on the active or passive blocks.

The shearing resistance was developed by considering the state of stress which exists in the soil. Whipple assumed that, prior to the arrival of the blast wave, the soil surrounding the arches was at rest. The other states considered were the active state of plastic equilibrium and the passive state of plastic equilibrium. The active state is developed when the soil undergoes a "stretching." The passive state develops when the soil mass has been compressed laterally. Movements develop within the soil as the arch deforms under blast loading. The author discussed the amount of deformation required for full development of the plastic or active states of equilibrium. He

used a relation similar to that developed by Terzaghi and which was explained earlier in this chapter. Whipple developed displacement-resistance functions which are idealizations of the work by Terzaghi and others.

In determining the values of the pressure ratios corresponding to the limiting states of the stress, the classic Coulomb assumptions have been used. The mass of the soil assumed to move with the arch is concentrated at the joints. This mass of soil changes according to the location of the joint, the direction of movement of the joint, and the depth of burial of the arch. A linear interpolation is used between the at rest and the plastic equilibrium states. Soil resistance is assumed to be a constant after its strain has exceeded that required for plastic behavior. The primary variables determining the state of stress within the soil mass are the direction and amount of deformation to which the soil mass is being subjected.

Essentially, the author considered a wedge of soil acting on each side of his arch and a wedge of soil acting on the top. He dealt principally with the wedges on the side which the arch either moves into or away from. This in turn determines the loads which the structure will experience. The loading is modified by the inertial effects of the mass of soil considered and the shearing resistance along the failure planes on the wedges.

2.7 SUMMARY

This review of the literature indicates that although there has been considerable work in the field of soil-structure interaction, there is no agreement concerning the soil-structure interaction process. As for the arching part of the problem, some investigators believe that an actual arch forms. Others feel that shear planes develop with the deformation of horizontal soil elements. The slip planes generally radiate vertically from the structure toward the surface. In actuality, the arching problem is probably just a problem of stress distribution in the soil. The majority of the experimental investigations have been in dry sand. Very few tests have been performed with a plastic material which exhibits a sizeable amount of cohesion.

In general, the analytical studies are divided into those relying on strength only and those relying on the deformation modulus of the soil. The strength studies usually depend upon the development of shear planes along at least a part of which a fully plastic region has developed. Most investigators allow the shear planes to continue their planes to the soil surface; others provide an empirical method for determining the limit of the shear plane. The studies using deformation modulus are in the minority, but appear to be applicable to certain particular conditions such as small deformations.

CHAPTER 3

EQUIPMENT, SOIL, AND TEST PROCEDURES

3.1 GENERAL

The test program as outlined in Tables 1 and 2 consisted of placing a structure or test device at various depths in a clay soil which was confined within a test chamber and applying several static or dynamic pressures to the surface of the soil. The deflections and accelerations of the top and bottom of the device as well as within the soil were observed during the tests.

Within the overall objective of this experimental program, i.e. to study the effects of soil arching in clay, there were other limited objectives to tie this program in with some of the previous work outlined in Chapter 2. Since some of the earlier fundamental work consisted of trapdoor studies, the initial static tests were made with a device designed so that its top could be moved up and down similar to a trapdoor. This device was located 30 inches or five structural diameters (5B) above the fixed bottom of the test chamber so that the effects of the boundary adjacent to the trapdoor could be studied. Other objectives of the program were to determine the effects of variation of the stiffness of the test structure and the effects of static versus dynamic surface pressures. These objectives necessitated the design of different test devices and instrumentation

for the various phases of the test program.

The following sections of this chapter describe the test chamber, test devices, instrumentation, soil, and test procedures used during this test program.

3.2 TEST APPARATUS

3.2.1 Test Chamber. The test chamber or loader used was the Small Blast Load Generator (SBLG) located at the U. S. Army Engineer Waterways Experiment Station (WES). This facility consists of series of mild steel, 5/8-inch-thick rings bolted together and fixed to a rigid concrete base, and topped by either a static or dynamic pressure bonnet, Figure 7. Rings are available in heights of 1/2, 1, 2, 3, 6, 12, and 24 inches and can be combined to provide any desired depth of test chamber. A more complete description of this test chamber is reported by McNulty. The operation of the generator is described by Boynton Associates and the U. S. Army Engineer Waterways Experiment Station (1963).

The dynamic overpressure is applied by two lines of commercially available, PETN-filled detonating cord placed in two parallel firing tubes. Methods for determining the effective overpressure-time relation were investigated and reported by Dorris. Actual dynamic pressure records for each test are shown in Appendix C.

The static overpressure is applied by high pressure air furnished

by a three-stage compressor through a specially built pressure-regulating console.

Since this test program was conducted with a highly plastic clay, a diaphragm was not used initially on the surface of the clay for the static tests. Previous preliminary work had shown that there was a danger of bridging over portions of the soil surface as the medium deflected under pressure. Early static tests showed that although there seemed to be no air leakage through the clay, it was possible for high pressure air to force its way around the outside of the clay specimen and escape.

To control the escape of the high pressure air, several membranes were tried. The most successful were a 600-gram Darex weather balloon and a specially constructed 3/32-inch-thick, synthetic elastomer, flexible diaphragm, Figure 8. The latter was designed and fabricated in time for use in the latter part of the static test program. The weather balloons were easily cut or damaged by the slightest sharp edge or indentation and had to be very carefully handled and placed in the bonnet. The static bonnet was modified to accommodate the balloon and to eliminate edges. Twice the balloons burst during the raising of the pressure and the tests had to be restarted. With the very short load duration in the dynamic tests, no diaphragm was required.

Within the SBLG, the test device was buried in the plastic clay

30 inches above the base and centered. The following section describes the test devices used.

3.2.2 Test Devices. The basic idea for the design of the initial static structure was that it would have the same diameter and control as the trapdoor used in the studies by both McNulty and Hendron (1968). Secondly, it should, with minor changes, be capable of allowing its vertical stiffness to be varied for the later static and dynamic tests. It was considered desirable to limit the weight of the device to that of an equal volume of buckshot clay. At a wet density of 120 pcf, this volume of soil weighed approximately 10 pounds.

The design of the static test device with controlled extension and contraction was based upon concentric aluminum cylinders as shown in Figure 9. The two inside cylinders were sealed by O rings and filled with transmission oil. The third cylinder served as a protection to allow the inside cylinders to move freely. The extension and contraction of the device were controlled by the fluid which was connected to a piston on the outside of the SBLG by nylon tubing. The device was calibrated so that the approximate position of its top could be controlled by the number of turns of the piston shown in Figure 10. The number of turns necessary to move the top of the device varied with the internal fluid pressure, so it was necessary to determine the exact movement of the top relative to the base of the

device with a Collins Model III, 0-0.2-inch (Model SS-102) linear variable differential transformer (LVDT) mounted as shown in Figure 9. In addition a potentiometer, Computer Instruments Corporation (CIC) Model III, 0-0.5-inch range, was mounted in the device. The LVDT was used for initial, small displacements and the potentiometer was used to measure the larger movements.

Connected to the base of the device were the three steel tubes shown in the center of Figure 11. Two of the tubes were connected to displacement measuring devices which will be explained in a later section. The large central conduit contained the tubing for the control fluid and the instrumentation cables.

The gap between the top of the device in the extended position and the outside cylinder was covered by two layers of 0-0.1-inch band steel, one connected to the top and one connected to the outside of the device. A layer of 0.003-inch Teflon was wrapped around the outside of the entire device.

For static Tests 6, 7, and 8, and all dynamic tests except 26 and 27, the hydraulic device was modified in order to allow its vertical stiffness to be varied, Figure 12. Since the steel spring rings were very heavy, it was necessary to eliminate as much metal as possible. The outside dimensions of the spring-ring device remained the same as those of the hydraulic device, but the weight of the spring-ring device was somewhat less, Table 3.

For the dynamic tests, the displacement transducers were the same as previously described except that a Kaman-Nuclear Model KD-1101-8, noncontact unit was substituted initially for the CIC Model III. The Kaman-Nuclear gage was unreliable, so its use was abandoned.

The spring-ring system design evolved from a metal bellows idea through a proving ring concept first suggested by Hvorslev (1966) to that shown in Figure 12. A detailed discussion of the development of the spring system is contained in Appendix B.

Design studies showed that by the use of three sizes of rings, 1/4, 1/8, and 1/6 inch, and by varying the number and placement of the spacers, it would be possible to attain the entire range of flexibility desired except for the stiffest structure. Springs were built and calibrated for each test. Calibration curves similar to that shown in Figure 13 were prepared for each test, Appendix B. The total force acting on the device was divided by the area of its top multiplied by the measured deflection. Thus, the stiffness of the device was measured in terms of pounds per square inch per inch.

The determination of soil stiffness is explained in Appendix A. The soil modulus was calculated by using both soil strain measurements and peak pressure wave propagation velocities. This modulus was divided by the height of the test device, 5 inches, to obtain the soil stiffness dimensions of pounds per square inch per inch.

The preliminary test program described in Appendix A was conducted to determine the variation of soil stiffness under various conditions of surface pressure and soil water content. Based upon this information, the design stiffness for the device was determined.

The stiffness of large scale structures previously tested against nuclear weapons was examined in selecting the relative stiffnesses of the test structures.

The majority of the devices used in the test program were designed to be less stiff than the soil because of the objective of determining if beneficial effects could be obtained from active soil arching. The 0.7 stiffness, Table 2, was selected for the majority of the tests since it corresponded to a stiffness that could be reasonably obtained with corrugated metal structures. In Tests 11 through 19, the device was designed to have a constant relative stiffness at peak design surface pressure. In reality this required varying the actual stiffness of the device as the design surface pressure was changed, because the soil modulus varied with changes in applied surface pressure, Appendix A. As it was not possible to determine the exact design surface pressure beforehand, the exact required relative stiffness was not obtained, Tables 1 and 2.

To study the effects of structure stiffness under dynamic conditions, a spectrum of relative stiffnesses varying from 0.03 to 566.0 in Tests 20-28 was planned, Table 2. The design stiffnesses

were not always obtained, especially for the passive arching tests.

Static Tests 6, 7, and 8 were used to supplement the dynamic data. Therefore, the devices were designed to be both stiffer and more flexible than the soil. Just as the soil modulus varied with the surface pressure, it also varied with the rise time of the pressure, Appendix A. Thus, the actual stiffness of the device for the same relative stiffness varied between the static and dynamic tests. In Test 6, the device was to be 0.5 as stiff as the soil; this test was to correspond to dynamic Test 21. Test 8 also contained a flexible device and was to correspond to Test 14. In Test 7, a device designed to be 3 times as stiff as the soil was installed, but it attained only a relative stiffness of 1.25. This test was supposed to correspond to dynamic Test 28.

In addition to the static calibration tests, dynamic tests were conducted on the test devices in the SBLG to determine their frequency and damping characteristics in air. The top was directly exposed to the blast and no soil surrounded the test device. A typical record for one of the tests is shown in Figure C-1. Table 3 contains the results of these tests and other characteristics of each test device.

For Tests 26 and 27 it was necessary to modify the test device still further. The spring rings were replaced by a solid steel cylinder constructed and installed as shown in Figure 14. All other

components of the device were exactly the same as those in Figure 12. Strain gages were bonded to the thin portion of the steel cylinder and were used to measure load. The device was calibrated in a static-compression machine and a curve of strain (voltage output) versus load was constructed.

3.3 INSTRUMENTATION

The measurements made during both the static and dynamic tests were bonnet pressure, soil and structure deflections, and soil and structure pressures. In addition, soil and structure accelerations were measured in all dynamic tests. Strains in the top and bottom of the test device and in the deflection rods were measured during some of the high pressure, dynamic tests.

3.3.1 Gage Locations. Gage location diagrams similar to Figure 15 showing the vertical and horizontal location of each gage within the test chamber were used for each test. The symbols shown in this figure were used throughout the test program to identify the type of gage, its location, and its instrumentation channel. As can be seen in the figure, the instrumentation was concentrated at the 35-inch level. This was the level of the top of the test device for all tests. A secondary instrumentation concentration was located above and below the test device. The locations of the gages were not constant throughout all the tests. As information

developed concerning the arching mechanism as well as the pressure and deflection contours associated with it, the limited amount of instrumentation available was moved. In addition, it soon became apparent that the pressure and deflection profiles changed with surface pressure and the type of test, so instruments were moved to what seemed to be critical locations.

During the preliminary test program and a gage placement test series reported by Hadala (1967a), the approximate locations of the zones of disturbance as affected by the walls of the SBLG were determined. As a result of these studies, the movement of soil deflection and pressure gages measuring the so-called "free-field" effects was confined to a very small area during all the tests.

Since the test program extended over a period of approximately fifteen months, the number and types of gages available did not remain constant. The soil pressure and deflection gages experienced a high mortality rate during the dynamic test program.

The basic concepts behind the layout of the gages in both the static and dynamic tests are outlined in the following paragraphs.

First it was considered important to know the vertical soil pressure profile at the 35-inch level. From this information it was hoped that clues to the mechanism and volume of soil involved in the arching would be disclosed. Secondly, the soil-pressure gages were placed to disclose the variation of soil pressure with

depth. The effects on the arching mechanism of the pressure wave as it passed the structure and moved below it were considered important. Thus, an array of vertical and horizontal gages was placed above and below the test device and in the free field when possible. The gages were used to determine the ratio of horizontal to vertical pressure and the variation of this ratio with depth. In addition, these gages were placed so as to measure the change in the direction of the principal stress in the soil if arching took place. As the test program progressed, it was found that the direction of the principal soil stress was not always vertical or horizontal but varied considerably within the medium as the load transfer progressed. Near the end of the test program, a technique of placing a three-gage array, vertical, horizontal, and inclined 45 degrees, first suggested by Drake was tried.

3.3.2 Description of Gages and Placement Techniques. The soil pressure cells used in all tests were 350-ohm, semiconductor, strain gage type, known as the SE gage. This gage was designed and built at WES (Ingram, 1965). These gages were placed with their surfaces flush with the soil surface as shown in Figure 16. The hole for the gage was formed with the "cookie cutter" shown in Figure 16. The cutter was developed during the test program. After the gage was placed, soil was mounded over it and compacted with a Harvard miniature compactor. Similar cut-and-cover techniques were used for the

gages measuring pressure normal to planes inclined at 90 and 45 degrees to the horizontal.

The soil deflection gages shown in Figure 17 were designed and constructed at WES. They consisted of an epoxy disk, 2 inches in diameter and 1/4 inch thick, density-matched to the soil, and connected to a 1/4-inch-diameter steel tube. This tube was slipped inside a 3/8-inch-diameter protective tube and connected to a transducer housed in a protective cylinder attached to the test chamber base. The transducers were either Bourns Model 108 or Collins Models SS-105 and SS-102 depending upon the range required.

The disks were the same size as the SE gage and were installed in a similar manner except that soil was not mounded and compacted over them. The connecting rods, shown in Figure 11, were installed without the disks prior to the placement of soil in the test chamber. As the soil level was raised, it was compacted around the stainless steel tubes by the use of a small, 2-inch-diameter, pneumatic compactor. The tubes were covered with Dow Corning 200 fluid to decrease the friction. Special precautions were taken not to bend or move the displacement rods.

Four soil deflection gages were normally used in each test. Two of these gages were used to measure the free-field deflection at the level of the top and bottom of the test device. The other two gages were moved during the test series in order to study the

variation of the soil deflection with depth and with radial distance from the centerline of the test device at the 35-inch level. The deflection gage results were used also to determine the secant modulus of the soil. This procedure is described in Appendix A.

Two similar devices were used to measure the deflection of the base of the test device. In Figure 11 the protective tubes and cylinders for these devices are shown placed in the center of the test chamber.

During the dynamic tests, accelerometers were placed in the free field at various depths and on the top and bottom of the structure. The accelerometers were used to study the effects of inertia and pressure rise time on the structure loads. In addition, the shock environment to which the structure was subjected and the relation of structural and soil accelerations as structural stiffness changed were studied.

Strain gage accelerometers of the Consolidated Electrodynamics Corporation (CEC) Model 4-202-0001 and Statham Model A57a were used in the 10-g to 1000-g range when possible. In some of the high pressure tests, the 2500-g Endevco Model 2261 was used. In the preliminary test program and when the strain gage accelerometers were not in range, the Columbia Model 504-53, 20,000-g piezoelectric accelerometer was used. Because of baseline shift and drift of the piezoelectric gages, strain gage accelerometers were used whenever possible. The

peak acceleration registered by the Columbia gage seemed to be reliable, but integration of the records to study velocity and deflection was not possible even with corrections for the shifts.

The accelerometers used in the soil were mounted on epoxy disks 2 inches in diameter and 1/4 inch thick. The composition of these disks was varied so that the weight of the disk and accelerometer was the same as that of an equal volume of clay. The accelerometer disks were placed in the soil in the same manner as the SE gages.

For the static tests, pressure gages to indicate bonnet and internal structural pressures were 0- to 60-psi and 0- to 300-psi Ashcraft Type 1082AC Bourdon gages and CEC pressure cells, Models 312 and 313, 0 to 100 psi and 0 to 500 psi, respectively. The results were read directly by the operator or recorded on a strip chart recorder. During the dynamic tests, bonnet pressures were measured using a 1000-psi, Model 211-34-C, Norwood gage.

3.3.3 Data Recording Systems. The signal conditioning and recording systems used for the static and dynamic tests were necessarily different. The salient features of each system are explained in the following paragraphs.

Figure 18 is a block diagram showing the layout of the system used for Tests 1 through 8. Essentially the pressure cells were controlled through one of three type 225, 10-channel, Baldwin-Lima-Hamilton (BLH) balance and switching units, but measurements were

either recorded on one of the two-channel Model 7100B, Moseley Strip Chart Recorders or read directly using a Model 201, Digital Voltmeter.

An entirely different measurement and control system was used for the dynamic tests. A block diagram of this system is shown in Figure 19. The cables from all gages exited from the SBLG through the ports shown in Figure 7 and were connected to a WES-constructed patch panel near the generator. The signal was fed through a B and F Model 6-200 B4 balance and calibration unit to either a Dana Model 2000 or an Alinco Model SAM-1 amplifying unit. A Kistler Model 5655-6 charge amplifier was used whenever piezoelectric accelerometers were used.

The test results were recorded on both light beam oscillographs and magnetic tape recorders. The oscillographs were CEC Model 5-119P4-36 using 7-363 galvanometers. The paper speed was 160 in./ in./sec. The tape recorders were Sangomo Models 472RB and 452R and Ampex Model ES-100. The recorders had a 20-KH frequency response and the signals were recorded at a tape speed of 60 in./sec.

3.4 TEST MEDIUM

The highly plastic clay used to construct the soil specimens for this test program was selected because of the experience at WES in its use. It is locally referred to as "buckshot clay." In recent

years this material has received rather wide use by investigators at WES and the Massachusetts Institute of Technology (MIT), Jackson and Hadala, Hadala (1965), and Richardson and Whitman (1963), and Whitman, Roberts, and Mao. Details concerning properties of the test medium are contained in the above references and in Table 4 and Appendix A.

3.5 SOIL AND TEST DEVICE PLACEMENT PROCEDURES

The soil placement procedures previously developed for footing tests and outlined in reports by Jackson and Hadala, Hadala (1965), Dorris, and Carroll were adapted to this test program. Air-dry clay was mixed to the desired water content in a pugmill. The material was delivered to the test site in a covered conveyance and kept covered during soil specimen construction. Sufficient moist soil to form a 3-inch compacted layer was placed in the SBLG. One compaction coverage was made on the soil layer with a 10- by 10-inch hand tamper as shown in Figure 20. Following this, four coverages by a Thor, Model D, mechanical backfill tamper were used. The layer surface was scarified and sprinkled lightly with water to promote bonding. Additional layers were constructed in a similar manner. Details concerning a study to determine the type and degree of compaction are contained in Appendix A.

In order to reduce friction between the clay soil and the metal rings of the SBLG, two layers of 1/16-inch, 50-durometer, nylon

reinforced neoprene were used as liners. The outside layer was normally continuous from top to bottom of the test chamber and the inside layer was segmented into 1- or 2-foot-high strips. The segments were initially taped in place, as shown in Figure 11. The tape on the inside liner was cut or removed as the soil specimen was built. Each liner was greased lightly with GS-403 Automotive and Artillery grease. Any excess grease was wiped off the liners prior to installation. Details concerning the development of this friction-reducing technique are contained in Appendix A and a report prepared by Hadala (1967b).

The technique used to place the test device within the soil is explained in Appendix A.

3.6 TEST PROCEDURES

3.6.1 Static Tests. The procedures used in the first group of static tests (1-5) were somewhat different than those used in the second group of tests (6-8). In the first group, the test device was that shown in Figure 9. The major objective of these tests was to study active and passive arching under conditions similar to the trapdoor studies, but with the so-called trapdoor located away from a fixed boundary.

For Tests 1-4 the device was placed in the soil with its top in the extended position and sufficient internal pressure was

exerted by the control cylinder shown in Figure 10 to hold the top into its stop throughout the placement and compaction procedure.

In Test 5, the test device was installed in the soil with its top in the fully collapsed position and with its inside pressure reading 0 psi.

After the device was placed in the clay at the desired height above the base and covered with the desired depth of clay, the static bonnet was placed on the top ring of the SBLG. The pressure in the bonnet was then raised to the desired test pressure at the rate of approximately 2 psi per minute.

As the pressure was raised, it was necessary to increase the pressure inside the device above the pressure in the soil in order to prevent the top from moving. Because of this, it was not possible to measure the actual pressure exerted by the soil on the device during this phase.

The deflections of the soil and the base of the test device as well as soil and bonnet pressures were monitored and recorded every 5 minutes during the pressure buildup. During this phase the device was essentially of infinite stiffness. The deflections of the base of the structure exceeded those of the soil at the same level. In other words, the soil under the device experienced what seemed to be a punching failure due to the excess loads it

experienced during the pressure buildup.

Upon the attainment of the desired bonnet pressure, the deflections and pressure within the soil were allowed to essentially stabilize. This usually took from 10 to 30 minutes, depending upon the surface pressures.

After all gages were read, the top of the test device was either raised (Test 5) or lowered (Tests 1-4) through a series of preplanned increments by use of the control piston.

Within 10-15 seconds there was a response in the deflection of the top of the device for any change in the inside pressure. The major portion of the deflection occurred within 10 to 60 seconds after the movement of the control piston was stopped. There was continued noticeable movement for another 5 to 10 minutes. This continued movement of the top was mainly due to the time it took for the fluid pressure within the entire system to stabilize plus the interaction of the effects of the movement of the test device base and the soil affected by the changes in pressure distribution. The deflection and pressure gages in the soil responded more slowly to the changed conditions, but stabilized at about the same time as the device deflection gage. The major portion of their change occurred during the buildup to design pressure in the bonnet. Changes due to arching were usually not as large.

After the top had reached its extended or contracted position, the device was allowed to remain in this position for approximately an hour. All gages were read and the values recorded at the end of this period. In most of the tests of this group, the top was recycled at least once.

Details concerning the exact sequence of operations and measurements taken for each test are given in Chapter 4.

For the tests in the second group, 6-8, the test device shown in Figure 12 was used. The fluid was no longer required to raise the top of the device; instead, a set of spring rings was installed. The top of the test device was allowed to deflect throughout the construction of the soil specimen, surface pressure rise, and reduction of the surface pressure.

The objective of the tests in this group was to study the difference in the arching as caused by an internally controlled deflection versus that caused by the deflection that might occur in a buried structure which is externally loaded. In addition, these tests were planned to serve as means for determining the effects of dynamic overpressures versus static pressures acting on similar structures.

The position of the top and base of the device as well as that of all deflection devices was accurately measured when they were installed. At the end of the buildup and compaction of the soil specimen, all gages were read and movement during compaction was noted.

Depending on the height of material above the device or deflection disk and the stiffness of the device and soil, the deflection during compaction varied from approximately 0.001 to 0.01 inch.

As pressure was applied to the surface, the deflections of the soil and test device as well as the pressures in the soil were observed.

At a depth of burial of 6 inches, the top of the structure began to respond in 1.2 to 1.8 minutes after pressure was applied to the surface. The top continued deflecting at a rapid rate for approximately the same amount of time after the pressurization ceased. The deflection gages under the device and in the free field at the 35-inch level responded to an increase in surface pressure in 0.4 to 0.8 minute at low pressures and almost instantly at pressures over 20 psi. These gages seemed to follow the pressure curve closely.

When the application of surface pressure stopped, the gages measuring soil and structural base deflection stopped their movement almost immediately. With a drop in pressure, free-field gages responded in 0.6 to 0.8 minute while the gages under the device responded in 1.6 to 1.8 minutes. The top of the device responded in 0.6 to 1.2 minutes.

Upon the complete release of bonnet pressure, all deflection gages rebounded rapidly for about 2 minutes. Measurable rebound was

observed for approximately 12 minutes.

With the top of the test device buried 12 inches below the soil surface and at surface pressures up to 125 psi, all deflection gages responded to an increase in bonnet pressure in approximately 1.8 minutes. The deflections continued for approximately the same amount of time after the pressure had stabilized.

After a surface pressure of 125 psi was reached, no definite breaks were noted in the soil and device base deflections when the surface pressure changed. All movements were slow and gradual.

With surface pressure in excess of 200 psi, and at a depth of 12 inches below the surface, no definite breaks were noted in the movement of any of the deflection gages. All movements were slow and continuous. Below 200 psi, the movement of the top of the device showed small but definite breaks in the deflection record almost instantaneously with a decrease in surface pressure. These steps became much larger below 140 psi.

When a surface pressure of approximately 40 psi was reached, the soil and device base began to respond rapidly to the decrease in pressure. The device base moved very rapidly when the surface pressure was below 15 psi. All gages attained practically a steady position in approximately 2 minutes after 0 surface pressure was reached. The test device remained in the soil specimen from 1 to 20 hours. All gages were read at intervals until a steady state was reached.

Upon removal of the SBLG bonnet, the soil surface was profiled and photographed if a noticeable deformation was found. The soil was then carefully removed so that its structure could be observed and the locations of gages and test device could be measured.

3.6.2 Dynamic Tests. In all dynamic tests except 26 and 27, the test device shown in Figure 12 was installed at a specified depth of burial within the soil specimen. For Tests 26 and 27 the device shown in Figure 14 was used. The top and base were not prevented from deflecting during compaction of the soil above the device, but these deflections were monitored.

All pressure and deflection gages were read when construction of the soil specimen was completed. Instrumentation hookup, calibration, and checkout normally took from 4 to 16 hours.

After the firing tubes in the bonnet were loaded with sufficient quantity of detonating cord to produce the planned surface pressure, all control passed to a central control room which contained the signal conditioning equipment, oscillographs, tape recorders, and test control programmer.

Upon completion of the firing and safety check of the firing tubes, all gages were reread to determine their final positions. The surface of the specimen was closely examined, profiled, and soil samples were taken. After the surface pressure was checked, a determination was made as to whether a repeat shot was required. If the

pressure from the initial shot was considered insufficient, then a new charge was prepared and fired. Tests 17, 25, and 27B and C are repeat firings on specimens prepared for Tests 11, 24, and 27A, respectively.

Upon completion of the profiling and sampling of the soil surface, the specimen was carefully dismantled. The soil was examined and the position of all instrumentation was measured. These measurements were made with a Lory, Type B point gage which could be positioned accurately on the ring flanges. In addition, the signals from the instruments were read as the instruments were uncovered so that any zero shift in the pressure gages or discrepancies in the base position of the deflection gages could be discovered.

3.7 DATA REDUCTION

For the static tests, all gages were read as outlined in Section 3.3.3 and the data were recorded by hand on master sheets. Readings were taken after all surface pressure changes, at selected time intervals, and after changes in the position of the top of the test device. Using previously prepared calibrations, the data were reduced and tabulated. Measurements made as the instruments were installed, after compaction, and after the tests also were recorded in tables. These tables were the master files from which all calculations and figures were prepared.

Data reduction for the dynamic tests was somewhat similar. Calibrations were prepared for the oscillograph and/or tape records. The time base for all data selection was determined by a zero timing line which was placed on the record when the explosion of the charge cut the timing wire placed in the SBLG bonnet.

After an examination of all records to determine the time at which critical events such as peak acceleration, peak deflection, peak pressures at various levels, and the time of arrival of measurable reflections occurred, the data were taken from the records by direct measurements at the preselected times. If later examinations showed gaps in the trend of the data, then these were filled by adding data between the time intervals. All data were tabulated so that they could be examined closely and conveniently extracted for calculations and figures.

In addition to direct extraction from the records, acceleration data which were to be processed in the computer to produce velocities, deflections, or a Fourier spectra were read with a Gerber Telereader to produce the data needed for the punch card input.

CHAPTER 4

EXPERIMENTAL RESULTS

4.1 GENERAL

The test program consisted of three groups of arching tests. The first two groups were static tests, Table 1. Group one, Tests 1-5, contained those tests in which the top of the test device was forced to move into or away from the soil above it. In group two, Tests 6-8, the top was allowed to deflect under pressure applied to the soil surface. Its resistance to deflection depended on its stiffness relative to the soil. The third group were dynamic Tests 11-28, Table 2. The top of the test device was allowed to deflect as the various input parameters forced it to respond.

In this chapter the detail results of each group of tests are represented by sets of curves. Trends are examined and discussed. Because of the voluminous amount of raw data available, all of the data are not presented. Appendix C contains the oscillograph records from the dynamic tests, including the preliminary tests. The actual records have been included since they may be of assistance to other investigators studying free-field behavior or soil-structure interaction. The static data do not lend themselves to this type of presentation and are therefore not included in raw form.

The figures in Appendix C also show the exact location of each

gage before and after the tests. These locations are not presented in any other section of this report.

The digested data from the static and dynamic tests are presented in the following two sections. Each section is subdivided into a particular measured or observed effect.

4.2 STATIC TESTS

4.2.1 Arching Curves. In this section the results of static Tests 1-8 are presented in the form of arching curves. These curves depict the test results in terms of pressure exerted on the top of the structure, pressure exerted on the surface of the soil, shear strength of the soil, deflection of the test device, and deflection of the soil (Figures 21-25).

Most of the significant data and calculations from the static tests are summarized in Table 5. This table contains the dimensionless parameters used to plot curves. All data points have not been plotted for each test but all significant points are included. The ordinate of the arching curves is the difference between the pressure acting on the top of the device and the pressure exerted at the soil surface divided by one-half the unconfined compressive strength of the soil. On the abscissa two scales are shown. The first is the differential deflection between the device and the soil at the level of the top of the device scaled by the diameter of the

test device. The deflection of the device is the total deflection of the top of the device. The deflection of the soil is the deflection measured at the same level as the device top and at a radius supposedly undisturbed by the sidewall friction and the arching action of the structure. The second abscissa is the total deflection of the top of the device scaled by the diameter of the device. There are two arching curves for each test. The solid curve is the differential pressure versus the differential deflection, and the dashed curve is the differential pressure versus the total deflection.

As can be seen in Table 5, the data used to draw the arching curves are a measure of the changes in conditions, pressure, and position that took place after the surface pressure had been attained. This had to be done since it was found very early in the test program that it is the change, particularly the instantaneous change, from the previous state that seems to dominate all results. The arching curves should be studied in conjunction with the actual data shown in Table 5.

Figure 21a shows the results of Test 1. In this test the top of the device was buried 2 inches below the soil surface. The data recorded during the time the soil specimen was being brought to test pressure (37.5 psi) are not shown by the arching curves. A structural pressure considerably higher than the surface pressure was required

to prevent movement of the device top. The same procedure was used in Tests 2, 3, and 4.

Only a small movement of the top of the device (0.001 inch) was necessary to start the unloading of the structure. The differential deflection curve eventually attained a position almost parallel to the deflection axis. The slope at the end of the test indicates that it might have been possible to increase the differential pressure to more than 24.5 psi if more deflection had been possible. Scaled deflections of greater magnitude would have been only of academic interest since it is not practical to build structures with allowable deflections this large. A larger deflection might have provided a more accurate measure of the maximum differential pressure which could be maintained at this depth due to a fully developed plastic zone around the structure. As the top was lowered, the base of the device continued to deflect although its rate of deflection decreased considerably (Table 5). After the top had been lowered 0.47 inch, the device was allowed to set in the specimen overnight. Results of the load creeping onto the device can be seen in Figure 21a. The minor change in load seems small compared to what might have been expected based on the amount of cover, the surface pressure, and comments by Finn and Tschebotarioff (1951).

As the pressure was removed from the surface of the test specimen, the arching curve took on the shape of a passive arching curve

since the top was acted on from within the device by a pressure in excess of that in the soil it tended to push up on the soil above it. The point shown on the figure as "end of test" was measured before the soil was removed from above the test device.

The arching curve for Test 2 is presented in Figure 21b. In this test the device was placed at a depth 6 inches below the soil surface. The curves start at the time the top of the device was first lowered. The arching curves turn parallel to the deflection axis. This indicates that either maximum arching had developed or the surface pressure was not sufficient to develop full arching. For this test it is the latter since the differential pressure is equal to the surface pressure (Table 5). From the point at which the curves turn sharply parallel to the abscissa and the differential pressure is 36.6 psi, the remaining points are probably not significant. After the top of the device had been fully retracted, it was raised in increments as shown in Table 5. The initial part of this curve takes on a shape similar to a passive arching curve. This passive portion of the curve might have taken on a different shape had more time been allowed and more points used. In addition, the shape may be the result of a void developed during the large deformations. The last two points on the passive curve are in doubt because of the sharp upward turn. This probably indicates that the top had hit its stops.

During the second rapid lowering of the top, the differential deflection curve starts practically along the same curve shown for the first lowering. Had more points been plotted, the shape might have been more similar instead of the straight line used between the points at 6 hours and 37 minutes and 6 hours and 44 minutes. The curve for the second lowering also turns parallel to the abscissa. There may be a question as to why the curve did not come to the same differential pressure as the first curve. This can be accounted for by the fact that the surface pressure was lowered during this period. Therefore, it was not possible to obtain the same differential pressure. The final pressure on top of the device was the same for both portions of the test. In other words, the soil was able to dissipate all the pressure acting on the surface of the soil specimen with sufficient deflection of the test device. The point shown as the end of the test was measured with the soil on the device and with zero surface pressure.

Figure 22 shows the arching curves for Test 3. The figure has been divided into two parts; 3a contains the arching curves when the surface pressure was 37.5 psi, and 3b shows the arching curve when the surface pressure was raised to 50 psi. After reaching a structural pressure of 1 psi, the device was allowed to stand overnight with no change in the piston controlling the deflection of the top of the device. During the 14.5-hour creep period, the surface

pressure remained at 37.5 psi and the top of the device moved down approximately 0.048 inch. The base of the device moved down approximately 0.027 inch and the differential deflection increased 57 mills. Pressure on the top of the device increased to 3.3 psi. It is evident that the soil creep had been sufficient to cause these results.

After the creep period, further lowering of the top of the device by 13 mills was sufficient to pull a vacuum on the inside of the test device. During this period, the base continued to deflect at approximately the same rate at which the soil in the free field was deflecting although the total deflection of the base of the device was less than the deflection of the free field. This could be expected because of the unloading of the soil underneath the test device. At this depth of burial, the surface pressure was not sufficient to develop the full strength of the material.

During the third phase of Test 3 the top of the device was raised through the positions shown in Table 5. The resulting arching curve in Figure 22a has the same shape as a passive arching curve beginning at the origin. The shape of this curve is significant in that it shows that as soon as the direction of the top of the device is changed, the load on the device increases rapidly. The load on the device does not follow the active arching curves back to the origin but takes on the characteristic shape of a passive

arching curve immediately. This type of action is in agreement with the curves previously presented by Terzaghi (1936c).

The point shown at 21 hours and 6 minutes does not appear to be a good point. The top was probably into the stop at this time. The double dot-dashed lines are hypothetical curves which might have occurred had the overnight creep and slight decrease in surface pressure not intervened.

Figure 22b and Table 5 show the change in the deflections of the test device as the surface pressure was raised to 50 psi. The shape of the curve between the final position at the end of the 37.5-psi test and the start of the 50-psi test is not known. In order to hold the top of the test device into the stops, the pressure on the inside of the test device was increased appreciably above 50 psi. As previously discussed, pressures during this time are not sufficiently dependable to use in plotting arching curves.

The first point shown in the 50-psi curve was recorded when the top of the device first began to lower. The shape of the active arching curve at this pressure is not the same as that shown in Figure 22a. The time lapse and compression of the clay seem to have had a decided effect. The shape of the curve and the differential pressure indicate that a surface pressure of 50 psi was not sufficient to develop the full strength of the material at this depth.

Table 5 shows the results of leaving the test device in the

soil at zero surface pressure for approximately 65 hours. The soil under the device moved up and the top of the device also moved up. The differential deflection indicates that the overall movement of the device in relation to the soil was up. The location of the device in relation to the soil after the soil was removed to the 35-inch level has been included in Table 5.

The arching curves for Test 4 are presented in Figure 23. The test device was buried at a depth of 6 inches, and the surface pressure was 75 psi. The active arching curves resulting from the lowering of the test device are characteristic of this type curve. The arching curves are generally parallel to the abscissa at 1 hour and 7 minutes. At this time, the deflection of top of the device was 91 mills and the differential pressure was approximately 36.6 psi. This pressure and deflection correspond very closely with the results noted in Tests 2 and 3, i.e., the curves pass through practically the same point. The scaled differential pressure of $\frac{2\Delta P}{q_u} = 3.3$ measured at 1 hour and 7 minutes is probably a good indication of the strength of the soil at this depth of burial. The slope of the arching curve indicates that either the soil was increasing in strength with time or that the much larger deflections were able to mobilize more strength. In the latter case, it means that even larger differential deflections might have generated greater differential pressures. The much higher differential pressure developed by further lowering

the top at 2 hours and 33 minutes was due to the stops.

The initial point plotted indicates a plus differential pressure or passive arching condition. This was the true condition since the device had been held in a stiff configuration while the surface pressure was raised. When the top was raised, a true passive arching condition resulted.

For the second lowering of the top of the test device, the arching curve was similar to the initial curve except that the initial part of the curve was steeper. This may have been due to the high pressures that were exerted on the top of the device at the end of the passive portion of the test and increased soil strength. This curve fell above the curve for the first lowering just as was noted in Test 2, but in this case the surface pressure was the same for both phases of the test. In addition to the fact that the origin for the second test was different, examination of the soil showed that failure planes had developed. The differential pressures during the second lowering depended on the type and extent of the failure planes developed and the remolding of the soil along these planes. The actual change in pressure was from a plus 36.1 psi at 4 hours and 39 minutes to a minus 36.1 psi at 6 hours.

The data in Table 5 for Test 4 show that the base of the device moved up during the first lowering of the top. The deflections

are shown with a negative sign since they are in the opposite direction to the deflection of the soil and the top of the device. This action resulted from the fact that the soil under the device was unloading from a high preloaded condition while the soil in the "free field" was being loaded. When the top of the device was raised, the base began to deflect, as expected.

Movement of the deflection measuring instruments after the surface pressure was released and the overnight creep at zero surface pressure also are shown. These data are actual deflection data and actual positions without reference to the base point established after the surface reached test pressure. This accounts for the unusual shape of the total deflection curve during this period of time.

The arching curves for Test 5 are shown in Figure 24a. The device was placed at a depth of 6 inches and the top was raised initially instead of being lowered. The surface pressure was 37.5 psi. The device remained in the soil 3 days prior to this test. Deflections are carried to four decimal places because of the small changes that took place in the soil deflections as a consequence of this long initial creep period. During this period of consolidation, the shear strength of the soil was increased from 12.6 to 16.9 psi. The arching curve during raising of the top seems to be similar in shape to other passive arching curves. There was a large change in the load on the device with only a small amount of movement of the device.

The point plotted at 2 hours and 26 minutes is probably not a good point since the sharp change in the shape of a curve is an indication that the top was into its stop.

The arching curve still had a small amount of slope at the time of the maximum deflection of the test device, but no major load change occurred after $\frac{\Delta D}{B} \times 1{,}000 = \pm 16$ was attained. Scaled deflections of this nature are out of the practical range for structures.

During the initial lowering of the top, the arching curve is very steep. Between 4 hours and 8 minutes and 5 hours and 46 minutes the curve begins to turn parallel to the deflection axis. There actually was a small decrease in the ΔP after 4 hours and 8 minutes. This may have been caused by the speed of the deflection and the time it took for the soil to follow. The differential pressures are practically equal to the surface pressure. This is an indication that the maximum strength of the soil probably had not been developed by the deflection attained at this surface pressure. Had a higher surface pressure been used, a greater differential pressure probably could have been developed.

After 4 hours of creep, the load on the device increased by 1.4 psi and the top of the device moved down approximately 10 mills. The pressure increased another 1.3 psi and the top moved down another 17 mills during the overnight creep period. With lowering

of the surface pressure, the curves indicate that the device began to load the soil and the arching curve takes on passive characteristics.

The arching curves for Tests 6, 7, and 8 are different from those in the previous tests. The top of the device was not controlled by internal pressure (Figure 12). This device had a spring system which allowed the top to deflect as the pressure increased on the device. The top of the device was not held in position while test pressure was attained.

The arching curves for Test 6 are presented in Figure 24b. In this test, the device was weaker or more flexible than the soil. The top of the device was buried 6 inches below the soil surface. During the raising of the surface pressure the arching curve is considerably flatter than in the previous tests in which the top was artificially lowered under constant surface pressure.

Examination of the arching curves for Tests 2 and 6 discloses similar first cycle differential pressures of approximately -1.2 psi at comparable differential deflections. Larger differential pressures ultimately were developed in Test 2 because of the larger deflections possible.

An unusual phenomenon which took place during Test 6 was the change in the direction of the differential deflection curve after time 47 minutes. At this time the rate of deflection of the base became considerably less than the rate of deflection in the free field.

As a result, the differential deflection decreased considerably until time 3 hours and 28 minutes. At this time, although the differential pressure was approximately 14 psi, the differential deflection was only 0.004 inch. The total deflection of the device was approximately 0.89 inch. No soil deflection gage was located close to the test device at the 35-inch level so it was not possible to determine if larger deflections existed at this level.

When the pressure on the surface was initially lowered, the arching curves took on the characteristic shape of a passive arching curve. The soil actually was being held by the surface pressure and the device was moving upward at a faster rate than the soil. Even with zero surface pressure, approximately 3 psi was exerted on the top of the test device.

When the surface pressure was returned to 38.5 psi, the top of the device deflected to approximately the same position relative to the base as existed in the first phase of the test. There was only a small difference in the total deflection of the device in spite of the fact that this was the second cycle and the test device had started from a position lower than its initial position.

The device was allowed to set in the soil specimen for approximately 63 hours with the surface pressure maintained between 38 and 39 psi. There was very little change in the deflection of the top after the first 16 hours although the soil under the device in the

free field continued to deflect at a slow rate. The effects of creep seem to have been minimal for this test and this test device. Pressure increased approximately 3.5 psi during the first 16 hours. In the next 47 hours, the load on the device increased by 0.3 psi. During the last 20 hours of the creep test, the load on the device did not change. Throughout this period, the deflection of the soil in the free field and the deflection of the base of the device were practically the same. Consequently, there was very little change in the differential deflection which could add load onto the device. The planned ratio of stiffness of the structure to the soil was 0.5. The actual calculated ratio was approximately 0.6. The total load experienced by the top of the structure during the creep period was approximately 0.7 of the surface pressure. The results of this test seem to indicate that creep effects at this pressure are minimal after the first 24 hours. Whether the same could be said in terms of weeks, months, and years is not known but the results seem to throw considerable doubt on some of the assumptions concerning the effects of creep on arching made by Spangler (1948) and Finn.

Figure 25a contains the arching curves for Test 7. In this test the structural stiffness of the device was designed to be three times that of the soil. The calculated stiffness of the structure in relation to the soil was 1.25. In spite of its stiffness, the structure did not exhibit passive arching. The structure actually

experienced a decrease in load of approximately 5.5 psi.

During this test, the pressure container, an enlarged weather balloon, broke and it was necessary to restart the test. The deflections and pressures at the time the pressure vessel broke were noted. During the second pressurization the deflections showed very little difference from the initial deflections. The flat portion of the arching curve which is parallel to the abscissa probably was due to relative stiffness. In other words, this was the pressure which could be exerted on this device buried at this depth with this surface pressure. As noted in the deflection curves for this test and later in the arching curves for the dynamic tests, the stiffness of the device alone is not a measure of the amount of load that a stiff structure will experience. In this test, the deflection of the base becomes rather large and actually exceeds the deflection in the free field at the level of the top of the device. The base deflection is high enough when added to the deflection of the top to force the differential deflection to become negative and thus result in the negative loads noted.

The arching curves for Test 8 are contained in Figure 25b. In this test, the device was designed to be less stiff than the soil. The surface pressure was 240 psi. The arching curve starts with the characteristic shape of an active arching curve then flattens out to take on the shape of the curves noted in Test 6. It is interesting

that the differential pressure reached a value approximately five times the strength of the material. The top of the test device was buried at a depth of 18 inches. The maximum differential pressure varied from 54 to 57 psi after the surface pressure reached approximately 175 psi. This indicates that a surface pressure of approximately 175 psi was required to develop the full strength of this material at this depth.

When the specimen was allowed to creep overnight, the load increased by 23 psi while the differential load decreased by 23 psi. The results seem to indicate that once full arching exists and failure planes have developed, creep is more prevalent. In addition, the creep is obviously more substantial at higher pressures. When material above the structure remains below its ultimate shear strength, creep is not substantial.

The arching curves exhibited passive characteristics when the surface pressure was released.

Some general conclusions concerning static arching curves are: they are hysteretic in shape; it is possible for active arching curves to be parallel to the deflection axis without full arching; and their shape is dependent upon depth of burial, surface pressure, and the manner in which structure deflections are induced.

4.2.2 Pressure Profiles. Figures 26 through 28 are pressure profiles which show the horizontal distribution of vertical soil

pressure at the 35-inch level in the specimen. Since the top of the test device was at the 35-inch level for all tests and since changes in the distribution of vertical soil pressure as affected by arching should be significant at this level, it was used to plot all horizontal pressure profiles. These figures are representative of the type of data produced in the test program.

An important point to note in these figures is the manner in which the soil pressure was affected by the arching onto or away from the structure. As the load on the structure was reduced, then the soil pressure in the vicinity of the structure increased. Conversely, when the structure attracted load, the soil pressure in its vicinity decreased. It is also important to note the radial distance from the test device at which this effect is experienced by the soil. Some of the soil pressures were the result of the lapse of time as the sidewall friction was overcome and the pressure worked its way downward through the soil specimen. Generally 3 to 4 hours were required for the pressure to stabilize within the entire soil specimen.

Figure 26a is the profile for Test 1. It is a good example of how pressure is affected by movement of the structure. As the surface pressure increased, the top of the device was held rigid. Since the rigid structure attracted load from the surrounding soil, the soil pressure gage at a radius of 4-1/2 inches registered

considerably less pressure than the gages at 5-1/2, 6, and 6-1/2 inches. As the top of the device was lowered, the pressures registered by the 4-1/2-inch gage began to increase rapidly, while the pressures at 5-1/2-, 6-, and 6-1/2-inch radius increased at a lesser rate. The gages at 10, 14, and 16 inches stabilized at a constant pressure fairly early in the test.

It seems reasonable to conclude that the structure did load and unload the soil and that the effects are noticeable to a radius of approximately 6-1/2 inches. Unfortunately the gage at the 8-inch radius failed to function properly.

From the gages remaining after 19 to 21 hours, it can be seen that there was virtually no change at the 16- and 5-1/2-inch radii, but there was a noticeable change in the pressure at the 4-1/2-inch radius and on the structure. The pressure on the structure increased and the pressure at the 4-1/2-inch radius decreased from the reading after 4-1/2 hours. There were some creep effects and they seemed to affect only the soil close to the device.

In Figure 26b a similar change in the soil pressure can be noted for Test 2. As the top of the device was lowered the structure unloaded and the soil in its vicinity was loaded. There seemed to be effects at least to the 6-1/2-inch radius. This figure also shows the effects of raising the top of the device after it had been lowered. The pressure on the structure increased and the pressure

acting on the soil decreased. Again the changes affected the soil to a radius of approximately 6-1/2 inches. Unfortunately, the gages at the 8- and 10-inch radii did not function.

Figures 27a and b show the results from Test 3. The top of the device was buried at a depth of 18 inches. In Test 1 the top was buried 2 inches and in Test 2 it was buried 6 inches. In this figure it can be seen that the pressures registered by the gages at a radius of 16, 10, and 8 inches did not stabilize immediately. The effects of sidewall friction are significant at this depth and at this surface pressure. It was only after approximately 17 hours that the soil pressure at these radii seemed to become constant. As the top of the device was lowered and the pressure on the device decreased, the soil pressure in the vicinity of the device increased. The pressure changes due to the device do not appear to extend further than 6-1/2 inches from the test chamber centerline.

As the top of the device was raised, Figure 27b shows how the pressures in the soil decreased. Slight effects were registered at a radius of 6-1/2 inches, but not at 8 inches. The soil pressure gages at the 8-, 10-, and 16-inch radii indicate that the soil specimen reached an equilibrium condition which was unaffected by any arching action.

Figure 27c shows the distribution of pressure for Test 4. The surface pressure was 75 psi. The important part of this profile is

that the pressure was sharply lowered at the 4-1/2-inch radius and slightly lowered at the 5-1/2-inch radius as the device was lowered. This is exactly opposite to the effects previously discussed for the lower pressure tests. At 6-1/2 inches, the gage indicated the beginning of the pressure buildup that was required by the active arching. The extent of the raised pressure could not be determined because of gage failure.

Figures 28a and b show the results from Test 6. The device was more flexible than the soil. In this test, surface pressure was raised and then lowered, raised again, held approximately 70 hours, and then lowered. The results of lowering and raising the surface pressure as well as the arching effects on the soil are clearly visible in the pressure profiles. The low soil pressure region at approximately 6 inches under active arching conditions was confirmed by all 37.5-psi tests.

During Test 6 as the surface pressure was raised, the pressure on the structure remained considerably less than the surface pressure. This is as it should have been since the structure was designed to have one-half the stiffness of the soil. At 37.5 psi, the modulus calculations indicated that the structure was actually 0.6 as stiff as the soil (Table 1). At time $t = 2{:}20$, the pressure acting on the top of the device was $0.64 \times P_S$.

The soil pressures in the vicinity of the structure show the

results of a considerable amount of structural unloading. These effects seem to extend to the 6-1/2-inch radius. There appeared to be two definite regions affected by the arching: one inside the 5-1/2-inch radius and one outside the 6-inch radius. When the surface was initially unloaded, Figure 28a, t = 4:05 and 5:11 , the structure did not unload as fast as the soil surface. The condition is somewhat similar to a passive test with the structure attracting load. These effects can be seen by closely studying the actions of the 4-1/2-inch gage. The area affected by the device appeared to extend to the 6-inch radius.

In Figure 28b, the creep effects can be seen by studying the curves for times t = 7:41 and t = 70:17 . The increase at the 14-inch radius was probably due to a reduction of sidewall friction. It is particularly interesting to note how the pressure on the structure increased with time from 22.6 to 26.6 psi. The soil pressure at the 4-1/2- and 5-1/2-inch radii remained virtually unchanged and the pressures at the 6- and 6-1/2-inch radii decreased. These changes would seem to indicate that the creep effects extended to a position high enough above the structure to spread the effects to the 6- and 6-1/2-inch region in the soil.

Figure 28c is an example of the pressure distribution resulting from the installation of a device which was supposed to be stiffer than the soil in which it was buried. The device was designed to be

three times as stiff as the soil but posttest calculations showed that it was only 1.25 times as stiff as the soil (Table 1). The arching curve in Figure 25a and the data in Table 5 show that the structure-soil system acted less stiff than the soil itself. Some of these peculiarities can be seen in the soil pressure profiles. The pressure at the 4-1/2-inch radius was considerably lower than the pressure on the structure. The pressures at the 6-1/2- and 16-inch radii are even higher than the surface pressure. Some of this pressure difference was gage overregistration. This can be seen in the before and after test pressure profiles. The soil pressure gages returned to almost their initial reading. This pressure seems to be a measure of the weight of the soil above the gages. Pretest and posttest pressure measurements of this nature were made for all tests. They have not been included in the figures in order to eliminate clutter.

To study more closely the area of the soil which was influenced by the arching action induced by the test structure, the equilibrium of forces acting on the soil surface and at the level of the device was calculated for each test. The force balance calculations required two assumptions: that a straight line distribution of pressure existed between any two successive gages, and that the vertical pressure profile was the same along any horizontal radius emanating from the top of the test device. The straight line distribution

assumption between the device and the gage may have been poor. More than likely there was an abrupt change of the pressure at the edge of the device.

As examples to illustrate the use of this type of calculation in conjunction with the pressure profiles, the data from Tests 1 and 6 are presented in more detail. If time t = 4:52 is selected for Test 1, then the surface pressure is 37.8 psi, Figure 26a.

Radii	Average Pressure	Force	Cumulative		
			Force	Area	Average Pressure
in.	psi	lb	lb	$in.^2$	psi
0-3 (Test Device)	13.3	376	376	28.3	13.3
3-4.5	30.4	1,075	1,451	63.7	22.8
4.5-5.5	46.7	1,462	2,913	95.0	30.7
5.5-6	42.5	765	3,678	113.0	32.6
6-6.5	40.3	794	4,472	132.7	33.8
6.5-10	41.8	7,578	12,050	315.0	38.2
10-14	45.4	13,684	25,734	615.4	41.7
14-16	34.7	6,537	32,271	803.8	40.2

The results of the calculations indicate that arching induced by the structure seems to have effects out to a region somewhere

between the 6-1/2- and 10-inch radii. Using the 4-inch gage at the 32.5-inch level, it is possible to assume a somewhat higher pressure region between the edge of the device and the gage at the 4-1/2-inch radius, for example 39 to 40 psi. This would bring the area involved in the primary arching within the 6-1/2-inch radius.

The higher average pressures at the 14- and 16-inch radii do not exceed P_S by very much and there were some inaccuracies in the measurements and calculations. Another and highly probable explanation resulting from a close examination of many low pressure profiles is that arching takes place between the sidewall of the test chamber and a portion of the soil specimen in the vicinity of the 10-inch radius. The sidewall friction causes differential deflections to take place between the soil at this boundary and the soil further out in the specimen.

Similar calculations for Test 6 at time t = 2:20 showed that the area involved in arching extended to approximately the 6-1/2-inch radius. The average pressure inside this radius at the 35-inch level was 38.1 psi versus a surface pressure of 37.5 psi.

The force balance calculations confirmed the results obtained by examining the pressure profiles.

Figures 29 through 32 depict the change in the distribution of vertical soil pressure with depth for several of the static tests. These curves have been plotted to show the distribution in the

so-called free field as well as the distribution measured by gages placed directly above, below, and beside the test device. Curves are presented for different time periods so the change in the distribution with deflection of the top of the device can be illustrated.

Figure 29a shows that the pressure distribution changed practically uniformly as the pressure on the surface increased. The gage at the 36-inch level and directly above the device did not attain the surface pressure at time $t = 0$. At this level, the horizontal gage indicated that passive arching increased as the surface pressure was raised. The gage measuring soil pressure near the test device at the 35-inch level showed that this pressure was considerably lower than the free-field pressure which was equal to the surface pressure. This behavior can be explained by the fact that the top of the device was held rigid during the buildup of the surface pressure. The gage measuring horizontal pressure at the 32-1/2-inch level and at a radius of 4 inches indicates that the vertical pressure exceeded the horizontal pressure while the surface pressure was increasing. At the time the surface pressure reached 37.5 psi the horizontal pressure was practically equal to the vertical pressure. The gages at the 30-inch level indicate that the pressure distribution was fairly uniform at this level. The gages at the 27-inch level seem to show that the pressure under the device

was higher than the free-field pressure. This is understandable since the device in its rigid condition has been loaded more than the free field. Therefore, the pressure underneath the device also should exceed the free-field pressure. After the surface pressure reached 37.5 psi, the soil pressure gages in the so-called free field continued to show change, Figures 29a, b, and c.

The lowering of the test device took 4 hours and 52 minutes. The surface pressure varied between 37.5 and 38 psi. During this period, the free-field gages showed the following changes: the 6-inch level gage went from 13.8 to 17.8 psi, that at the 24-inch level went from 36.9 to 37.5 psi, the 27-inch gage from 24.2 to 27.2 psi, the 30-inch gage from 42.3 to 43.7 psi, and the 35-inch gage from 37.4 to 38.0 psi. The variations and readings seem reasonable except for the free-field gage at the 27-inch level.

During this same period of time, the gage at a radius of 4.5 inches and at the 35-inch level went from a reading of 20.7 to 49.3 psi. The low reading was due to the attraction of load by the stiff device and the high reading was induced by the lowering of the top of the device. The 5.5-inch gage went from 38.5 to 44.3 psi, the 6.5-inch gage from 35.4 to 41.4 psi, and the 10- and 14-inch gages changed less than 1 psi.

In Figure 29b the horizontal gage at the 32-1/2-inch level indicates that the ratio of the horizontal to vertical pressure was 1.

At the end of the active arching test, Figure 29c shows that the pressure in the soil near the device exceeded the pressures in the free field at the same level. The results of the arching extend to the 30-inch level. The horizontal gage did not show this same rise; thus, the vertical pressure was greater than the horizontal pressure. The close-in soil pressure gage at the 27-inch level indicates very little if any effect from the active arching induced by the structure.

From time 4 hours to 4 hours 52 minutes shown in Figure 29c, very little change in the pressures was indicated by the free-field soil gages. The free-field gage at the 27-inch level does not appear to have been functioning correctly. The soil gages near the device continued to show an increase in pressure with the lowering of the top of the device and therefore a decrease in the pressure acting on the top of the device.

Figure 30 contains the distribution of soil pressure and its changes with movement of the test device for Test 2. Figure 30a shows the distribution that resulted when the top of the device was lowered. The results are similar to those in Test 1 except for the gage located 5 inches above the device. As the device unloaded this gage also unloaded. This indicates that some arching was taking place above this level. The close-in gage at the 35-inch level displayed a characteristic unloading as the structure loaded. The close-in horizontal pressure gages registered higher pressures

than the average vertical pressure at the 32-1/2-inch level. This is a reflection of the unloading caused by the structure. In this test the close-in and free-field gages at the 30-inch level registered similar pressures. The difference between the free-field and close-in gages at the 24-inch level seems to be dependent upon the sidewall friction effects. The gages in the so-called free field indicated a gradual rise in pressure with time. This seems to be another manifestation of the sidewall friction. When the top was raised, Figure 30b, the gage registering soil pressure directly above the device showed an increase in pressure whereas the gage at the 35-inch level near the device indicated a decrease in pressure. These are the expected trends. The gage underneath the device at the 24-inch level registered a sharp increase as the structural load increased. Note how the ratio of the horizontal to vertical pressure at the 32-1/2-inch level reversed.

Figure 30c shows the pressure distribution as the top was lowered the second time. Note how the gage directly underneath the device unloaded as the device unloaded. The gage directly over the device also unloaded. Whether this change can be directly attributed to arching is not known, but the change at the 4-1/2-inch radius is opposite to the surface pressure. This would indicate arching effects rather than surface pressure effects.

Figure 31 shows the results of changing the technique for

placing the friction-reducing material around the inside of the test chamber. For Test 3, the inside layer was segmented in horizontal strips so that it could move more freely (Appendix A). Increased free-field pressures at the 6- and 24-inch levels resulted. The device was buried at a depth of 18 inches for this test.

While the device was in its stiff configuration, Figure 31a, the line of gages directly above it were not experiencing as much pressure as the free-field gages. The horizontal pressure above the device was less than the vertical pressure. The direction of the major principal stress must have been near vertical. The gages measuring soil pressure underneath the device experienced pressures higher than those in the free field. The 4-1/2-inch radius gage at the 35-inch level indicated a higher pressure than the free field. All other trends were as expected for passive arching.

The profiles in Figures 31a and b at times $t = 0:07$ and $t = 2:41$ must be compared to see the results of lowering the top of the test device. The profile at $t = 17:11$ shows the overnight creep effects.

The lowering of the top of the device caused no change in the horizontal or vertical pressure gages at the 47-inch level. A decrease in the vertical and horizontal pressures was registered by the gages at the 38-inch level above the device, and a slight decrease was registered by the 41-inch gage. These results seem to indicate

that the arching takes place within 1 diameter above the device.

The 4.5-inch gages at the 35- and 30-inch levels showed the increased pressures resulting from the structure unloading to the soil in its vicinity. The gages under the device reflected the decrease in the load on the device. The change at the 27-inch level was very marked. All free-field gages indicated an increase in pressure at t = 2:41 .

The creep period shown in Figure 31b also indicates some interesting results. All free-field gages except the one at the 38-inch level registered an increased pressure which was probably due to the gradual release of the sidewall friction.

Above the test device there were some noticeable changes. Although there was virtually no change in the vertical pressure at the 47-inch level, there was a sharp increase in the horizontal pressure. At the 41-inch level there was a sharp decrease in the vertical pressure, and at the 38-inch level some increase in the vertical pressure. These results seem to indicate that with time, the arching phenomenon propagates upward into the soil. It appears to be a time-dependent behavior in the clay. During the creep period, the pressure on the top of the device increased approximately 2 psi.

The pressure increases registered by the close-in gages at the 30- and 35-inch levels could have been the result of the arching action discussed above or friction phenomenon at the chamber walls.

The 27-inch gage under the device shows the results of the changes in the pressure on the device and in the free field.

As a result of studying Figures 31a and b closely, it can be seen that the arching phenomenon may not be attributable to any simple arching theory. The direction of the principal stress may change more than once above the structure depending upon its depth of burial, amount of deformation, and the time effects.

When the top of the device was raised, the vertical pressure indicated by the gage above the test device at the 41-inch level increased considerably. The vertical pressures at the 38- and 37-inch levels registered no such increase, but the horizontal pressure at the 38-inch level showed a large increase. The principal stress at this level changed directions. The 4-inch radius at the 38-inch level was probably outside the arching zone of action. At time $t = 2{:}41$, the structure registered a pressure of 1 psi while the vertical pressure gage at the 38-inch level indicated a pressure of 27.5 psi. At time $t = 21{:}06$, the structure had a pressure of 59.6 psi acting on it while the gage at the 38-inch level showed a pressure of 29 psi. One other possibility was a broken gage. A posttest check of the gage at the 38-inch level did not disclose any problems. Again, it must be surmised that the arching effects extended at least one structure diameter above the device. The sharp changes in pressure at the 41-inch level after the creep period

indicate that the arching actions propagated above this level. The actions of the gages at the 47-inch level indicate that arching effects did not reach this level.

The increased load on the top of the device also caused the gages below the device to register an increase in pressure. The results are more marked at the 24-inch level. Thus, it can be seen that effects are noticeable at least one structure diameter below the device.

The gages in the vicinity of the structure at the 35- and 30-inch levels in Figure 31c show very strong decreases in the vertical soil pressure as a result of the structure. Such action is normal for the passive arching condition. The horizontal gage at the 32.5-inch level also reflects this change. By this time, the free-field gages seem to have stabilized with the exception of the ones above or at the level of the device. The actions of these gages as seen in Figures 31b and c strongly indicate that the arching action had effects as far out as 16 inches from the centerline as time progressed. The stress reversal in Figure 31b is especially interesting considering the action of the other free-field gages.

Figure 31d shows changes in the pressure profile as the top of the device was lowered. Surface pressure had been increased to 50 psi. The increase in pressure with the top held rigid had increased all pressures above the device about the same amount except at the

47-inch level. The rigid structural effects also are manifested in the pressures registered by the close-in gage at the 35-inch level.

As the top of the device was lowered, the pressure 6 inches above and below the device also dropped. No change was noticed in the vertical pressure at the 47-inch level, but the horizontal pressure decreased. The pressures registered by the close-in and free-field gages at the 30- and 35-inch level show an increase in load. An increase in load also was observed at the 38-inch level in the free field.

Thus it can be seen that at $P_S = 50$ psi and $H/B = 3$ the active arching action has marked effects at least 6 inches above and below the structure and 16 inches in a horizontal direction from the structure. Stronger reactions were noted at a radius of 4.5 inches than at the 16-inch radius.

Profiles similar to those shown in Figures 29-31 were drawn for all static tests. The results were examined in a manner similar to the figures shown. The results of this examination are reflected in the conclusions drawn in Chapter 5.

In some of the tests, the horizontal and vertical gages were placed above the device in order to examine the ratio of the horizontal to the vertical pressure and how this ratio changed with arching in the soil. In Test 3 horizontal and vertical gages were placed 3, 6, and 12 inches above the device. Unfortunately, the gage

measuring horizontal pressure at the 6-inch level did not function. Figure 32a shows the stress ratio at the 38- and 47-inch levels above the device as well as that at the 32-1/2-inch level beside the device.

As the top of the test device was lowered, the vertical pressure at the 38-inch level dropped from 30 to 27 psi and the horizontal pressure dropped from 25 to 16 psi. The vertical pressure at the 41-inch level dropped from 30 to 29 psi. At the 47-inch level the vertical pressure increased 1 psi while the horizontal pressure increased 5 psi. At the 32.5-inch level there was a 5-psi increase in the average vertical pressure and a 6-psi increase in the horizontal pressure. The increase in vertical pressure at the 32.5-inch level is due to the pressure relieved at the 35-inch level by the top of the device as it was lowered.

During the overnight creep period, the vertical pressure at the 38-inch level increased to 29 psi while the horizontal pressure increased to 20 psi. The pressure acting on top of the device increased from 1 to 3.3 psi during the same period. The increase in the ratio of the horizontal to vertical pressure is in the correct direction and indicates that the arching action works its way up from the device progressively with time.

The gages at the 47- and 32.5-inch levels also showed an increase in the horizontal-to-vertical pressure ratio. At the 47-inch level, the vertical pressure stayed virtually constant while the

horizontal pressure increased from 16 to 30 psi. At the 32.5-inch level the vertical pressure increased by only 2 psi while the horizontal pressure increased 6 psi. At both levels the increase in the ratio seems to be the result of the high degree of saturation. The vertical and horizontal pressures are approaching each other as the soil approaches 100 percent saturation.

During the further lowering of the top of the test device the horizontal pressure at the 38-inch level decreased slightly while the vertical pressure stayed practically constant. Notice that the horizontal-to-vertical pressure ratio decreased just as it did during the previous lowering. There were also small decreases at the 47- and 32.5-inch levels which were probably insignificant.

During the next step, the top of the device was raised to cause a passive arching condition in the soil. At the 47-inch level, the vertical and horizontal pressures remained relatively constant. This indicates that arching action had very little if any effect at this level.

At the 32.5-inch level, there were considerable pressure changes. The horizontal pressure decreased 12 psi while the average vertical pressure decreased 13 psi. These decreases resulted from the action of the test device as it attracted load away from the soil in its vicinity.

In Phase 6 of Test 3 the surface pressure was raised from 37.5

to 50 psi while the top of the device was held rigid in its extended position. At the 38-inch level the vertical pressure increased 10 psi while the horizontal pressure increased approximately 7 psi. Directly over the device the vertical pressures must have been considerably higher since the device experienced pressures in excess of 70 psi. At the 47-inch level there was practically no change in the pressure ratio.

Upon lowering of the top of the test device under the higher pressure conditions, the horizontal pressure at the 38-inch level decreased about 18 psi while the vertical decreased only about 3 psi. At the 47-inch level, there was a 3-psi decrease in the horizontal pressure measured at a radius of 3 inches with no change in the vertical pressure measured at a 3.5-inch radius. Notice that the direction of change in the horizontal-to-vertical pressure ratio is the same for steps 4 and 7 at the 47-inch level. In spite of all the placement problems, these changes seem to be caused by more than just chance.

Figure 32b shows the ratio of horizontal to vertical pressure at selected elevations in the soil specimen for Test 8. The curves terminate at different times because of water migrating into the gages and the connectors. The high pressure to which the gages were exposed, along with the length of time, eventually caused all of them to cease functioning. Gages were placed to measure soil pressures

acting on horizontal, vertical, and 45-degree planes at selected radii and levels as shown in the figure. The horizontal-to-vertical pressure ratio at a particular location is plotted versus the surface pressure.

The gages on the centerline directly above the device (35-inch level) and at the 41-inch level show that the ratio varied from approximately 0.55 to 1.15, while the ratio at the 47-inch level decreased from 0.70 to 0.57. The figure seems to indicate that the arching action had measurable effects to at least one structure diameter above the roof. The increase in the horizontal pressure with increase in surface pressure is an indication of the unloading action of the soil above the device as it deflected and is similar to the behavior hypothesized by Terzaghi (1943). At the 47-inch level the vertical pressure gage followed the surface pressure within 1 psi. The horizontal pressure did not show a comparable buildup during this period. The horizontal pressure was approximately 10 psi less than the surface pressure from P_S = 20 psi to P_S = 125 psi .

The gages at the 4.5- or 5-inch radius at the 35- and 41-inch levels show the strong influence of the increase in vertical pressure as the soil above the structure unloaded. After the surface pressure exceeded 10 psi, the close-in vertical gages began to show the influence of the additional load arched onto the soil. This change was sharpest at the 41-inch level. The switch from passive to active

arching can be seen in the action of these gages. These results are similar to Test 3 and appear to substantiate the explanation given for the behavior of the gages at the 41-inch level in Test 3.

In general, the gages located along the centerline or 5-inch radius started at a horizontal-to-vertical pressure ratio between 0.4 and 0.8. As pressure was applied and the structure deflected, the ratio approached a zone between 0.9 and 1.1 and remained constant when P_S exceeded 80 psi. The gages located at a 10-inch radius started at a ratio between 0.8 and 1.2 and also tended to move to a range between 1.0 and 1.1 as the surface pressure increased. Undoubtedly the actions were governed by a combination of the degree of saturation, arching, and sidewall friction effects.

Because of the anomalies that were noted in the horizontal-to-vertical pressure diagrams and pressure profiles and because it was desired to determine the change in the direction of the principal stresses, a series of 3-gage arrays of pressure transducers was used in Test 8. The use of this arrangement was suggested in a paper by Drake. The principle involved is simple, but placement of the gages and analysis of the results are more difficult.

If a body is assumed to be in a state of plane stress and if the values of three stress components at some point in the body are known, it is possible to determine the stress components on a plane which passes through the point at a known angle with the plane of one of

the known stress components and whose normal lies in the same plane as the known stress components, Crandall and Dahl. Considering the small wedge of material represented by the triangle in Figure 33a, the equilibrium requirements $\Sigma M = 0$ and $\Sigma F = 0$ can be expressed by three equations assuming the stress components to be uniform over each face. Manipulation of the equations using the trigonometric relations between the sides of the triangle and the double angle relations results in the following relations:

$$\sigma_x = \frac{\sigma_h + \sigma_v}{2} + \frac{\sigma_h - \sigma_v}{2} \cos 2\theta + \tau_{hv} \sin 2\theta \qquad (4)$$

$$\sigma_y = \frac{\sigma_h + \sigma_v}{2} - \frac{\sigma_h - \sigma_v}{2} \cos 2\theta - \tau_{hv} \sin 2\theta \qquad (5)$$

$$\tau_{xy} = - \frac{\sigma_h - \sigma_v}{2} \sin 2\theta + \tau_{hv} \cos 2\theta \qquad (6)$$

The relations are expressed in the form normally used to represent the stress components in a Mohr's circle of stress.

Since it is not possible to measure the shear stress acting on a plane by the use of a soil stress gage, the value of the shear stress must be calculated. By placing the soil stress gages in such a way as to measure the stress acting normal to the vertical, horizontal, and 45-degree planes, it is possible to further simplify the equations shown above. With $\theta = 45$ degrees as the gages are shown in Figure 33b, the equations become:

$$\sigma_x = \frac{\sigma_h + \sigma_v}{2} + \tau_{hv} \tag{7}$$

$$\sigma_y = \frac{\sigma_h + \sigma_v}{2} - \tau_{hv} \tag{8}$$

$$\tau_{xy} = - \frac{\sigma_h - \sigma_v}{2} \tag{9}$$

Thus with the 3-gage array, σ_h , σ_v , and either σ_x or σ_y are measured directly, depending upon whether the 45-degree gage is placed as in Figure 33b (1) or (2). Knowing the three stress components, it is possible to find τ_{hv} and τ_{xy} . With these values known, a Mohr's circle of stress similar to those shown in Figure 33d can be drawn for each array.

Using the Mohr's circle, it is then possible to find the principal stress, the maximum shear, and the location of the planes they act upon. In addition, by drawing a series of Mohr's circles as the surface pressure increases and the test device deflects, it is possible to study the change in the direction of principal stress and planes of maximum shear. Thus with several arrays of soil stress gages, it was hoped that a closer study of the arching mechanism in the soil could be accomplished.

In Test 8, it was possible to place 8 gage arrays in the soil specimen with the number of SE gages available. Six of the arrays were placed at the 35-, 41-, and 47-inch levels at radii of 5 and

10 inches. Two additional arrays were placed above the test device at the 41- and 47-inch levels.

The one additional SE gage available was placed to measure horizontal soil pressure 1 inch above the test device. It was assumed that with the stress acting on the top of the test device known, the direction of the principal stress would be obvious. As noted in the previous discussion of Figure 32b, the horizontal stress was large but did not appear to be large enough to be the principal stress. A 45-degree gage at this location might have helped eliminate some of the doubt concerning what was happening in the soil just above the test device.

Figure 33d is one of the sets of Mohr's circles drawn during the analysis of Test 8. The circles are identified by the surface pressure below each circle. The direction of the principal stress changed as the surface pressure increased. Because of the gage difficulties previously enumerated, it was not possible to carry the circles to the design pressure of 240 psi. It can be seen that the shearing stress was still increasing at P_S = 150 psi . The gages in the array shown in Figure 33d lasted longer than any of the others. When one gage in an array was lost, it was not possible to continue the calculations.

Figure 34 shows the results from all the arrays used in Test 8. The centers of the circles represent the intersection of the

centerlines of the three gages and are located in proper position with respect to the test device. The solid lines represent the direction of the principal stress at a particular surface pressure. The radial arrows between the solid lines show the change in direction of the principal stress as the surface pressure increased. Normally only two solid lines are shown since the change in direction was continuous from its initial direction to its final position at the highest pressure. This was not always the case. Note the circle for the 10-inch radius at the 47-inch level. The principal stress moved from +14.50 to -29 degrees while P_S increased from 10 to 20 psi. The direction moved back to +44 degrees between 20 and 60 psi. Then it moved up again to a final position of 35 degrees at 70 psi. The extreme directions of the principal stress are shown when they differ from the initial or final directions.

The dashed lines used in the circles of Figure 34 indicate the location of the planes of maximum shear. In most cases the maximum shear occurred in the Mohr's circle for the maximum recorded surface pressure, similar to Figure 33d. This was not always the case. For example, in the circle depicting the 10-inch gages at the 35-inch level, the maximum shear occurred with a surface pressure of 60 psi. Mohr's circles drawn for higher surface pressures were smaller than the 60-psi circle. This seems to indicate that a shear failure occurred.

Note the directions of the shear planes. One set of the planes is vertical in all cases. The planes tend to point toward the test device.

The final direction of the principal stresses is also interesting. At the 4.5- and 5-inch radii at all levels, the principal stress was directed away from the soil above the device. In all cases the principal stress moved from some other orientation to this final position.

The arrays at the 10-inch radius of the 35- and 41-inch levels indicate that the direction of the principal stress is from the outside or toward the sidewalls. This is a very interesting result since it seems to confirm the earlier tentative conclusions concerning the high stresses noted at the 10-inch radius in the pressure profiles, Figures 26a and 27a and b, for example.

The Mohr's circles for the gage array at the centerline of the 41-inch level were a series of very small circles. This indicates that the load was practically uniform in all directions throughout the time the gages were registering.

The 3-gage array investigation makes the results from Test 3 seem more plausible. Note the steep attitude of the principal stress at the 4-1/2- or 5-inch radius at the 35- and 41-inch levels. It can be seen that the vertical component of these stresses will be large in relation to the horizontal component. While over the device, the

vertical component at the 41-inch level is smaller than the horizontal component.

4.2.3 Deflection Curves. Figures 35-40 compare the deflection of the soil and the test device in some of the static tests. These curves are typical of the results from all of the static tests.

There were always two gages measuring the deflection of the base of the device relative to the fixed bottom of the pressure chamber and two gages measuring the deflection of the top of the test device relative to the base of the test device. The total deflection of the top of the device was the sum of these two deflections. Normally the results of the two base gages were averaged. Since the two gages measuring the deflection of the top of the device had maximum travels of 0.2 and 0.5 inch, the result used was taken from the gage which was more accurate in the range of deflections being measured.

Four soil deflection gages were used. In some tests, these gages were arrayed vertically in the so-called free field and in some they were arrayed horizontally at the level of the top of the device. There was always one gage at the level of the top of the device, 35 inches from the base of the test chamber, and one at the level of the base of the device, 30 inches from the floor. These gages were placed in the so-called free field, that is, in an area that should not have been affected by sidewall friction of the pressure chamber or by the arching effects in the soil around the structure.

During the test program it was found that it was the change from a previous deflected configuration within any time increment which was important to immediate load changes. In examining the curves, note the relative change in the position of the soil gages and also the position of the soil gages relative to the top and base of the device. It is the changes in position and the rate of these changes with respect to one another which show the regions affected by arching and how they are affected.

Figure 35 shows the plot of the deflections for Test 1. During the buildup of surface pressure, the base of the device moved further than the soil at the same level. This is understandable considering the fact that the top of the device was held rigid and the device was thus stiffer than the soil.

During the test, the gage placed at a radius of 5.5 inches registered more deflection than the gages further from the centerline at the level of the top of the device. The pressure profile in Figure 26a shows that this region was experiencing a rather high pressure because of active arching. Further, the rate of deflection at the 5.5-inch radius was higher than that at the 8- and 16-inch radii. The 8- and 16-inch deflections were approximately equal. Thus, the region affected by active arching extended to a radius of 5.5 inches at the level of the top of the device (35-inch level), but not to a radius of 8 inches.

During the overnight creep period, all deflection gages showed approximately the same amount of movement. The top of the device and the gage at the 5.5-inch radius showed the greatest creep deflection.

When the surface pressure was removed, all gages rebounded. The base of the device moved to a position approximately the same as the soil at the same level. The top of the device moved up, but not as far as the soil at the 5.5-inch radius. This gage moved much less than the gages in the so-called free field.

The deflection-time curve for Test 3 is presented in Figure 36. In order to save space and more closely examine the changes, deflection is shown as the surface pressure rose to 37.5 psi, then the curve is restarted at zero.

The data shown in this figure indicate that the movement necessary to completely unload the device at this surface pressure is relatively small compared to the overall movements in attaining the test pressure. The base deflection shows the effect of the unloading of the device as the top moved down. There was very little difference in the deflection of all the soil gages. The differential movement necessary to develop arching is shown to be very small. At maximum arching, the differential deflection was only slightly larger than 1 percent of the device diameter.

Considerable movement by all the gages was noted during the overnight creep period. The top of the device deflected more than

any of the other gages. The soil gages at the 5.5- and 8-inch radii registered large deflections. These resulted from the increase in the load arched from the device into those regions.

When the top of the device was raised, the data in Figure 36 show a sharp increase in the deflection of the device base. In addition, a substantial decrease in the deflection of the soil at a radius of 5.5 inches was noted. Both of these results were the result of the loading of the device as its top was raised or pushed into the soil above it. When the surface pressure was raised to 50 psi, a sharp increase in all deflection gages, especially those at the base of the device, resulted. When the top of the device was lowered at this higher pressure, the effects were similar to those noted earlier in the active phase of the test at $P_S = 37.5$ psi .

Figure 37 shows the deflections resulting from raising the surface pressure in Test 5 and the three days of creep with the rigid device.

After one day of creep at $P_S = 37.5$ psi, most of the soil deflection had taken place. The base showed the effects of the increased load on this stiff device as it attracted load from the surrounding soil. The close-in pressure gages and the 10-inch-radius deflection gage also reflect this result. The vertical soil pressure gage at the 30-inch level registered approximately 35 psi. The pressure gage 6 inches above the base and 16 inches from the

centerline registered 34 psi. This indicates that sidewall friction was not appreciable.

The deflection time curves for Test 6 are displayed in Figure 38. This test was different from those previously shown. The deflections of the device top resulted from an increase in the external pressure on the top. Deflection of the top was not controlled by pressure from inside the device. As the pressure on the surface was raised to the desired test pressure, the base of the device deflected more than the soil at the same level. Evidently at low pressure the device acted stiffer than the soil. As the surface pressure increased, the load was arched from the device onto the soil. The deflection of the soil at the 35-inch level is comparable to the total device deflection even though the device was more flexible than the soil. Without soil deflection gages within the area affected by the arching, it is not possible to determine the actual differential deflection which produced the active arching condition. From the data presented, it is obvious that arching did not extend to the 14-inch radius at the 35-inch level. Therefore, differential deflections measured with reference to this gage are probably of minor significance.

When the load on the device decreased, the deflection gage in the soil at the 30-inch level approached the deflection of the base. All gages showed rebound as the surface pressure was lowered. The

soil at the 30-inch level and the base of the device rebounded to approximately the same position.

As the surface pressure was raised to design pressure the second time, the total deflection of all gages was higher since they started from positions lower than their original positions, but their movement during the second pressurization was less. The reason for this was that the soil was stiffer. The total deflection of the top approaches that of the soil at the 35-inch level at peak pressure. The soil deflection at the 35-inch level was larger than the total deflection of the device at the 35-inch level.

Figure 39 shows the deflection-time curve for Test 7. In this test, the device was designed to be stiffer than the soil. While the pressure on the surface was increasing, the pressure container broke. The surface pressure reduced to zero. A new diaphragm was installed and the pressure increased again to 37.5 psi. Time was measured from the second pressure initiation.

An important point to note is that the deflection of the base even exceeded that of the soil at the 35-inch level until high surface pressures were reached. This is the reason why the arching curve did not reflect passive arching as planned. When the pressure on the device is increased, then the base of the device must deflect more than the soil around it. The amount of pressure which is exerted on the device will determine how much the base deflection

exceeds that of the soil around it. Later discussions in this report will point out that factors other than the stiffness of the structure are important in determining the relative stiffness of the structure. The type of footing as well as the depth and stiffness of the soil affected underneath the structure has a great deal to do with the actual loads a stiff structure experiences.

Figure 40 shows the deflection-time curves for Test 8. Deflection gages were arrayed at 5.5-, 8-, and 16-inch radii at the 35-inch level. Another soil gage was located at a radius of 16 inches at the 30-inch level. In this test the device was more flexible than the soil when the surface pressure reached 240 psi. Early in the test, the base of the device and the gage at the 5.5-inch radius indicated that the device was acting as if it were stiffer than the soil. Since the device stiffness was designed to be 0.7 at a pressure of 240 psi, the relative stiffness of the device does change as the surface pressure changes. As the surface pressure increased, the load on the soil near the device increased. This behavior was indicated by the movement of the deflection gage at a radius of 5.5 inches. This figure also shows that during overnight creep, the soil at 5.5-inch radius actually deflected below the top of the structure because of this increase in pressure. The base of the device showed a decrease in its rate of descent as the load was arched off of the device. The deflection gage at a radius

of 8 inches also indicates that this region was experiencing higher pressures than the soil at the 16-inch radius.

4.2.4 Soil Profiles. One of the objectives of the experimental program was to determine how the arching mechanism operates within the soil. In Chapter 2, several hypotheses concerning arching were discussed: Engesser, Terzaghi (1936b, c), Mason, Selig (1960, 1961), and others. Most of the experimental work to date has been with sand. Many of the tests involved rather large deformations such as those conducted at Illinois Institute of Technology. Depicting deformation by using layered sand of different colors is a formidable task but determining deformation patterns in clay was found to be even more difficult. In an attempt to determine these deformation patterns, three approaches were used. First, careful measurements were made of the exact location of all instrumentation, the test device, and the soil layers as they were installed and removed from the test chamber. In some tests, roofing nails were used as bench marks on the various soil layers. In conjunction with these static measurements, the soil deflection gages were located to determine the movements taking place during the tests. Because of the shortage of this type of instrumentation and the interference with soil compaction, the gages were moved as required during the testing program. These results were discussed in Section 4.2.3.

The second approach used was to remove the soil from the test

chamber in blocks or layers when possible. With care, it was possible to remove large, relatively undisturbed blocks of soil from the specimen. These blocks were then broken to expose the soil structure within them. The structure was carefully studied and field notes, sketches, and photographs were used to record the results. In many cases, the structural changes were so subtle as to be indistinguishable using normal photography. Some of the more dramatic photographs have been included in this report. Various lighting schemes and photographic papers were tried without notable success.

As a third approach to the study of the soil structure, X-ray photography was suggested. Dr. E. L. Krinitzsky, head of the Geologic Research Section at the Waterways Experiment Station, has perfected a technique for using radiographs in the study of sediment structure. Although the use of radiography by geologists in paleontology studies dates from 1896, its use in the study of sediments started around 1962. Haase has prepared a report on Dr. Krinitzsky's techniques.

Radiography has been used previously in soil mechanics work. Most of the work has centered around the tracking of lead pellets embedded in sand to determine displacements. Recent work in this field has been reported by Davis and Woodward, Bloedow, and Roscoe, Arthur, and James. Berdan and Bernhard reported studies they made on density measurements by X-ray techniques. Baker and Janza have reported

their studies to determine the utility of flash X-ray techniques in soil dynamics research.

For the purposes of this experimental program, a series of undisturbed, block soil samples were taken along a vertical plane. The plane extended from the soil surface to a point 6 inches below the test device and from the opposite edge of the test device to the test chamber wall. The soil blocks were normally 4 inches wide by 6 inches deep and as long as could be handled without damage. From these blocks 15-mm slabs were cut with piano wire, mounted, waxed, and X-rayed. The negatives were mounted in mosaic and photographed. Perry has explained the techniques in detail.

Full-size radiographs were made from untested soil specimens. Three specimens were used: (a) no test device, (b) flexible test device, and (c) stiff test device. These mosaics were compared with those taken from tested soil specimens. These radiographs disclosed residual deformation patterns and density changes. Some of the full-scale mosaics have been reduced to page size for this report but do not disclose the density deformation patterns clearly enough to warrant inclusion of more than an example. The deformation patterns are more discernible when full-size X-ray negatives are examined using a light table.

The only significant depression in the soil surface appeared during Test 1. The depression, as shown in Figure 41a, was generally

circular in shape and approximately 0.375 inch deep at the center. Exact dimensions are shown in Figure 42. The diameter of the bottom of the depression is smaller than that of the test device located 2 inches below the surface, while the diameter across the top of the steepest part of the slope is almost exactly 6 inches. The slope tapers into the plane soil surface at about an 8-inch diameter. The steepest part of the surface seems to be intersecting the surface at about a 30-degree angle.

The radiograph in Figure 41b shows that a hump developed outside the depression. The figure also shows that there was a definite change in the slope at a point approximately 0.3 inch inside the edge of the device. The steeper slope fell within a 6-inch radius.

Figure 41b also shows what appears to be deformation lines radiating in a dome shape from the soil above the device. The soil beside the device at the 35-inch level shows the change in density and the deformation pattern caused by the high loads arched onto the soil. It is of interest to check the pressure pattern experienced in this area as shown in Figure 26a. Figure 41b gives the appearance of an actual arch having formed over the device and abutted on the soil beside the device. The pattern caused by the friction between the soil and the side of the device is clearly visible in the radiograph.

Figure 42 is a composite sketch of the survey information recorded before and after Test 1. The right side of the sketch was

taken along the south radial and the left side along the west radial. The soil pressure and soil deflection gages are included in order to check deformation magnitudes. The deformation patterns shown for the 30- and 35-inch layers were located by the use of roofing nails, as previously described.

No definite shear planes were located by any of the techniques used. The evidence examined indicates that shear planes might have developed as hypothesized in Figure 42 had sufficient deformation taken place.

Figure 43a is a photograph of the posttest soil surface from Test 2. After approximately 7 hours of exposure to a pressure of 37.5 psi, there was no depression on the soil surface. The surface pressure was raised to 63 psi for 20 minutes and the depression shown in the photograph appeared. The cracking on the surface is the result of drying. The white powder is talc which was used on the diaphragm. Notice the seal used between the edge of the soil and the test chamber.

The dimensions of the depression are more visible in Figure 43b. The inside, flat portion of the depression had a diameter varying between 2 and 3 inches. The diameter of the outside extremity of the slope varied between 4-1/2 and 6-1/2 inches. The sketch shows the north-south cross section. The posttest soil surface sloped generally toward the depression in the center. The deflection of the gages indicates that the soil at the 35-inch level also sloped toward the

center. The soil in the immediate vicinity was 0.7 to 1.0 mm lower than the test device. Soil pressure gage S-13 deflected the same amount as the depression 1 inch above it. The deflection of soil deflection gage D-1, 0.625 inch, was greater than the deflection at the same radius at the 35-inch level and less than the surface deflection at the same radius. The X-ray technique was not being used at the time of Test 2. No clear failure surface was disclosed in the visual investigation of the soil.

Figure 44 is a picture of the radiograph mosaic constructed for Test 3. This mosaic was full size and examined with a large 2-power magnifying glass. The deformation patterns in the soil beside and under the device are particularly noticeable in the high-pressure areas, Figure 27. At the 35-inch level strong deformations can be seen at the 4-1/2- and 10-inch radii. The pattern under the device appears to conform with classical bearing capacity theory, Terzaghi (1943). In addition, deformations were noted between the 37- and 38-inch layers, the 40- and 41-inch layers, the 42.5- and 43.5-inch layers, and the 45.5- and 47-inch layers.

The friction effects between the test chamber and the soil at the 38-inch layer and between the test device and the soil at the 32.5-inch layer are clearly visible in Figure 44. Sometimes it was possible to locate the high- and low-pressure regions by the amount of compression between the layers. There is a rather large space at

the 38-inch level directly above the device. This soil layer is practically indistinguishable at the 5-1/2- and 6-1/2-inch radius at the same level. Directly above the device the soil was less dense. This can be seen in the radiograph and appears to be characteristic of active arching.

Using the deformation patterns noted in the radiograph, the sketches made during the visual inspection of the soil, and the surveyed gage and roofing nail deflections, the diagram in Figure 45 was constructed. A definite fold pattern was noted above the edges of the test device up to a height of approximately 6 inches. In addition, the domelike formations are shown at heights of approximately 3 and 6 inches. At heights of 7 to 8 inches above the device, the inverted dome or depression is shown. While examining these figures, it should be remembered that during Test 3 the top of the device was cycled, i.e. lowered, raised, and lowered. Thus, two different arching phenomena are involved in the soil deformation patterns.

Test 4 had to be conducted twice. During the first test, a leak developed in the pressurization system and the full test could not be performed. The top was not cycled, only lowered. Figure 46a is a photograph of the depression and shear pattern found at the 38-inch layer, 3 inches above the test device. Figure 46b is a profile of the depression. The outside crack pattern had a diameter of

approximately 8 inches. The inside crack pattern had a diameter of approximately 6 inches. The more or less flat bottom had a diameter of 3 inches. The soil surface at the 41-inch level was plane and showed no signs of the crack pattern.

The second time Test 4 was conducted, the top of the device was cycled, i.e. it was lowered, raised, and then lowered again. Figure 47a is a picture of the hump or arch that appeared at the 38-inch level above the device. Note how easily the soil separated over the hump. The soil over and outside the hump had a slick, shiny appearance.

Figure 47b is a sketch of the hump and other soil deformations as recorded by the gages or the profiles. The top of the hump was at the 38-inch layer, so the hump itself was within the 35- to 38-inch layer. This was a homogeneous layer of soil completely placed at one time. Consequently, no horizontal compaction planes intersect the hump. The top of the 38-inch soil layer can be seen as a step at the right side of Figure 47a. The hump itself was approximately 1 inch high and 9 inches in diameter at the base. The deformations recorded by D-1 and S-13 confirmed the profiles as measured.

It is interesting to note that S-11 at a radius of 4-1/2 inches did not deflect as much as S-10 at 5-1/2-inch radius. Figure 27c shows the pressure profile and confirms that there was a higher pressure at the 5-1/2- to 6-inch radii. The test device itself was

depressed considerably more than the soil surface at the 35-inch level. The soil under the device deflected approximately 0.69 inch, while the soil at the 30-inch level and at a radius of 10 inches also deflected 0.69 inch. There is a faint indication of a hump on the soil surface in the profile, Figure 47b. The edges of this hump have been connected to the edges of the test device. These connection lines pass through the edges of the 37- to 38-inch hump.

Test 5 was principally a passive test. The initial movement of the top of the device was up. In Figure 48a, the soil surface is shown. A small hump can be seen on this surface. The raised portion was approximately 0.19 inch high. A profile of the raised surface is shown in Figure 49.

Figure 48b is a picture of the dome that formed over the test device. The structure and density of the material in this dome were different from those of the material around it. Notice how the soil seems to be stratified and bent around the dome. The two pieces of soil broke apart just as they are shown in Figure 48b. A profile of the arch or dome is shown in Figure 49.

The layer of soil shown in Figure 50a broke away from the 35- to 38-inch layer of Test 6. This plug of soil was directly above the test device. Well-defined planes rising at approximately 45 degrees can be seen in the right-hand portion. The edges of the test device were approximately as shown by the arrows. The plug of soil in

Figure 50b also came from the 35- to 38-inch layer but between the 6- and 14-inch radii. The soil broke out as shown.

This study of the soil deformations indicates that there are definite patterns associated with the arching phenomenon. The patterns appear to be considerably different in the active and passive cases. These patterns are discussed in detail in Chapter 5.

4.3 DYNAMIC TESTS

4.3.1 General. Tests 11 through 28 are termed dynamic tests since pressure was applied to the soil surface generally in much less than a millisecond by the use of high explosives. Depending on the pressure desired, the peak was normally reached in less than 1 to 3 msec. The wave form can be approximated by a step pulse.

Tests 11 through 14 were designed to measure the effects of surface pressure on arching when the depth of burial and the relative flexibility of the device were held constant. After examining all the available data concerning the constrained modulus of clay, it was found that the information required to plan the stiffness of the test device at the selected water content and pressure level was not available. The preliminary dynamic test program, explained in Appendix A, was conducted to determine soil stiffness, as well as to establish limiting values for the parameters to be measured. Based on the preliminary tests, the constrained modulus values shown in

Table 3 were used to design the springs of the test device. A very slight variation in water content and/or surface pressure made a large difference in the constrained modulus of the soil.

Tests 11, 15, 16, and 18 were designed to investigate the effects of depth of burial of the structure on arching. In Tests 11, 15, and 16, surface pressure and relative stiffness were held as close to constant as possible. Test 18 was designed to give an indication of the effects of pressure in the determination of the depth at which arching behavior indicated the structure was fully buried.

Test 17 was a repeat test on the Test 11 specimen using a slightly higher surface pressure. This test was designed to determine the effects of repeated low pressure shocks on arching.

Test 19 was designed to determine primarily the maximum shear strength of the clay that could be mobilized in the arching mechanism. It was also used to study the effects of depth of burial in conjunction with Test 13.

Tests 20 through 28 were used to investigate the effects of structural stiffness on arching. In addition, these tests were designed to determine if it is possible to take advantage of active arching by varying the structural stiffness within a practical range. The extent to which passive arching increases the load a structure experiences was also studied.

In the following sections the pressures, deflections, and accelerations measured in the soil specimen and the structures as well as the observed soil profiles will be presented and discussed.

4.3.2 Arching Curves. Table 6 is a summary of the arching data measured and the calculations made for each dynamic test. Detailed data are not presented for Test 28 because of the measurement difficulties experienced and previously explained. The data were selected for times corresponding to specific critical points within the test, such as arrival of peak stress, peak acceleration or peak deflection, as well as those points necessary to give a continuous picture of what was occurring between the structure and the soil. All times are measured from the so-called "0 time"; i.e., the time at which the explosion in the bonnet broke the timing wire. The surface pressure is used as a measure of the arching since it was the most reliable pressure measurement available.

The soil pressure given is that measured in the so-called "free field." The gages used for the measurement were normally located at a radius of 10 to 16 inches from the centerline of the test chamber. The selection of the radius used was based on a study of the pressure profiles given in the next section of this report.

Deflections in the free field, D_S , were measured by the deflection of a disk buried at the same depth as the top of the test device and located from 14 to 16 inches from the centerline of the test

chamber. Normally this distance was found to be outside the influence of the arching around the test device and inside the effects of the sidewall friction.

In the next three columns of Table 6, the deflection of the base of the device with reference to the fixed base of the test chamber (d_b), the deflection of the top of the device with reference to its base (d_t), and the deflection of the top of the device with reference to the fixed base (or total deflection of device, D_T) are presented. In the next column, ΔD is the relative deflection of the top of the device with reference to the so-called free field at the same depth of burial. The values of the soil and the total structural deflection at the 35-inch level were used to calculate ΔD .

ΔD cannot be used without some reservations. As will be shown in the following sections, what was thought to be an undisturbed region was not always completely undisturbed. Depending upon the overpressure, depth of burial and flexibility of the structure, and the reduction in sidewall friction, there may have been no completely undisturbed area within the SBLG for some of the tests. In addition, the pressure distribution at any level including the surface was not always uniform, nor was the soil specimen perfectly homogeneous in spite of the precautions used. A more complete discussion of the distribution of soil deflections is contained in Section 4.3.4.

The forces shown in Table 6 as acting on the top of the test

device were calculated using the equation of motion:

$$m\ddot{x}_{(t)} + c\dot{x}_{(t)} + kx_{(t)} = F_{(t)} \qquad (10)$$

where m is the mass of the top of the device plus a percentage of the springs, as explained in Section 3.2.2; c is the coefficient of damping; k is the spring constant of the test device. m, k, and c vary with each test device configuration. $\ddot{x}_{(t)}$ is the absolute acceleration of the top of the device measured at a specific time, t. $\dot{x}_{(t)}$ is the velocity of the top of the test device with reference to the base of the test device at time, t. $x_{(t)}$ is the deflection of the top of the test device relative to its base at time, t. $F_{(t)}$ is the force acting on the top of the test device at time, t. The values given in Table 6 are in terms of force per unit area acting on the top of the test device. P_T corresponds to $F_{(t)}$ divided by 28.26 in^2, the area of the top of the device.

ΔP is the difference between the pressure exerted on the surface of the soil specimen and that exerted on the top of the device. This value is used as a measure of the amount of soil arching that existed. There are some inherent inaccuracies involved in this value, but it is believed to be the most accurate possible representation, considering the inherent inaccuracies in measuring the actual free-field pressure. As can be seen, two major inaccuracies exist; one, the force lost to the sidewall friction of the test chamber, and two,

the fact that the transmission of the surface pressure, initiation or peak, is not instantaneous. There was considerable time lag between the time of peak surface pressure and the arrival of the peak at the level of the top of the device, depending on the depth of burial and the peak overpressure. This problem will be discussed further in Section 4.3.6.

The last four columns of Table 6 are the dimensionless parameters which were used to plot the arching phenomenon. The first of these four contains the term $\frac{2\Delta P}{q_u}$ which is the differential pressure divided by one-half the average unconfined compressive strength of the soil above the test device. These strengths were obtained as explained in Appendix A. Saturated buckshot clay when loaded rapidly allows little drainage to occur and behaves as if $\phi = 0$. This is discussed in more detail in Appendix A. Under the conditions specified, the shear strength of the material at failure is approximately equal to the cohesion. As explained in Peck, Hanson, and Thornburn, the unconfined compressive strength, q_u, can be related to the cohesion by the following formula,

$$q_u = 2c \tag{11}$$

Therefore, the shear strength is equal to $\frac{q_u}{2}$. If the pressure on the soil surface and the relative deflection of the structure are

sufficient, a failure condition will be created in the soil above the device and the differential pressure should be related to the ultimate shear strength of the soil. This concept will be discussed in more detail in Chapter 5.

If, on the other hand, the deformations are not sufficient or if the surface pressure is not high enough, then the differential pressure is related to some percentage of the ultimate shear strength, depending on the amount of deformation and the height of soil involved. When this condition occurs, P_T/P_S may be a better parameter to use in correlating test results.

Two dimensionless deflections are shown, $\Delta D/B \times 1{,}000$ and $D_T/B \times 100$. The first is a measure of total deflection of the top of the device relative to the deflection of the free-field soil at the same level. This deflection has been scaled by the diameter of the top of the test device, B . The validity of this scaling is discussed in the arching study by McNulty. The problems inherent in using this parameter were discussed earlier in this section.

The second parameter is the total deflection of the top of the device scaled by the diameter of the top. This parameter is a more accurate deflection measurement but may not be directly related to arching since it is the differential deflection of the structure with respect to the soil which is required to develop a relative movement

within the soil. The question is "where does this differential movement take place?"

The load, as determined by any arching action, which acts on the top of the structure for a sufficient length of time to be important in design must be related to the total movement of the top, base plus the top relative to the base, and not just to its instantaneous movement relative to the base. Of course the length of the force pulse and the type of structure also must be considered. Arching curves drawn using the relative deflection of the top are very similar in shape to those drawn using scaled total deflection of the top.

The remainder of this section will be devoted to a discussion of the arching curves for each test. The arching curves and the accompanying data in Table 6 constitute an overall summary of what seemed to be the important results from a particular test. All the points listed in Table 6 have not been plotted in order to save space and to prevent an erroneous impression being formed from the very early and late data. At the earlier test times, the high differential pressures were the result of the use of surface pressure in these calculations. At this time, the buildup in soil pressure at the level of the device was normally lagging by several milliseconds. In addition, at these early times, much of the driving force was dissipated in overcoming the inertia of the soil above the device. The inertia of the device has been included in the calculations for the

force on its top and does not contribute to the lag.

Later data points, especially those marked by an asterisk in Table 6, are affected by at least two phenomena. First, the pressure on the surface was decreasing at a faster rate than that in the soil. Second, noticeable reflections from the base of the test chamber tended to drive the base of the test device up and increase the soil pressures.

At the later times, it can be seen that most active arching tests take on the appearance of a passive arching condition. In addition to the more rapid decay of the surface pressure, the device which had been depressed to a maximum was trying to expand and unload. The compressed soil above the device was resisting this motion and thus causing a condition in which the top of the device was actually loading or punching into the soil; thus a passive arching condition existed. From a design point of view, this does not appear to be important, since the loads are less than those already experienced by the structure. This phenomenon could become important in the case of multiple hits or reflection from lower strata occurring before the structure has a chance to rebound or unload.

In Test 11, the structure was 0.7 times as stiff as the soil and was buried 18 inches below the surface. The design surface pressure was 37.0 psi. Figure 51a is a plot of the arching curve for Test 11. The first point plotted was at 6 msec. The peak soil pressure

arrived at the 35-inch level at approximately 12 msec. At 13 msec the arching curves turn horizontal. The curves continue in the horizontal direction until approximately 15 msec. The maximum differential deflection and the maximum deflection of the top of the device occurred at these times. The reflections from the base appeared to arrive at the 30-inch level at 13.5 msec and at the 35-inch level at 15 msec, Figures C2 and C3, Appendix C. The effects of the reflections also can be seen in Figure 51a.

The time between 13 and 15 msec was selected as the worse condition to which the structure was subjected although the differential pressures were lower at times 17 and 20 msec. These seem to be the result of the reflections and the decrease in the surface pressure. From a design standpoint, it would seem that the minimum differential pressure which should be considered is the 9.5 psi which occurred between times 13 and 15 msec. The maximum load on the device, 26.3 psi, occurred at 13 msec. This should be the design load.

At 50 msec, the surface was actually unloading faster than the structure. After 50 msec, the top was loading the soil and a passive condition existed. The appearance of this curve indicates that the soil above the device did not fail completely, but that the maximum load experienced depended on the surface pressure and the development of something less than the full shear strength of the soil.

The structure used in Test 12 was similar to that used in

Test 11. The device was buried at the same depth, 18 inches, but was subjected to a surface pressure of 70 psi. In the arching curves for this test, Figure 51b, the effects of the buildup in pressure at the level of the device and the inertia of the soil above the device can be seen. This type of action was typical for most of the tests at $P_S \leq 70$ psi , but the early points have been omitted from many of the figures to simplify the curves. In Test 12, almost all the points have been plotted as an example.

The dynamic arching curves appear to be upside down when compared with the static arching curves. In the dynamic curve, the sequence of action and travel times were significant. As the pressure at the level of the test device rose and the force on the surface was able to overcome the inertia of the soil, the plot of differential pressure versus the scaled deflection rose from some value in excess of -5 as determined by the surface pressure. At 10 msec, the curve turned horizontal. This is an indication of the relatively long-term load of 55 to 57 psi which this structure experienced. The load on the structure remained practically constant from approximately 10 msec to 18 msec. The differential pressure ranged from 11 to 13.5 psi in relation to the surface pressure, and 6.5 to 12.5 psi in relation to the soil pressure at the 35-inch level. The maximum load on the structure occurred at 12 msec. This was the critical load. It is not only a maximum, but it is also the

approximate load which the structures experienced for some period of time. Active arching did exist in this test. The minimum differential pressure of 11 psi experienced indicates that arching was not fully developed.

At time 18 msec the deflection seemed to be affected by the reflections driving the base. Inspection of the oscillograph records in Appendix C, Figures C-6 and C-7, shows that the reflections appeared to arrive at the 30-inch level just before the 18-msec timing line and at the 35-inch level just after 18 msec. There may have been earlier reflections but they do not seem to have been of sufficient strength to affect the results. The arching curves in Figure 51b also show strong reflection effects at 18 msec. The data in Table 6 for Test 12 show that the maximum overall deflection of the soil and structure did not occur until after the arrival of the reflections. The effects of the reflections appear to be rather strong at 24 msec. The oscillograph records in Appendix C confirm this conclusion.

The sharp upturn in the arching curve and its excursion on the passive side is caused by the conditions previously discussed for Test 11. By time 100 msec the structure was loading the soil above it. The final position or that position which was measured at the end of the test was very near the starting position of the structure. The appearance of this curve is such as to indicate that the soil

might have experienced a complete failure condition, but the differential pressure was not sufficiently high. The differential pressure is a reflection of the amount of load that this differential deflection will develop at 70-psi surface pressure and an 18-inch depth of burial.

In Test 13 the flexible device was again buried 18 inches below the soil surface but was subjected to 151-psi surface pressure. The minimum differential pressure of 32 psi occurred between 12.5 and 13.5 msec, Table 6. The maximum load on the device at this time was approximately 106 psi. This appears to be the design load. The considerable diminution of the surface load indicates that active arching did occur under dynamic conditions. Upon comparing the soil pressures at the 35-inch level and the pressure acting on the test device between 7 and 13.5 msec, it can be seen that the decrease in the pressure on the device ranged between 40 and 50 psi.

The maximum deflection of the top relative to the base of the device occurred at 13.5 msec. The total deflection continued to increase until 50 msec. This was caused by the continued deflection of the device base. In spite of the strong reflections which became appreciable prior to 15 msec, the base of the device continued to respond to the initial impact from the surface, Figures C-10, C-11, and C-12, Appendix C.

Note the size of the inertia terms early in the test. This

effect can be seen also in the arching curves, Figure 52a. The curves flatten out at the critical times and break sharply as the reflected pressures affect the structure response.

Test 14 consisted of a device 0.7 as stiff as the soil, buried at a depth of 18 inches and subjected to a surface pressure of 245 psi. Several difficulties were encountered in trying to record and analyze the data from this test: first, the accelerometers in the top of the device did not function; secondly, the reflections were very strong and may have started affecting the results as early as the 9-msec mark, Figures C-14, C-15, C-16, and C-17, Appendix C. It was not possible to correctly calculate the damping and inertia terms in the equation of motion without the accelerations, Table 6. Using a Fourier spectral analysis of the structure and soil acceleration records for Test 13, it was found that the transfer function between the soil and the top of the structure was approximately 2 for peak accelerations and approximately 1.5 for peak velocities. Using this information and the acceleration record for the soil at the 35-inch level, it was possible to estimate the accelerations and velocities for the top of the device in Test 14. As can be seen from the record for soil accelerometer 4 in Figure C-17, Appendix C, the damping and inertia terms were probably not too significant at 9, 10, and 11 msec. They probably had significant values at 4, 5, 6, 12, and 13 msec.

The arching in Figure 52b indicates that the critical time

prior to the strong reflections was between 10 and 12 msec. The maximum deflection of the top occurred at 12 msec, but the arching curve indicates that the reflections may have had appreciable effects by this time. As previously noted, the actual soil pressure records show some reflection as early as 9 msec. The maximum differential deflection occurred at 11 msec. The first peak pressure arrived at the 35-inch level at approximately 7 msec and definite signs of the reflection can be seen at the 35-inch level at 12 msec (column 2 of Table 6).

Disregarding the reflections, inertia, and damping as explained in the previous paragraph, it would appear that the design load was approximately 190 psi between 9 to 10 msec. The minimum differential pressure is between 35 and 60 psi considering the surface pressure, and 20 to 45 psi considering the soil pressure at the 35-inch level. Even without the acceleration and velocity terms the results appear to be consistent with those found in Test 13.

Test 15 was made with a device 0.7 as stiff as the soil. It was buried 2 inches below the soil surface and subjected to a peak surface pressure of 39 psi. The load on the device was practically constant between 5 and 16 msec, Figure 53a. The differential pressure was approximately 6 psi in comparison to the surface pressure. The deflection of the top of the device was fairly constant throughout the critical portion of the test, but the maximum deflection of the

base did not occur until 20 msec. The magnitude of the base deflection was sufficient to cause the maximum total and differential deflections to occur at 20 msec.

Because of the nearness of the surface, dynamic amplification of the load on the structure was involved and is discussed in detail in a later section of this chapter.

Inspection of the deflection and acceleration records in Figures C-20 and C-21, Appendix C, did not disclose any significant vibration of the top. The system appears to be very close to a critically damped one. One interesting observation in several of the dynamic tests was the fact that early in the test as the soil pressure was fairly low and the inertia term was large the pressure on the top of the device was practically equal to that on the soil at the same level. In this test at 1 msec, P_T was 18.2 psi versus a $\bar{P}_s$ of 17 $\pm$ 2 psi in the soil. This is probably due to the time it took the device to react and the fact that the relative stiffness changed with pressure. The oscillograph records in Figures C-18 and C-19, Appendix C, indicate that noticeable reflections arrived at the level of the device base at 13 to 14 msec, and at the level of the top of the device at 16 msec.

Test 16 was performed with the same device as that used in Tests 11 and 15. The depth of burial of the top of the device was 6 inches. The maximum surface pressure was 37.5 psi. The maximum

soil pressure arrived at the 35-inch level at 14 msec, but the soil pressure at this level was fairly constant between 5 and 20 msec. The maximum soil deflection did not occur until 50 msec. The maximum deflection of the structure base occurred at 18 msec. The deflection of the top of the device was fairly constant between 8 and 10 msec.

The maximum differential deflection occurred at 10 msec with a second maximum occurring at 18 msec.

The critical phase of Test 16 occurred between 6 and 14 msec, Figure 53b. At approximately 14 msec the first major reflections were apparent at the 30-inch level, Figure C-22. The strong reflections began at the 35-inch level at about 15 msec. The arching curve indicates that some reflection effects may have been experienced as early as 10 msec. The maximum average pressure experienced by the top of the structure before strong reflections was about 25 psi. The differential pressure with reference to the surface pressure ranged from 10.5 to 12.5 psi. The arching curve indicates that fully developed arching conditions probably did not exist during this test.

The $\frac{K_T}{K_S}$ curve in Figure 53b will be explained in Chapter 5. This curve depicts the change in relative stiffness as the soil pressure changed and the effect of this change on the arching curve. This change ties in with the explanation of the observed soil and structural pressures early in Test 15.

Test 17 was a repeat test on the same soil specimen and test

device as that used in Test 11. A slightly higher surface pressure, 40.5 psi, was used. This test was designed to check the effects of repeated shocks. The results are compared with Test 11 and the other tests in the pressure versus depth series in Chapter 5.

In Test 17, the peak pressure wave arrived at the 35-inch level between 8 and 12 msec, Table 6, but the deflection of the soil and the base of the device peaked at 17 msec. The top of the device maintained a fairly constant deflection between 10 and 20 msec. The maximum differential deflection at the 35-inch level occurred between 12 and 14 msec.

The arching curves for Test 17 in Figure 54a indicate that the critical time before the strong reflections occurred between 8 and 14 msec. Inspection of the oscillograph records, Figures C-26 and C-27, Appendix C, shows that the reflections became noticeable at the 30-inch level between 12 and 14 msec and at the 35-inch level at 14 msec.

The maximum average pressure on the top of the device ranged between 27.5 and 28.5 psi with the maximum occurring at 8 msec. The differential pressure with reference to the surface ranged between 11.5 and 13.0 psi. With reference to the measured soil pressure at the 35-inch level, the differential pressure ranged between 10 and 15.5 psi.

Again it is interesting to note how closely the soil and

structure pressures compare early in the test, 2- to 5-msec range. This type of information should be an important consideration for the designer who desires to take advantage of arching.

In Test 18, the top of the device was buried 42 inches below the surface, the deepest in the test program. The device was subjected to the highest pressure used in the test program, 310 psi. The experiment was designed to develop a fully buried condition at 240 psi.

In examining any of the arching curves, it is best to look at the data in Table 6 at the same time. This is particularly true for Test 18. To get a feel for what took place during the test, it is also worthwhile to look at the oscillograph records in Appendix C. For this test, Figures C-30 through C-33 are a dramatic description of the tremendous effects of the reflected pressures which exceeded 1,200 psi. The arching curves in Figure 54b also show these effects.

The strong precursor of the reflected pressure wave appeared at the 30-inch level in the 11- to 12-msec time frame, and at the 35-inch level at 12 msec. The arching curve indicates a strong reaction to the reflected pressures at 12 msec. Maximum arching occurred at 12 msec when the differential pressure with respect to the surface reached 140 psi, and 134 psi with respect to the soil pressure at the 35-inch level. Figure 54b shows that the arching goes through several stages depending upon amount of pressure at the level of the

structure, the amount of soil deformation, and the amount of structural deformation. For example at 8 msec, Table 6, the pressure on the structure and on the soil at the 35-inch level were practically equal. The majority of the force of the structure was involved in overcoming the inertia of the top. At this time the structure was evidently approximately of the same stiffness as the soil in its vicinity. The average structure pressure of 245 psi acting on the top of the device was the maximum pressure experienced by the structure and must be considered by the designer. The differential pressure with relation to the surface was 53 psi. The very high accelerations imparted to the device by the rapid rise in the pressure at the 35-inch level had a load amplification effect. Note the shape of the pressure waves at the 35-inch level in Figure C-30 and the accelerations in Figure C-33.

As the soil pressure at the 35-inch level increased to its peak at 9 and 10 msec, the inertia term in the equation of motion changed sign and the plateau seen in Figure 54b was obtained. The pressure acting on the top of the device ranged between 203 and 207 psi. The differential pressure was 87 psi with respect to the surface and 82 to 98 psi with respect to the soil pressure at the 35-inch level. It would be desirable to design for the 200-psi pressure since this pressure stayed on the structure for a period of time and the

acceleration spike which contributed the high inertial forces noted at 8 msec was very sharp.

The minimum differential pressure, 47 psi, for Test 18 occurred at times 14 and 15 msec. The load on the structure ranged between 220 and 223 psi. The waveforms in Appendix C and the arching curves in Figure 54b indicate that the results at this time were affected by the reflections discussed in the previous paragraphs.

It is interesting to note in Table 6 that, in spite of the strong reflections, the soil and the structure continued to deflect throughout the major portion of the test. This is in contrast with some of the lower pressure tests in which the direction of the motion started changing at about the time the reflected pressure reached the 30- to 35-inch levels.

Test 19 was designed to determine the maximum arching that could be expected above a flexible structure buried at a depth of one structure diameter. The structure was of approximately the same stiffness as that used in Test 13 and somewhat stiffer than those used in Tests 11, 12, 15, and 16. Peak surface pressure was 157 psi.

The peak pressure at the 35-inch level occurred at 6 msec. Although the initial reflected wave was not as strong as that noted in the previous test, it could be detected at the 30-inch level at 8 msec and at the 35-inch level at 9 msec, Figure C-34. The very strong peak reflections hit the device at 14 msec.

The soil and entire structure continued to move downward during the first 100 msec of the test, Table 6. The maximum differential deflection occurred at 100 msec. The top of the structure reached its first deflection peak at 5 msec. It peaked again at 50 msec because of the reflection effects.

The arching curves for Test 19 in Figure 55a indicate that the shear strength of the clay was fairly well developed. The maximum load on the device, 132 psi, occurred between 5 and 6 msec. The differential pressure in relation to both the surface and the soil at the level of the top of the device was approximately 25 psi. Maximum arching reached a value between 23 and 30 psi during the 8- to 10-msec time frame, depending on the datum chosen.

It is interesting to note the similarity of the structure and soil pressures at 3 msec. Note also the residual load on the device after the surface pressure had decreased to zero and the pressure on the soil at the 35-inch level had reached 19 psi. This is a function of the ability of the soil to hold the top down and only let it expand slowly with time. The soil and structural pressures eventually reached 4 psi several hours after the test.

The structure used in Test 20 was a very flexible one ($K_T/K_S \approx 0.29$). The arching curve in Figure 55b shows that the differential pressure was relatively constant for a long period of time while deflection was increasing rapidly. In this particular

test, the minimum differential pressure did not occur at the time at which the device reached its maximum deflection, but at 8 msec. The variation in differential pressure was very small throughout the active arching phase.

The soil pressure at the 35-inch level reached a peak at 6 msec and stayed relatively constant until 14 msec, Table 6. Maximum deflection of the soil and structure was reached at 17 msec. Maximum differential deflection occurred at 11 msec. The maximum load on the device, 9.3 psi, and the minimum differential pressure, 23.5 psi, occurred at 8 msec. Maximum arching of 25 to 26 psi occurred at 6, 10, and 11 msec. From these figures and the shape of the curve in Figure 55b, it appears as if the shear strength of the material was close to being fully developed.

Test 21 used a device with a relative stiffness, K_T/K_S , of approximately 0.42. The appearance of the arching curve, Figure 55c, is more nearly like those shown for the static tests. The peak soil pressure arrived at the level of the top of the device at approximately 6 to 8 msec. Figures C-42 and C-43 indicate that a noticeable reflected pressure wave reached the 30-inch level at 8 msec and the 35-inch level at approximately 10 msec. The arching curve confirms these observations. Between about 4 and 12 msec, the load on the test device seemed to be fairly constant. Fluctuations in the differential pressure between 4 and 12 msec appear to be mostly a

contribution of the inertia term in equation 10. The minimum differential pressure prior to the time of the arrival of the reflection and the decrease in the surface pressure was 20 psi. At 10 msec the device had reached its maximum deflection and the spring force was at a maximum. The design load experienced by the device at 10 msec was 15.5 psi. This load appeared to remain on the structure for sufficient time to be fully effective. After 10 msec, the characteristic backward and upward swing of the arching curve can be observed. This was caused by the decrease in the surface pressure and the reversal of the loading.

In this test the soil reached its maximum deflection at 12 msec, the structure at 10 to 12 msec, and the top deflection was fairly constant from 8 to 100 msec. The maximum differential deflection was reached at 10 msec and corresponded fairly accurately with the maximum load and minimum differential pressure.

The Test 22 device was stiffer than those used in Tests 20 and 21, but was also less stiff than the soil that it replaced. It can be seen in Table 6 and Figure 56a that the contribution of the inertia term at the early times was much less than the spring force. This is opposite to the results noted for the very flexible structures. The stiffer the structure, the less the contribution of the inertia term at the early times. At times 1.5 and 3 msec, there were large differential pressures but these should be considered in

light of the contribution of the inertia term and the arrival of the peak stress at the level of the top of the device.

The critical point or that point at which the differential pressure appeared to be a minimum and the structure pressure a maximum was at 5 and 6 msec. The load on the device was approximately 26 psi and there was very little contribution from the inertia or damping terms. At this time, the top of the device had not reached its maximum deflection but it was very close to it. Actually the deflection of the top was fairly constant from 5 to 100 msec. Its maximum deflection occurred at 10 msec and the maximum total deflection of the device did not occur until 14 msec. The maximum differential deflection occurred at 6 msec.

Reflections appeared in the oscillograph records, Figures C-46 and C-47, at the 30-inch level between 8 and 10 msec and at the 35-inch level at approximately 10 msec. The reflections seem to have a definite effect on both the soil and structure deflections.

Test 23 was made using the most flexible device in the test program, $K_T/K_S = 0.3$. The shape of the arching curves shown in Figure 56b was normal for active arching curves. There was a definite turn horizontal at 4 msec. The portions of the curves from 4 to 12 msec indicate active arching. The sharp turn at 12 msec was caused by the beginning of the reflection effects. As in the other tests with flexible devices, the contribution of the inertia term was very large

in comparison to that of the spring, Table 6.

The critical time seemed to be approximately 2 msec. At this time the pressure on the device was 12.6 psi, Table 6. The soil pressure at the 35-inch level averaged 12.5 psi at the same time. As previously explained, in spite of the weakness of the device, early in the test before the pressure builds up in the soil, the device is much stiffer relative to the soil than at later times after the maximum pressure is exerted on the soil. It is true that these early conditions normally do not last long and in some cases may not be significant for design purposes.

The data in Table 6 indicate that the top of the device experienced a negative pressure of approximately 0.8 psi at 10 msec. Whether this is a real negative pressure or an error in the calculation of the inertia term is not known. In examining the test device after the test, the soil was found stuck firmly to its top. The adhesion was sufficient to allow the soil to exert tension on the top. The accelerations were sufficient to drive the top at a very high velocity. At times 10 and 12 msec all the pressure available at the surface had been reduced by the shear developed in the soil. The shear strength of the soil was probably close to being fully developed. A higher surface pressure exerted on this same device would have been required to determine if the shear strength of the soil was actually fully developed.

The reflection seemed to arrive at the 30-inch level at approximately 8 msec and at the 35-inch level at about 12 msec. This is also the time at which the structure recorded its maximum differential deflection and its minimum load. The maximum deflection of the soil and structure did not occur until 15 msec.

In Test 24 the test device was stiffer than the soil which it replaced. The characteristic shape of the curve was different because the structure was loading rather than unloading, Figure 57a. This type of action is generally termed passive arching.

Table 6 shows that prior to 4 msec the differential pressure was negative. This was partially due to the fact that the differential pressure was being measured with reference to the surface pressure and the pressure at the level of the top of the device had not had time to rise to the level of the surface. Unfortunately, the soil pressure gages did not function properly during this test and there was no accurate measure of the time of arrival of the peak pressure at the level of the top of the device.

The maximum differential pressure, 10 psi, and also the maximum pressure acting on the top of the device, 41.6 psi, occurred at 6 msec. This was the worse condition experienced by the structure.

The contributions of the inertia term were small. Note that the inertia contributions became smaller and smaller as the structure became stiffer and stiffer. As the mass and stiffness of the springs

increased, the accelerations logically decreased.

At 6 msec, the maximum deflection of the top of the device relative to the base of the device occurred. Although there was a larger relative deflection at 12 msec, this appeared to be the result of reflections.

Test 25 was made with the same test device as Test 24 and in the same soil specimen, but at a higher pressure. It can be seen in Table 6 and Figure 57b that the early results and the shape of the arching curves resemble those of the previous test. The maximum load was exerted on the structure at 7 msec. This was also the time at which the maximum relative deflection of the top of the device occurred. The maximum load was 77.4 psi and the differential pressure was approximately 25.5 psi.

The surface pressure was 1.7 times that used in Test 24 while the maximum device pressure was 1.86 times as high and the differential pressures were as much as 2.5 times those in Test 24.

Note that the differential deflection reversed at the time of maximum load. Close examination of the test results at this time indicates that the base of the device started to move faster than the soil at the same level because the load on the device exceeded the free-field pressure. The high rate of movement of the base of the device caused the change in direction of the differential deflection. Note the shape of the arching curve between the 500-msec point and

the final position. The total deflection curve shows that the device actually moved up after the pressure was removed, yet the differential deflection curve indicates that the relative position was down. This seems to be the result of the fact that the base of the device has been driven further and harder than the soil and thus did not rebound to the same extent as the soil in the free field. The soil and structure deflections showed two peaks, 16 and 50 msec. These were probably due to the reflections.

The arching curve for Test 26 shows the characteristic shape of a dynamic, passive arching curve, Figure 58a. Again the direction of the differential deflection is reversed after the maximum load was exerted on the top of the structure. This resulted from punching of the base into the soil.

The test device used in this test was extremely stiff as compared to the soil, but there was no sharp increase in the differential pressure as compared with Tests 24 and 25 as might have been expected. These results indicate that beyond a certain stiffness of the structure the base punches into the soil, and the limiting load a structure will attract is governed by the bearing capacity of the soil below the base of the structure. This behavior did not appear to govern the behavior of flexible structures. As the top of the device deflected, the load on the device decreased before the interaction of the base with the soil had an appreciable effect. The

decrease in the load on the top of the device did have an effect on the base deflection, but it was not as significant as noted with the very stiff devices.

The maximum load in Test 26 occurred at 8 msec. The results of this test are somewhat questionable because when the test device was removed and inspected, it was noted that some of the strain gages measuring the load on the top of the device had been damaged. In Test 26 the maximum load on the device of approximately 40 psi actually occurred between 4 and 10 msec with very little variation within this time frame. Whether this was due to the discrepancy in the instrumentation or was the actual load on the device could not be determined.

The maximum differential deflection occurred between 6 and 7.5 msec. The deflection of the top of the device was practically constant between 4 and 12 msec. The maximum deflection of the soil and the device did not occur until 20 msec.

As a result of the strain gage damage, this test was repeated as Test 27A with a new soil specimen and the same test device. The maximum load of approximately 42 psi was on the device from 4 to 8 msec with very little variation, Figure 58b. The load measured in this test is practically the same as that measured in the previous test, although the differential pressure was larger since the surface pressure was lower. The spring load was practically constant between 6 and 12 msec with the maximum of 42 psi occurring at 8 msec. The net

load was practically constant between 4 and 8 msec with a maximum of 42.5 occurring at 6 msec. The differential pressure was practically constant between 4 and 12 msec with a maximum of 11.5 psi occurring at 6 and 7 msec. The maximum deflections occurred between 14 and 16 msec. The shape of the arching curve was as expected, Figure 58b.

Test 27B was a repeat test at a higher pressure (41.5 psi) on the same specimen used in Test 27A. The arching curve is shown in Figure 59a. The maximum load of 47 to 50 psi occurred between 6 and 14 msec. Whether the loads at 12 and 14 msec were the result of reflections could not be determined. The maximum load on the spring occurred at 12 msec, but the maximum calculated load occurred at 6 msec. The arching curve indicates that the critical time was from 6 to 7 msec. The negative inertia load was also at its maximum at 12 msec. As a consequence of this, the net pressure on the top of the device was slightly higher at 6 msec. The differential pressure of 8 psi was the same at 6 and 12 msec. Some of the points after the arrival of the reflection were omitted in order to simplify the arching diagram.

Test 27C was a repeat shot on the same test specimen used in Tests 27A and B. The surface pressure for this test was 64 psi. The maximum load on the structure occurred between 8 and 16 msec, Figure 59b and Table 6. The maximum net load actually occurred at 14 msec. The maximum spring load of 84 psi occurred at 14 msec. Reflections occurred after 14 msec.

At 500 msec the load on the device was zero. Again the characteristic shape of the passive arching curve was observed for this test. The previous discussions relative to the deflection of the base and the differential deflection are also pertinent to this test.

Note in Table 6 that maximum deflections of the soil and structure did not occur until 20 msec. This agrees with the other high pressure tests in which the deflections continued for a longer period of time relative to those that occurred in the 31- to 37.5-psi tests. The maximum differential deflections occurred at 12 to 14 msec and occurred at the same time as the maximum load on the structure.

4.3.3 Pressure Profiles. In this section, three types of pressure distribution figures are presented and discussed: the horizontal distribution of vertical pressure at the 35-inch level, the vertical pressure distribution with depth, and the ratio of the horizontal to the vertical pressure above the test device. Although these profiles were drawn for each test, only certain selected curves are presented. These are typical of the distributions observed.

First, the distribution of the vertical soil pressures at the 35-inch level, the level of the top of the test device, is discussed. Certain selected times are shown in each figure to illustrate the buildup and decline of the pressure at this level and how these pressures were affected by the arching onto or away from the structure.

Figure 60a shows the pressure distribution for Test 11 and illustrates the distribution at low pressure with a device more flexible than the soil buried at a scaled depth of burial of 3. The gages at the 10- and 14-inch radii indicate that sidewall friction had some effects on the distribution at this level and these radii. The buildup at the 14-, 10-, and 6-1/2-inch radii indicates the time necessary for the gages at the 35-inch level to reflect the changes in the surface pressure. This figure also shows that the gages at the 4-1/2-, 5-1/2-, and 6-1/2-inch radii are definitely influenced by the load arched away from the device onto the soil. At 100 msec, the soil was unloading and there was some indication that the structure was starting to load the soil and thus reduce the pressure peaks around the structure.

In Figure 60b, Test 12, it can be seen that the sidewall friction problem experienced in Test 11 had been overcome by the measures explained in Appendix A. The gages at the 10-, 14-, and 16-inch radii were in the free field. The gages at the 4-, 4-1/2-, 5-1/2-, and 6-1/2-inch radii were influenced by the structure. The structure in this case was more flexible than the soil and was buried at a scaled depth of 3. At 70 psi, the soil pressure distribution is considerably different from those shown in Figures 3 and 4 and postulated by Monfore and Finn. This could be due to the fact that as the structure depressed it allowed the soil to move toward the area

vacated, and thus the soil became less confined and consequently yielded. There is some indication that the area 6-1/2 inches from the centerline was also influenced by the arching action since there was less pressure in this area than would have been expected from observing the gages at 10 and 14 inches.

Figure 60c illustrates the distribution of the pressure for Test 13. This is an example of the effect of a high surface pressure of 151 psi on the pressure distribution. The gage at the 4-1/2-inch radius indicated the unloading of the device onto the soil as the pressure increased. The gages at the 8-, 10-, and 14-inch radii indicated that the arching did not measurably influence this region. The high pressure region near the device and the low pressure region at the 6-1/2-inch radius are similar to those found in Test 12. Unfortunately, the gages at the 5-1/2- and 6-inch radii failed to function and the distribution within the high pressure region is not known.

Figure 61a shows that the pressure distribution for Test 15 was considerably different from that of the previous tests. The test device was less stiff than the soil, but in this case it was buried only 2 inches below the soil surface. The influence of the arching can be seen at the 4-1/2-inch radius, but it is not sharply defined because of the small amount of arching.

The distribution for Test 16, Figure 61b, should be compared

with that for Tests 11 and 15. The pressure level and test device were similar but the device was buried at a depth of 6 inches or a scaled depth of 1. The shape of the curve is somewhat similar to that for Test 11. The major difference is that the gage at a radius of 4-1/2 inches for Test 16 registered a pressure which was considerably lower than that registered in Test 11. The gages at the 6-1/2-, 10-, and 14-inch radii measured pressures which were somewhat higher than those measured in Test 11. This is explained by the depth of burial. The gage at 18 inches certainly indicated that sidewall friction was playing a role at this radius at a 6-inch depth of burial. The 10-, 14-, and 16-inch radii gages were probably in the free-field region. The pressure buildup at the 5-1/2-inch radius can be seen as the arching increased and as the pressure at this level increased. The soil appeared to be affected by the arching to at least the 6-1/2-inch radius. There was a marked difference between the pressure distribution for Tests 15 and 16. This is explainable by the depth of burial.

The pressure distribution for Test 17, Figure 61c, was different from that for Test 11, even though it was a repeat test on the same sample. Again it seemed that the area around the 5-1/2-inch radius received most of the pressure arched onto the soil. The area in the vicinity of the 4-1/2-inch gage was not loaded as in Test 11. The structure appeared to be arching with respect to the regions farther

from the device. The gage at the 10-inch radius was influenced by the active arching.

Figure 62a, Test 20, shows that for this weak device the load seemed to be arched to the region between the device and the 6-1/2-inch radius, with the majority of the load applied near the 4-1/2-inch radius. This is in contrast to Figure 61b which shows that the larger concentration of pressure was at the 5-1/2-inch radius for Test 16. Note how the pressure increased in the close-in regions as the arching increased.

In Test 21, Figure 62b, the distribution indicated a low pressure region very near the device and a very high pressure region at the 5-1/2-inch radius. The shape of the curve is very similar to that for Test 20 except for the drastic change at the 4-1/2-inch radius. This lack of pressure buildup at the 4-1/2-inch radius seems to have influenced the high pressure at the 5-1/2-inch radius. The soil appeared to be affected to a radius of approximately 6 inches by the arching.

Figure 62c illustrates the pressure distribution for Test 22. The profile appears to be somewhat similar to those for Tests 20 and 21 except for the 8-inch gage. The pressures at the 6-1/2-, 10-, and 14-inch radii were very similar.

Test 23 results were dissimilar to those for any other test, Figure 63a. Although the pressures between the 4-1/2- and 6-1/2-inch

radii were higher than those acting on the device, they were lower than the surface pressure and the area was small. High pressures were experienced in the large region between the 6-1/2- and 12-inch radii. Due to the large deflections experienced by this extremely flexible device the load was distributed over a larger area farther from the device. These large deflections allowed the soil near the device to unload as it moved toward the centerline and thus the higher pressure region developed progressively farther from the centerline as the deflection increased. The pressure in the region at the 14- and 16-inch radii seemed to be uniform and undisturbed by the arching. The low pressures at the 12-inch radius seem consistent with similar regions at the 10-inch radius in Tests 20 through 22 and at the 6-1/2-inch radius for Tests 12, 13, 15, and 17.

Figure 63b draws the profile for Test 26, a passive arching test. Note that its shape is considerably different from those resulting from the use of the flexible device. The pressure at the 4-inch radius was very near the pressure experienced by the structure. There was a low pressure region at the 5-1/2-inch radius instead of a high pressure region as noted for the flexible devices. The 6-1/2-inch gage seemed to confirm the readings of the 5-1/2-inch gage. A region with pressures higher than the surface pressure existed at the 8- and 10-inch radii.

The times plotted in Figures 60-63 indicate the pressure

profiles when arching was a maximum and a minimum. The zones in the soil affected by the arching are shown. The curves also show the buildup and decay in the arching as time progressed.

In order to examine these pressure profiles more closely, a force balance similar to that used for the static tests was made at certain selected radii. The times for these calculations were selected such that the pressure at the surface and at the level of the device had become fairly stable. A straight line distribution of pressure between the gages was assumed. The forces at the 35-inch level and at the surface were calculated by taking the average pressure between any two gages and multiplying it by the area over which it was effective. The same type of calculation was made for the device itself.

In Test 12, the time at which the maximum load was exerted on the test device was 12 msec, Table 6. At this time, the surface pressure was 68 psi. At 6 to 11 msec, the surface pressure was 69 psi. The force balance at the 35-inch level disclosed the following average pressures:

Radius	Average Pressure at 12 msec	Average Pressure at 15 msec	Radius	Average Pressure at 12 msec	Average Pressure at 15 msec
inches	psi	psi	inches	psi	psi
4.5	64.5	--	10.0	65.2	66.4
5.5	70.4	69.8	14.0	65.1	67.7
6.5	70.9	71.0	16.0	65.9	68.1

From the 12-msec information, it appears that the area affected by the arching extended to a region somewhere between the 6.5- and 10-inch radii. At a 7-inch radius the average pressure was 69 psi.

The force balance at 15 msec also showed that the area most affected by arching was between the 6.5- and 10-inch radii. The force balance seems to confirm the results observed in Figure 60b. The average pressure at the 35-inch level was 68 at a radius of 7.35 inches. The results also show that the force lost to sidewall friction at the 16-inch radius was not significant for this test.

Similar calculations were made for Test 13. Again the influence of the sidewall friction was minimal. This indicates that as the surface pressure increased, the force necessary to overcome the sidewall friction was a smaller percentage of the total load. The soil sample actually slipped inside the Small Blast Load Generator and sidewall friction loss was insignificant. A summation of forces at the level of the top of the device at 13.5 msec disclosed that the equivalent surface pressure was approximately 154 psi. The area influenced by the arching extended to a radius of approximately 5.5 inches.

A force balance was made for Test 16 at 10 and 16 msec. At 10 msec, the total force acting on the 35-inch level was 30,370 pounds or an equivalent pressure of 29.8 psi. The pressure at the surface, taking into consideration the travel time, was approximately 37 psi.

This indicates a force loss in excess of 7,500 pounds. If the radius of interest is reduced to 10 inches, the force acting at the 35-inch level was 11,720 pounds. This is equivalent to an average pressure of 37.3 psi. This pressure is reasonably close to the surface pressure. Using the 37.3-psi pressure as a datum, it was possible to determine at what radius the arching has an influence within the soil. At both the 10- and 16-msec times, this radius was found by similar calculations to be approximately 6.5 inches or slightly larger than one structure radius outside of the device.

As an example of a passive arching test, the curves in Figure 63b for Test 26 were examined at 8 and 14 msec. By the time this test was performed, the sidewall-friction problems had been solved and the losses experienced at the 35-inch level were very minimal. The force balance disclosed that the area affected by the arching was inside the 6.5-inch radius at both times.

In Figure 64a the pressure distribution for Test 12 is presented at four times. In this way it is possible to see that there was a pressure buildup at the 6-inch level considerably after the maximum structural load occurred or minimum arching took place. In this test the horizontal-to-vertical pressure ratio at a radius of 16 inches remained less than 1 throughout the test. This is an indication that the principal stress remained close to vertical in this region throughout the test. At the 4- to 4.5-inch radius the figure shows

that the ratio was much less than 1. Thus high vertical stresses were predominating.

Figure 64b shows the pressure profiles for Test 13 plotted at 4, 10, and 12.5 msec. These times are fairly early because of the high reflections which took place in this test. At 12.5 msec the pressure at the 6-inch layer had not risen to surface pressure level. This was not due to the friction dissipation, but to the fact that the peak of the pressure wave had not reached this level. For instance, the pressure at the 6-inch level reached 115 psi at 15 msec and 385 psi at 20 msec.

At the 47-inch level, the horizontal and vertical gages located along the centerline indicate that the ratio of the horizontal to vertical pressures was slightly greater than 1 at the times plotted. The curves also indicate that the pressure in the free field was very similar to that at the centerline. Any arching action that existed at this level was only minor, since the pressure distribution was not disturbed. No horizontal gage was placed at the 41-inch level, but the vertical pressure was similar to that recorded at the 47-inch level for 10 and 12.5 msec. At the 38-inch level, the horizontal-to-vertical pressure ratio near the centerline was 1 at 4 msec, larger than 1 at 10 msec, and jumped back to a value considerably less than 1 at 12.5 msec. These readings indicate that the

direction of the principal stress over the device changed during the test.

The 4.5-inch gage at the 35-inch level clearly indicates the unloading action of the structure to the soil. This loading at the 35-inch level evidently affected the gages farther out at the 30- and 24-inch levels. The gages under the device at the 27-inch level registered higher pressures than those in the free field.

Figure 64c for Test 14 shows the buildup of pressure with depth. The pressure in the free field was practically uniform to the 24-inch level. The close-in gages at the 35- and 30-inch levels clearly indicate the arching action as the structure unloaded to the soil in its vicinity. The gages underneath the device at the 24- and 27-inch levels show the sheltering action which the flexible structure provided. The ratio of the horizontal to vertical stress at the 32.5-inch level varied from near 1 to less than 1 as shown in Figure 64c.

There were a series of horizontal and vertical gages above the test device at the 47-, 41-, and 38-inch levels. At the 47-inch level, the pressure and pressure ratio did not change noticeably in the 4- to 8-msec time frame. The ratio of horizontal to vertical pressure varied from 0.84 to 0.88 during the test. The principal stress was near vertical during the entire test and appeared to have been unaffected by the presence of the structure. At the 40- to 41-inch level, the ratio varied from 1.0 to 1.14 during the test.

The horizontal pressure had begun to predominate at this level; therefore, it appears to have been affected by the arching action around the structure. At the 38-inch level, the effects of arching were more noticeable, as can be seen in Figure 64c. Initially the 3.5-inch radius gages showed a horizontal to vertical ratio of 1.83. With time the ratio dropped to approximately 1. The changes of the ratio of horizontal to vertical soil pressure indicate that a large component of horizontal stress developed as the structure deflected and the soil tended to fail. As the pressure increased, the soil became saturated and the pressure ratio moved toward 1.

At the 5.5-inch radius of the 38-inch level the horizontal-to-vertical pressure ratio varied from 1.35 at 4 msec to 1.06 at 8 msec. At the 8-inch radius, the ratio was 1.16 and 1.05. The 10-inch radius gages registered a ratio of 1.25 at 4 msec and 0.84 at 8 msec. From these ratios it appears that the arching effects extended to a radius somewhere between 6 and 10 inches.

The distribution of soil pressure with depth for Test 18, Figure 65a, is very interesting since this test used the highest surface pressure on the tallest specimen in the test program. As in previous tests, the buildup of pressure at the 6-inch level was slow. Even with an incident pressure in excess of 300 psi, the entire specimen was not loaded until a considerable time after the pressure initiation at the surface. In Figures C-30 and C-31, Appendix C, the

effects of the clay soil on the shape of the pressure pulse as it traveled through the soil can be seen. The effects of the steep front also can be seen in Figure 65a at 8 and 12 msec. Strong reflected pressure in excess of 1,000 psi occurred after 15 msec. Table 6 shows that the maximum load acted on the structure at 8 msec.

The pressure gradient between the top and bottom of the structure, seen in Figure 65a, probably contributed to this high loading. Between 8 and 14 msec the loading in the free field at the 30- and 35-inch levels appears to be fairly uniform. By 14 msec the free-field pressures at the 71-inch level were decaying.

The horizontal and vertical pressure gages located above the device at the 53-inch level indicate that the vertical pressure was approximately the same as that found in the free field. The ratio of the horizontal to vertical pressures varied from 1.07 to 1.0. Except for the very early time frames, prior to 8 msec, the ratio exceeded 1. Table 6 and Figure 65a indicate that the structure experienced very little load until 8 msec.

At the 47-inch level the horizontal-to-vertical pressure ratio was considerably less than 1, varying from 0.76 to 0.83 during the time span shown in Figure 65a. From 8 to 12 msec the vertical pressure at this level was higher than that found 6 inches above or below it.

At the 41-inch level the horizontal pressures were very high.

The horizontal-to-vertical pressure ratio varied from 1.11 to 1.20. This is a strong indication of arching action at this level.

At 8 msec the horizontal-to-vertical pressure ratio was 1.00 at the 38-inch level. Some arching action was taking place at this level. The lower vertical pressures at this level as compared to the levels above it also indicate the unloading effect of the flexible structure 3 inches below.

Figure 65a indicates that the structure affected the loading of the soil above it to approximately the 53-inch level. The majority of the unloading appeared to occur at a height of approximately 6 inches above the device, one structure diameter.

At the 35-inch level, the loading of the soil by the structure is very noticeable in Figure 65a. The effect also can be seen at the 30-inch level at the early time frames; the structure evidently sheltered the soil directly underneath. This can be seen at both the 24- and 27-inch levels.

Figure 65b for Test 19 shows two curves derived from data taken very early in the test. There was a characteristic pressure buildup at the 30- to 35-inch level near the device as it unloaded onto the soil. Note that this action occurred between 3 and 6 msec.

At the 32.5-inch level there were gages measuring horizontal pressure both in the free field and next to the device. The free-field gages showed horizontal-to-vertical pressure ratio considerably

less than 1 throughout the major portion of the test. The close-in gages varied from a ratio of approximately 1.9 to 1.

In this test a gage measuring horizontal pressure was placed under the device at the 27-inch level. The ratio of horizontal to vertical pressure at this level was, as expected, considerably greater than 1 throughout the test.

Figure 66a shows the distribution of soil pressure for Test 22. This test was very interesting in several respects. First, the vertical pressure gages directly above the device at the 38- and 40-inch levels show that the soil unloaded as the device deflected. The horizontal pressure gage above the device confirmed the arching action. It indicated a horizontal-to-vertical pressure ratio greater than 1. The horizontal-to-vertical pressure ratio in the free field at the same level was considerably less than 1. The greatest unloading is shown by the vertical pressure gage at the 38-inch level.

Figure 66b shows the soil pressure distribution for Test 23. This device was the most flexible one used in the test program. A 6-inch layer of soil was placed above the device. The array of gages along the centerline above the device indicated that arching influenced the soil up to at least the 39-inch level. The horizontal-to-vertical pressure ratio at the 39-inch level was much greater than 1 and remained constant for the two times shown in the figure. The characteristic large decrease in the vertical pressure and the high

ratio of horizontal to vertical pressure also were observed at the 37-inch level. The gages close to the device at the 35-inch level did not show the normal sharp increase in pressures because the very flexible device caused the high stresses to be arched over these gages.

The horizontal and vertical gages below the device at the 27- and 24-inch levels indicated interesting results. At the 27-inch level the vertical pressure rose sharply at 10 msec to exceed the free-field pressure, while at 4 msec the pressure appeared to be fairly uniform. The horizontal pressures were less than the vertical pressures at both time intervals. At the 24-inch level the vertical pressures indicated the sheltering action of the structure. The horizontal pressures exceeded the vertical pressures at this level.

Figure 66c for Test 25 does not contain many gage readings since this was one of the tests in which gages were placed vertical, horizontal, and at 45 degrees. Only the vertical and horizontal gage results are in the figure. At the 35-inch level, the gages close to the test device registered less than the gages in the free field. The actions above and beside the device indicate that it was a stiff device and therefore attracted load.

Figures 67a, b, and c are examples of the pressure versus depth curves for the preliminary dynamic tests. No test devices were installed for these tests. In these figures it is important to note

the pressure buildup with time and depth. At high pressures, Tests C and F, the test chamber attained fairly uniform pressure conditions by 8-10 msec after the initiation of the bonnet pressure. Uniform pressure conditions at the 30- to 35-inch levels were attained prior to 6 msec. For the lower pressure test, Figure 67b, the sidewall friction effects are evident. Uniform pressure conditions at the 30- to 35-inch levels were attained at 10-14 msec. The scatter in the pressure data is an indication of the magnitude of scatter that should be visualized in inspecting Figures 64-66. Comparison of Figure 67 curves with the curves in Figures 64-66 illustrates the effects of the structure on the soil pressures.

Figure 68 consolidates the data on the horizontal-to-vertical pressure ratios. The full range of the ratio's variation throughout each test is shown by the length of the arrows. This ratio appears to be a good indication of the type and extent of arching taking place.

Figure 68a shows the variation of the horizontal-to-vertical soil pressure ratio above the device for Test 13. Although there was probably some arching action at the 38-inch level, the higher horizontal pressures at the 41- and 47-inch layers indicate that there was a large amount of arching action at these levels. From Figure 68a, it can be seen that the arching action acted at least to the 47-inch layer for a pressure of approximately 150 psi.

Figure 68b shows the horizontal-to-vertical pressure ratio for Test 14. In this test, the device was buried at the same depth of burial as for Test 13, but the test pressure was approximately 245 psi. At the 38-inch level the vertical pressure exceeded the horizontal pressure except for an initial spike at 4 msec. At the 41-inch level, the horizontal pressure exceeded the vertical pressure. At the 47-inch level, the vertical pressure exceeded the horizontal pressure. Evidently most of the arching occurred below the 47-inch level and above the 38-inch level.

In Test 14 an array of horizontal and vertical pressure gages was distributed in a horizontal direction between the 35- and 37-inch levels. Figure 68c shows the variation of the horizontal-to-vertical pressure ratio with radial distance from the centerline of the test chamber. Close to the device the horizontal pressure exceeded the vertical pressure by a considerable margin. At the 8-inch radius, the horizontal pressure exceeded the vertical pressure but not by as much as at the 5.5-inch radius.

Figure 68d shows the horizontal-to-vertical pressure ratio for Test 18. At some depths the horizontal pressure exceeded the vertical pressure and at locations in between these depths the vertical pressure exceeded the horizontal pressure. A large amount of load transfer appeared to have taken place in the vicinity of the 41-inch level. At the 47-inch level, the vertical pressure predominated.

The horizontal pressure predominated again at the 53-inch level.

Figure 68e shows the variation of the horizontal-to-vertical pressure ratio for Tests 20, 23, 24, and 25. Test 20 used a flexible device and Test 23 used the most flexible structure of the series. The devices used in Tests 24 and 25 were stiffer than the soil.

For Test 20, the horizontal-to-vertical pressure ratio 4 inches above the device was considerably greater than 1. This result was confirmed in Test 23. In the free field at the same level, the ratio was less than 1 which indicates that arching had no effect at the 14-inch radius.

In addition to confirming the results of Test 20, Test 23 indicates that a very large horizontal-to-vertical pressure ratio existed 2 inches above the device. With this very weak device and the relatively low pressure, a large amount of arching evidently was taking place at this level. The pressure ratios beside and below the device also are shown for this test in Figure 68e. At the 32.5-inch layer, the gages at the 4-inch radius indicated the unloading that took place near the device during this test. The gages at the 16-inch radius appear to indicate that the pressure distribution from the 35-inch level or actions instigated by the chamber walls changed the direction of the principal stress.

The results shown for Tests 24 and 25 show what can be expected when the structure is stiffer than the soil. In this case, the soil

above the device experienced large vertical loads. Horizontal and vertical gages were located at the centerline and at a 2-inch radius for these two tests. The pressure ratio were much less than those for the flexible device or for the free field in most cases.

From pressure ratio curves and the pressure distribution profiles with depths, it appears that the height of soil above the device that was affected by arching action was dependent upon the surface pressure and the stiffness of the device at a given depth of burial. This subject is discussed more fully in later sections of the report.

As explained in Section 4.2.2, an effort was made to determine the direction of the principal stress and the shear planes within the soil specimen by the use of a series of three gage arrays of soil pressure transducers. The derivation and explanation given in Section 4.2.2 will not be repeated in this section. This technique was tried during Test 24 and the repeat test on the same specimen, Test 25. Because of the high mortality rate of the SE gages during the latter part of the dynamic test program, only four arrays could be installed. During the tests, at least one gage in every array except one failed to function. This array was located 3 inches above the test device as shown in Figure 69.

With the small amount of information available, it was not possible to draw significant plots of stress within the soil specimen.

However, the results from the one functioning array in Test 24 are interesting. The Mohr's circles of stress for various times are shown in Figure 69a. As the surface pressure increased and the effects of the test device were felt by the soil, the direction of the principal stress moved to a position which pointed toward the top of the test device. This progressive movement can be seen in the figure. Note that after 3 msec, this direction remained relatively constant. The direction of the principal stress was that to be expected in a passive arching test. Compare this final direction with that shown in Figure 34. In this figure, the final direction is away from the test device as is to be expected for an active arching test.

Similar results were noted at the 41- and 47-inch levels above the device in Test 8. The maximum shear stress of 33 psi and the maximum principal stress of 54.8 psi occurred at 8 msec. The surface pressure at this time was 32 psi. The maximum pressure on the device, 41.6 psi, occurred at 6 msec. The Mohr's circle for 4 msec, not shown in Figure 69, indicated a small amount of tension. There was a large jump in the amount of pressure acting on the device at this time, Table 6. At 8 msec, considerable tension is indicated. What appear to be tension cracks in the soil are shown later in this chapter.

After 8 msec, the Mohr's circles began to decrease in size despite the fact that the surface pressure remained relatively constant

until sometime after 20 msec. The 20-msec circle is shown in the figure as an example. After 4 msec, the centers of the circles were shifted sufficiently to the right to always indicate that tension existed. At 100 msec, the surface pressure was 25 psi, and 1 psi of tension was shown.

The direction of the planes of maximum shear are indicated in Figure 69b.

Figure 70 shows the results of Test 25. A maximum surface pressure of 52 psi was utilized in this test. The previous test on this soil specimen may have affected the initial direction of the principal stress. Note that the final position for Test 24 was 39.4 degrees and the initial direction for Test 25 was 30 degrees. The direction at maximum was 38.5 degrees for Test 24 and 38.3 degrees for Test 25. At 100 msec, Tests 24 and 25 results indicate directions of 39.3 and 39.4 degrees, respectively.

The characteristic buildup of concentric circles to a maximum at 10 msec and the decrease in circle size after this time were noted in Test 25. The center of the circles again shifted first to the left and then back toward the origin after 4 msec.

The maximum pressure on the device, 77 psi, occurred at 7 msec, Table 6. The principal stress at the location shown in Figure 70b was 81 psi, the vertical stress was 44 psi, and the 45-degree stress was 80 psi at this same time.

4.3.4 Deflection Curves. In this section the deflection versus time curves for the soil and the test device are discussed. Normally there were two deflection gages under the base of the device and two deflection gages measuring the deflection of the top of the device relative to its base. In addition, there were usually four deflection gages in the soil. These gages were either arrayed horizontally at the level of the top of the device or vertically in the free field above and below the device. Differences among these curves and between these and those for the static tests involve primarily total deflections and the relation of the structure's deflection to that in the soil.

Figure 71a for Test 11 shows that the deflection of the device base was greater than that of the soil at the same level even though the indicated load on the device was less than that in the free field. Evidently the device, which was denser than the soil, was driven by the dynamic effects. The total deflection of the top of the device was very close to that registered by the soil 10 inches from the centerline at the 38-inch level. The deflection at the top of the device was large as compared to the soil in the so-called free field at the same level. Thus, the top and bottom of the flexible structure deflected more than the soil in the free field at the same level.

Test 12 involved a structure of the same relative stiffness as

that in Test 11 but the surface pressure was almost twice that in Test 11. In Figure 71b the soil deflection at the 5.5- and 6.5-inch radii was approximately the same as the total deflection of the device. This indicates that the structure and the soil in its immediate vicinity deflected together or interacted so that the pressure exchange maintained approximately the same deflection. All three of these deflections were greater than the deflection in the free field at a radius of 16 inches. These results are consistent with the pressure profile in Figure 60b.

The base of the device moved farther than the soil at the same level. As will be seen throughout the dynamic deflection data, the relative deflection of the base was in the opposite direction during active arching tests to that found in the same type of static test.

The deflection-time curve for Test 15, Figure 72a, depicts the results when a flexible device was buried with only 2 inches of soil above it. Total deflection of the top of the device up to approximately 8 msec was the same as the soil at the 5.5-inch radius. After this time, the total deflection exceeded the deflection of all soil gages. At 100 msec the deflection at the top was approximately the same as at the 5.5-inch gage.

The deflection of the base of the device was about the same as the soil at the 30-inch level until approximately 8 msec. Then the base deflection began to exceed that of the soil by a considerable

amount. At 18 msec it was practically the same as the soil deflection at the 5.5-inch radius at the 35-inch level, and exceeded the deflection of the soil at a radius of 5.5 inches at the 30-inch level. During rebound, the base deflection was approximately the same as that at the 5.5-inch gage at the 30-inch level. Notice that the 5.5-inch gage in the soil at the 30-inch level deflected more than the 14-inch gage after approximately 13 msec. This pattern of greater deflections near the device was seen in all of the active arching tests, both static and dynamic. This deformation pattern is consistent with the pressure data discussed in the previous section. It also shows the time required for the pressure change induced by arching to take effect at the 30-inch level.

In Test 16 the device was buried at 6 inches and was more flexible than the soil. The deflection-time curves in Figure 72b are similar to those for the previous tests. The effects of depth of burial can be observed if the results are compared with the curves from Tests 11 and 15. In this test the deflection of the base of the device exceeded that in the free field at the same level. The total deflection of the top of the device was approximately the same as that of the soil at the 5.5-inch radius at the 35-inch level and exceeded that of the free field at a height of 38 inches.

Test 18 was a deep, high pressure test. The test device was buried 42 inches below the surface. The deflection curves in

Figure 73a indicate that it took several milliseconds for the pressure to reach the deflection gages. The deflection of the base of the device started sooner than the soil at the same level, but was only slightly larger than the deflection in the soil at that level until the reflections hit the device. The total deflection of the top of the device was approximately the same as the deflection of the soil at a radius of 8 inches at times less than approximately 10 msec. Then, the effects of arching seemed to take over and the soil showed the effect of being loaded by the device. At about 13 msec the deflection of the 8-inch gage at the 35-inch level showed the results of the load being arched onto the soil by the structure. The deflection of the structure exceeded that of the soil in the free field at the same level throughout the test. The structure deflection was not plotted for the time interval in which the severe reflection occurred.

The deflection curves in Figure 73b are examples of the data which resulted from the use of a very flexible device at a depth of burial of 6 inches in Test 23. Early in the test, the deflection of the base of the device was less than that of the soil at the same level. At 8 msec and later times, the base deflection exceeded that of the soil at the 30-inch level. The very flexible device deflected more than the soil at the 41-inch level. This is a good measure of

the large amount of deflection which may be expected with such a structure.

The deflection-time curves for Test 24 in Figure 74a are a good example of the type which resulted from using a device stiffer than the soil. The deflection of the base of the device exceeded that of the soil at the same level by a considerable margin, except very early in the test. This deflection was understandable since the stiff device attracted an increased load. Because of the device stiffness, the top showed very little deflection. The deflection of the soil at a radius of 12 inches exceeded that at a radius of 5.5 inches. This was due to the device attracting load from the soil in its vicinity.

Figure 74b shows the deflection-time curves for Test 27B. These curves resulted from the loading of a very stiff device buried 6 inches in the soil. The symbol used for the base deflection is also the total deflection of the top. The base deflection far exceeded the deflection of the soil at the same level. Early in the test, until about 6 msec, the deflection of the base was almost equal to the deflection at the 5.5- and 6.5-inch radii at the 35-inch level. The deflection of the soil at a radius of 5.5 inches was not as large as that at a radius of 6.5 inches at the 35-inch level. This was due to the attraction of load from the soil by the stiff structure.

The deflection curves for preliminary tests E and F in Figure 75

can be compared with tests at somewhat similar pressures and depths of burial in Figures 71a, 72b, and 74. The curves in Figure 75 show the deflection in the soil at the 24-, 36-, and 42-inch levels. The relative deflections and times of initiation appear reasonable.

4.3.5 Acceleration Data. For all of the dynamic tests, accelerometers were placed in the free field of the soil specimen and also on the base and top of the test device. From the records of these accelerometers, it is possible to study the variation of acceleration with depth. In addition it is possible to see the relation between the accelerations of the structure and free field. In Figures 76 and 77, much of the acceleration data has been consolidated. All accelerometer records are available in Appendix C.

In Figure 76 the variation of the soil and structure acceleration with depth and surface pressure is shown. Only peak accelerations are included. Accelerations due to reflected pressures are excluded. All tests included in Figure 76 were designed so that the relative stiffness of the structure and soil would be the same. This was not possible in all cases as is shown in Table 2, but the stiffness was close enough to allow a comparison of the acceleration data. The stiffness chosen was such that the structure would be 0.7 as stiff as the soil.

As might be expected, there was an increase in the structure and soil accelerations at a particular depth of burial with an increase

in the surface pressure. There are some abnormalities in the free-field data. These are points which do not plot within the data for a particular surface pressure. These points have been numbered with the test numbers that correspond to these data. Two tests in particular seem to present erratic data--Test 15 in the 37- to 39-psi group and Test 19 in the 151- to 157-psi group. In both of these tests shallow depths of burial were used, i.e. 2 inches for Test 15, and 6 inches for Test 19. The point plotted at the 6-inch depth for the free field of Test 18 also appears to be low compared to the remainder of the data from this test and Test 14 data.

For the device used in these tests, it was found that the structural accelerations exceeded the free-field accelerations at the same elevations. The one exception was the top of the structure in Test 15. In Test 15 the structure was so near the surface that anomalies were likely considering the rise time of the pressure pulse at this depth. There appears to be a linear relation between depth and both structure and soil accelerations. For example, the 37- to 39-psi data show three structures at three depths of burial. Except for Test 15, all data appear to plot on a straight line. Similar occurrences were noted in the 151- to 157-psi data and in the 240- to 245-psi data. In general, the soil accelerations were less than the structure accelerations, except as previously noted, and the acceleration of the structure base was less than that of the top. The

results appear reasonable considering the relative flexibility of the device, except for the anomalies noted in Tests 15 and 19.

The data from the repeat tests on the Test 11 specimen indicated interesting results. Although the pressure was only about 3 psi higher than that used in Test 11, there was considerable change in the accelerations of the structure and the soil. This change does not appear to be due only to pressure. The densification of the soil and the increase in soil saturation had some effect.

If the free-field accelerations at a particular depth, for example 23 inches, are examined, there appears to be a direct relation between the surface pressure and the soil accelerations. These results are logical and confirm previous work in this area (Newmark and Haltiwanger). An examination of structure accelerations at the same depth also shows that a linear relation exists between surface pressure and these accelerations.

An important point to note in Figure 76 is the sharp decrease in the structure and soil accelerations with only a small increase in depth. This phenomenon is important to both the structure and equipment designer.

Figure 77a is a more detailed picture of the relation between accelerations at a particular depth and surface pressure. The test devices involved were designed to have the same flexibility in relation to the soil at a particular pressure level for all four tests.

As previously explained, the test results showed that the relative flexibility was not exactly identical.

Figure 77b shows the variation of structural acceleration with a change in structure stiffness. All tests were at a constant scaled depth of burial of 1. The free-field soil data also have been plotted so that the consistency of the data can be studied. There are several important points to note in this figure. First is the high acceleration of the top of the very flexible devices (Tests 20 and 23), and second, the consequent low acceleration of the base of the flexible structures. Third, the acceleration of the base tended to increase as the stiffness of the device increased. Fourth, note the consequent decrease in the acceleration of the top as the structural stiffness increased. The acceleration of the top of the structure exceeded that of the free field except for the stiff devices in Tests 26 and 28. This was not true for Test 24, but there was very little difference between the soil and structure accelerations.

These phenomena are reasonable since the flexible structure absorbs much of the initial load in the large deflections of the top. Consequently, the base was loaded slowly by a small load. In the stiff structures, large loads were immediately transmitted to the base, Test 26. For Tests 24 and 26, Figure 77b shows that the acceleration of the base actually exceeded that of the top by a small amount. Structures of intermediate stiffness, i.e. those of

Tests 22, 24, and 28, showed very little variation in the acceleration of the top with change in stiffness but the acceleration of the base decreased with a decrease in structure stiffness.

The environment within the test chamber during Test 14 at P_S = 245 psi was so severe that many instrumentation cables were severed with a consequent loss of data. Several of the accelerometers in the soil and both the accelerometers on the top of the device were lost in this high pressure test. The range of accelerations used for the top of the Test 14 device was determined by use of both the spectra data and the actual accelerations in Test 13.

4.3.6 Dynamic Effects. In order to examine the dynamic response of the test device, it was necessary to study the form of the pressure wave at the 35-inch level. The initial arrival and rise times were of particular interest. In examining the pressure records, a number of difficulties arose: the times of initiation and maximum pressure peaks were not distinct in some cases; the pressure wave did not arrive at the 35-inch level uniformly; and the waveform was different at various radii, depths, and pressures.

At low pressures, 35-70 psi, the initiation times were earlier near the center of the test chamber. At higher pressures, the initiation times at the 35-inch level were practically uniform.

At low pressures the initial slope of the pressure-time relation decreased before the maximum pressure was attained, Figure 78a. The

device was not loaded instantaneously. The load increased with time similar to the trace shown in Figure 78b. The pressure rise time varied depending on the surface pressure and the depth of the structure, Figures 78c and d. The degree of dynamic amplification of the load, if any, depended on the rise time at the level of the top of the device, 35 inches from the test chamber base.

The length of time the load remained on the structure and the small amount of load decay in the time frame considered important were such that the maximum load could be considered to be maintained indefinitely. The characteristics of the pressure traces can be seen in the figures of Appendix C. These traces vary from the relatively long rise times with precursors for the deep, low-pressure tests, such as Figure C-3, to the almost instantaneous rise to a peak somewhat less than the maximum as shown in Figure C-14.

Table 7 contains the rise times measured for each test. Time, t_r , was developed by constructing an idealized pressure wave similar to that shown in Figure 78a. The curve was constructed with equal area under the curve between initiation and maximum. Most pressure traces rose sharply from initiation to an intermediate pressure. This was followed by a slower buildup to maximum pressure. The rise time, t_o , was developed using equal areas but only the steep portion of the trace was considered.

The test device was idealized as a single-degree-of-freedom (SDF)

system. In no case was the load sufficient to exceed the elastic range of the spring system. Some degree of damping existed in all test structures, Table 3. In the machined cylinders, the damping was considered to be negligible.

From the previous work in the dynamic design of aboveground structures--for example, Newmark (1949, 1962, 1964)--it is known that the time rate of application of the load to a structure can have a significant effect on the load and the structure response. For the idealized loading function and model assumed, the dynamic amplification factor (AF) approaches a maximum of 2 as shown by Merritt and Newmark. The equation for the AF was found by solving the equation of motion for the SDF system and forcing function assumed. The system was considered to be initially at rest and without damping.

$$AF = \frac{X}{X_{st}} = 1 + \frac{T}{\pi t_r} \sin \frac{\pi t_r}{\pi_r} \tag{12}$$

When damping was added to the system, the magnitude of the amplification factor was reduced. The reduction factor was derived from the complete solution of the equation of motion. The final values for the AF are shown in Table 7.

It was not possible to actually distinguish or measure dynamic effects by examining the test records. The flexible structures exhibited loads less than the average soil pressure and the stiff

structures exhibited higher loads. But by examining the values of the P_T/P_S and K_T/K_S columns in Table 2, the AF columns in Table 7, and the test records in Appendix C, a pattern was distinguished. When the values of P_T/P_S were modified by the AF's and compared with the actual values of K_T/K_S, it was found that very little if any amplification was involved in Tests 11, 16, and 20 through 28. These were low-pressure tests with scaled depths of burial varying from 1 to 3. Appreciable amplification seemed to occur in the high-pressure tests, 12-14 and 17-19. The amplification generally fell between the factors calculated for t_r and t_o, but tended more toward the value calculated using t_o.

In the process of determining rise times, the initiation time of the soil pressure gage nearest the device was checked against the initiation times of the displacement gages and accelerometers in the test device. Generally, the accelerometers attached to the top of the device and the close-in soil gage initiated at approximately the same time. The device deflection gages lagged the other gages by 0.5 to 1.0 msec.

The deflection gage and the accelerometer traces in some of the high-pressure tests, such as 12, 13, and 14, appeared to vibrate at a frequency which was unrelated to the measured period of the structure. The period of these vibrations varied from approximately 14 to 16 msec. Close examination of the motion of the whole soil specimen

disclosed that the period of its motion was similar to that measured by the device gages.

Examination of the deflection records also disclosed that there was very little rebound, except that caused by reflections, while pressure was maintained on the soil surface. The device appeared to act like a system approaching the critically damped condition. The damping factors shown in Table 3 were calculated for the unburied state. Once the structure was buried and pressure exerted on the surface, the soil pushed down on the top and held it near the point of maximum deflection until the surface pressure was released. Oscillatory motion such as that shown in Figure C-1 was not possible. No free vibration was observed after the surface pressure decayed.

The data discussed in this section indicate that rise time was important in determining the load on the test structure depending upon its depth of burial and the surface pressure to which it was subjected. Sizable amplifications appeared to be present even at a scaled depth of 7 when the surface pressure equaled 310 psi. Even under controlled conditions, there was considerable scatter in the rise times measured for tests at the same depth and surface pressure. Except for the low pressure tests, 40 psi or less, the step-pulse of infinite duration would appear to be a realistic assumption for the loading condition just as it is under field conditions with large-yield nuclear weapons. At pressures below 40 psi, the depth of

burial can have a large effect on the rise time, Figure 78d. From these results it appears that a very shallow depth of burial can be very important in the design of structures for low pressures. Rise times and their dependence on pressure, depth, and soil water content will be discussed in more detail in Appendix A.

4.3.7 Soil Profiles. The three techniques for investigating soil deformations which were described in Section 4.2.4 for the static tests also were used for the dynamic tests. First, careful measurements were made of the exact location of all instrumentation, the test device, and the soil layers as they were installed and removed from the test chamber. Second, as the soil was removed after the test, sketches and photographs were made of the soil deformations. Third, X-ray photographs were made of undisturbed block soil samples after some of the tests.

The soil deformations were investigated to determine the soil deformation pattern characteristic of passive and active arching. In this way it might be possible to confirm the soil mechanism involved in the arching action. Another objective was to determine if there was a difference between the static and dynamic arching actions. The remainder of this section is devoted to an explanation of the deformation patterns observed and measured. Only representative photographs and sketches are shown since the soil action appeared to be similar for similar-type tests.

Test 12 contained some distinct and interesting deformation patterns which are shown in Figure 79. The surface appeared to move down uniformly. Upon the removal of the top 3 inches of soil, the surface at the 50-inch level contained a distinct hump approximately 16 inches in diameter. This hump is shown in Figure 80a. As can be seen in Figure 79, part of the hump was above the original level of the soil in spite of the 3/4-inch reduction in overall sample height. Much of the soil inside the radius had a livery appearance. Inside the hump, a depression with approximately a 5-1/2-inch inside diameter was noticed, Figure 80b. This depression was not directly over the centerline but offset into the southeast quadrant by approximately 3 inches. A ridge 1/4 to 1 inch in width existed around the outside of the depression, Figure 79.

When the soil above the 50-inch layer was examined, the fracture pattern indicated in Figure 79 was observed. Throughout all the tests, these fracture patterns were very distinct when found. Figure 81a shows a piece of soil in which the deformation pattern has been exposed. Note the slickenside, glossy appearance. In this piece of soil two fractures can be seen, but only part of the top one was exposed.

A similar hump and depression were found at the 47-inch level. The critical dimensions are shown in Figure 79. The extent of the hump and depression are not exactly circular but irregular.

Dimensions are given along the south and west radii when possible. Note that the dimensions of the hump and depression were not the same as for the layer above. Again the fracture pattern in the soil was examined. It was almost a mirror image of the fracture pattern above the depression. Also the invert of the hump-depression pattern was found in the soil above the 47-inch layer. The ridges were very distinct, as can be seen in Figure 81a.

The hump-depression pattern at the 41-inch level was distinct in the northeast and northwest quadrants. The depression was not directly below the depression found at the 47-inch level; it was approximately 5 inches away in a northwesterly direction. The white substance in Figure 81b was used in an attempt to make the hump stand out in the photograph.

At the 38-inch layer, the hump and depression were distinct. The depression developed closer to the centerline and was much larger than previously observed. The outside dimensions were 8-1/2 inches along the north-south axis and 7-3/4 inches in an east-west direction. The depression was very livery in appearance.

The soil directly above the test device was fractured in the pattern shown in Figures 79 and 81a.

In general, the depressions appeared to become smaller with height above the device while the hump appeared to grow larger. The deformation patterns were not continuous from top to bottom. For example, the

depression could not be followed in the intermediate layers of soil. Over the depressions, a plug of soil in the shape of a dome was generally found. For Test 12, the presence of the structure affected the soil deformations to a height at least 15 inches above the structure.

An X-ray mosaic was constructed for Test 13. The depression-fracture pattern described for Test 12 was partially observed in the radiographs. The depression was distinct at the 38- and 50-inch levels. The fracture pattern was distinct in the 35- to 38-inch layer and the 53- to 50-inch layer. No deformations were noted on the soil surface.

Since Test 14 was one of the two tests above 200 psi, it was studied as closely as possible. These observations are shown in Figure 82. Most of the observations were made along the south radius so only half of the sketch has been detailed.

The surface appeared to move down uniformly except for a small mound that existed over the centerline (Figure 82). At the 50-inch level, no depression was observed, but the radiograph mosaic in Figure 83 shows that one existed. It was off center to the left, as shown in this figure. A depression 5-1/2 inches east-west by 4-1/2 inches north-south was seen clearly at the 47-inch level. It also was off center similar to the depression at the 50-inch level. Note that the mosaic shows the inverse of the depression clearly at the bottom of the first layer. Because of the necessity of reducing the

size of the mosaic for publication, it is not possible to see clearly the deformations and patterns which were clear in the full-size mosaic. When the full-size mosaic was inspected with a magnifying glass, it was possible to follow the deformation patterns in the soil layers above the depressions.

The large mounds which were seen in Test 12 were not clearly discernible in Test 14. Figure 83 clearly shows a ridge at the 15-1/2-inch radius at the 44-inch level. In addition, at this same level it shows a ridge at the 7-inch radius. Part of a very distinct depression was observed at the 38-inch level. The radius of the portion seen was between 4 and 4-1/2 inches. This appears to be large so the center may have been offset. Notice the lip on the depression. This type of formation was seen around all the depressions found in this test.

The profile of the variation of soil pressure at the 35-inch level has been included in Figure 82. Note how the profile of the soil corresponded to the pressure profile. In addition, Figure 83 shows the strong deformations that occurred at the 35- and 33-inch layers in the high pressure region between the 4-1/2- and 6-inch radii.

As in the previous dynamic tests, there is a pattern of deformations which appears to be associated with active arching under dynamic loading conditions. The radiograph assisted in the location

and study of the deformations, but direct observation was a more sure and satisfying means of investigation. The fracture patterns observed in Test 14 were similar to those observed in Tests 12 and 13. In Test 15 with 2 inches of cover above the device, the soil surface moved down uniformly. No depression or mounds were observed.

The mound-depression pattern was found to exist in Test 16. Again the surface was plane, but the pattern was seen clearly at the 44-inch level. The depression had an inside radius of 5-3/4 inches. The mound had an outside diameter of approximately 19 inches.

No unusual deformations were observed in Test 17.

Test 18 was the deep test, $H/B = 7$, in which the maximum surface pressure reached 310 psi. The surface did not disclose any distinct deformation patterns. There was a slight mound at the centerline as shown in Figure 84. A distinct pattern was noted at the 71-inch level where a set of depressions was found, Figure 84. These deformations were very distinct and deep. The fracture pattern shown in Figures 84 and 85 was observed. Inside the depressions, the soil had a glossy appearance and gave evidence that movement had taken place.

At the 68-inch level, the double depression pattern was observed again, Figure 84. Between the 71- and 68-inch layers, the soil was not extensively fractured except right under the center depression and at the ridges.

At the 65-inch level, three more or less concentric depressions were observed. In studying Figure 84, note that the depression patterns are shown along several radii, so the depressions may not match those directly above them on the sketch. The middle two depressions at this level were livery in appearance. The fracture pattern between the 68- and 65-inch levels was as shown in the sketch.

The depressions at the 62-inch level were unusual. Along the northwest radius there were three distinct ridges, while in the southeast quadrant only one ridge appeared to be present. The ridges all seemed to blend into each other as the depressions were not concentric about the centerline.

The double depression pattern was seen at the 59-inch level. Figure 86a shows the distinct ridges noted in the 62- to 59-inch layer. The fracture pattern over the depression also can be seen.

At the 53-inch layer, the double depression pattern as shown in Figure 84 was present. Figure 86b is a side view of the soil between the 53- and 56-inch levels. A mirror image of the ridge pattern at the 53-inch layer can be seen at the bottom of the sample.

Test 19 was a medium pressure test at a scaled depth of 1. The main objective of this test was to fail the soil to the surface. By accomplishing this, it would be possible to determine how much of the soil strength had been mobilized. Based on the information developed in Tests 13 and 16, it seemed that complete failure should occur

under the conditions specified for this test.

As can be seen in Figure 87, the soil surface does not exhibit failure planes; in fact there seems to be a slight mounding of the surface at the centerline. This mound appeared to have a diameter varying from 8 to 9 inches. As previously stated, no distinct depressions were found on the soil surface for any of the dynamic tests, regardless of the pressure and structure depth of burial.

At the 38-inch level, the first layer below the surface which could be examined, the deformation pattern was very distinct, Figure 87. A large mound which varied in diameter from 14 to 16 inches was present. Approximately at the center of the mound, a depression with mounded sides as shown in Figure 87 was observed. The inside diameter of the depression was delineated by a crack pattern similar to that shown in Figure 46. The fracture pattern above the 38-inch level is shown in Figure 87.

At the 35-inch level, the soil in the vicinity of the device was depressed below the rebound position of the top of the device. In fact, the soil was below the maximum depressed position of the device. The pressure profile at the 35-inch level gives an indication of the reason for this depression, Figure 87. In addition, the large pressures at 14-inch radius were consistent with the deflections measured at this radius.

In Test 20, the soil surface appeared to have depressed

uniformly with only slight signs of a lower region near the center of the test chamber. At the 38-inch level, a mound approximately 1/2 inch high and 10 to 17 inches in diameter was observed. In the center of the mound a small depression approximately 5 inches in diameter was found. The characteristic fracture patterns, previously described, were found in the 35- to 38- and 38- to 41-inch layers.

No important deformations were found in Tests 21 and 22.

In Test 23, there appeared to be an 8-inch-diameter low area on the soil surface which was about 4 inches off center. The deformation gage on the surface deflected the same amount as the soil in its vicinity. No mounding or depressions were found at the 38-inch level.

For Tests 24 and 25, the soil surface appeared to move down uniformly. The soil at the 38-inch level was well bonded even though the glossy-livery soil surface was present. There were no mounds or depressions. The soil was bonded well at the 35-inch level.

Test 26 was made with the very stiff device. The soil was closely examined in this test and Test 27 to determine the characteristic deformations for passive arching conditions. The deformations were not definite enough to determine a pattern. In both tests, the surface appeared to move down uniformly with some slight downward slope from the test chamber walls toward the centerline.

The fracture pattern shown in Figure 88 was somewhat different from that seen in the active tests. In the 38- to 41-inch layer very

little if any fracturing was observed. At the 38-inch level, a combination depression and mound was observed near the center of the test chamber, Figure 88. The mounds in the northwest and southwest quadrants rose out of a depressed area. The depression was not uniform. One area was about 1/2 inch lower than the rest. There was no large mound area as was seen in the active tests.

No high pressure, passive arching tests were performed. Previous results indicate that pressures higher than 50 psi are required before deformation patterns become distinct.

4.4 SOURCES OF ERROR

The greatest problem with error seemed to occur during the static tests. The detail results from three of the initial static tests are questionable because of air leakage around the test medium. In order not to bridge over the top of the test medium no diaphragm was used initially. Although it had been hoped that the clay around the sides of the test chamber would seal itself, this was not the case. There is evidence that air may have gotten into the clay near the test device. The results from these tests are erratic. Later, weather balloons were used to contain the air used to apply the surface pressure until a diaphragm was secured which could deform to the extent required by the clay. The balloons seemed to work well except that they were very easily punctured. Details concerning

the balloons and diaphragms used are contained in Section 3.2.1.

Another source of error in the early static tests was the hydraulic system used to raise and lower the device. This system had more elasticity in it than had been planned and the time required for pressures to equalize inside the test device was not constant. Initially, deflection gages were not placed in the test device to measure the deflection of its top. The volume of the test device was calibrated against turns on the pressure cylinder. Even though much care was exercised in the calibration, the calibration curves were not linear since the deformation of the system was such as to change the calibration at each pressure level.

Tests have been conducted on the soil pressure gages to determine the best method of placing these gages and the probability of measuring the actual pressure in the buckshot clay. The tests indicated that the SE gage, placed as described in Section 3.3.2, was generally accurate to $\pm$10 percent for dynamic pressures, Hadala (1967a) and Ingram (1967). At low static pressures, generally below 10 psi, the gage tended to be inaccurate, especially after remaining in the specimen for long periods of time.

It was necessary to recalibrate the SE gages during the dynamic test program. These gages were subjected to harsh treatment by the high pressures, especially the reflections. Calibrations did change and gages were damaged.

The reflected pressures were also a source of error. The records in Appendix C show that the pressures reflected from the base of the test chamber sometimes exceeded the peak surface pressure by a factor varying from 3 to 6. It was not difficult to see the arrival of the peak reflected pressure during high pressure tests, but in the low pressure tests it was more difficult to decipher. The data in Table 2 were based on velocity calibrations and careful examination of the pressure records. Only the data measured prior to the reflections were used.

These reflections sometimes had drastic effects, such as breaking the instrumentation cables. It was necessary to coil the cable in the soil, leave slack along the sides, and to protect the cable with plastic tubes.

Data about which there was any doubt were not included in the report. Several of the static and dynamic tests were repeated because of questionable data or the loss of instrumentation. The results included in this report have been carefully checked several times and are believed to be reasonably accurate.

CHAPTER 5

DISCUSSION AND ANALYSIS OF EXPERIMENTAL RESULTS

In this chapter the information developed in Chapter 4 is summarized and conclusions are drawn from the results. The static and dynamic results are presented separately and then compared. Each test variable is examined separately in an attempt to analyze its effect on arching.

The ultimate objectives of the program were to determine if soil arching takes place in rapidly loaded clay soil, and to provide a guide that will enable designers to incorporate the beneficial effects of arching in their structural design; therefore, major emphasis is placed on what appears to take place in an analysis of the behavior in these arching experiments and on the development of curves which relate the pertinent variables in terms which may be usable to designers.

5.1 STATIC TESTS

Although the static test program was limited, the results are presented in order to compare them with static trapdoor tests and the dynamic tests. The conclusions must be judged with the limited number of tests in mind.

5.1.1 Soil Deformation Patterns. The deformation patterns observed and measured were complicated by the fact that in many of the

tests the top of the test device was cycled through both active and passive phases. Another complication was the fact that the zone of soil affected by the arching phenomenon extended upward and outward with the increase in time, depth of burial, and surface pressure.

Based on the soil pressure profiles at the level of the top of the device, Figures 26 through 28, the soil pressure profiles above and below the device, Figures 29 through 32, the soil deformations, Figures 35 through 40, and the soil deformation patterns, Figures 41 through 50, two composite soil deformation patterns were constructed. Figure 89 depicts the deformations for active arching and Figure 90 those for passive arching. The effects of surface pressure are discussed in Section 5.1.3, the effects of depth of burial in Section 5.1.4, and the effects of time in Section 5.3.

In Figure 89 the depression located above the device appeared to become smaller with distance from the top of the device. The diameter of this very distinct depression varied from 4 to 5.5 inches depending upon the depth of burial. The type of depression and the soil deformations around it are clearly shown in Figures 41, 42, 43, and 46.

As illustrated in Figures 41 and 42, a ridge varying in diameter from 5 to 6.5 inches was found around the depression at the centerline. This ridge appeared to be part of a deformed zone in the soil around the depression.

At $H/B = 1/3$ and $P_S = 37.5$ psi , the depression was clearly visible at the soil surface, Figure 41. When the depth of burial was increased to $H/B = 1$ at the same surface pressure, no surface depression was visible. The soil specimen prepared with $H/B = 1$ was subjected to a surface pressure of 63 psi after the $P_S = 37.5$ results were examined. A depression was found at the surface, Figure 43. When depth of burial was increased to $H/B = 3$ and the surface pressure held to a maximum of 50 psi, the soil depression pattern extended to a height one structure diameter above the device.

At a surface pressure of 75 psi and with $H/B = 1$, the depression pattern did not form at the soil surface, but the depression was clearly visible 3 inches above the device, Figure 46. Cracks or shear zones were found in the soil around the depression.

Cracks similar to those found in the $P_S = 75$ psi test also were observed in Test 8 in which the surface pressure was 240 psi and the depth of burial was 18 inches, $H/B = 3$. In this test, the depression pattern was found at a height two structure diameters above the device.

A parabolic dome as depicted in Figures 50 and 89 formed on top of the device during the active arching tests. A soil formation of this nature appears more likely to be associated with passive arching. Initially, it was felt that the dome formation formed during the preliminary phase of the active arching tests when the

hydraulically controlled device was held rigid. It was during this period that the surface pressure was raised from zero to test pressure and the soil was more compressible than the structure. But the active arching tests made with the spring-ring device, in which arching was induced by increasing the pressure on the outside of the device rather than decreasing its internal pressure, showed the same phenomenon, Figure 50.

In Tests 4 and 8, P_S = 75 and 240 psi and H/B = 1 and 3, respectively, the dome formation was observed above the central depressions described above. In Test 4, the dome was observed in the soil layer 3 to 5 inches above the device. A similar dome-depression was seen 2-1/2 diameters above the device in Test 8.

Large soil fracture patterns similar to those depicted in Figure 89 also were observed in the active arching tests. These fracture patterns appeared to be associated with high soil pressures around the soil depression, Figures 44 and 45. The fractures also can be seen in Figure 50.

Similar deformed zones were located beside the device at the level of its top, Figures 45 and 89. The high pressures which existed in the deformed zone at this level were confirmed by the pressure profiles in Figures 26 through 28b.

To summarize the soil deformations under active arching conditions, the clay appeared to follow the device as it depressed. This

movement propagated upward in the form of a rather distinct depression. The soil was pushed out and up, away from the depression. As the depression formed, the zone beside the depression was loaded and deformed by the differential movement. The deformation pattern was not continuous, but a series of deformations developed with time as movements and pressures were sufficient to deform the soil. This created a series of loaded areas and is consistent with the high pressures observed at a considerable distance from the device.

The majority of the unloading and loading of the soil was accomplished in the first 3 to 6 inches above the device. Therefore, the majority of the load was redistributed just outside the device. As the area near the device was loaded and as the deformation propagated upward, the loaded zone moved outward from the device.

The lateral expansion of the zone affected by arching is a manifestation of the stress gradients developed. The wet, viscous clay used in the experiments tolerated only small stress gradients. Thus, for equilibrium to be satisfied, the load arched around the structure had to be taken by increasingly larger areas with time rather than building up high stress gradients in a small area. The whole active arching mechanism under static conditions appears to involve the development of shear and compressive stresses by relative movement. The more movement the larger the zone affected by arching and the greater the magnitude of the load arched off the structure. The

higher the surface pressure, the more differential movement required for the same percentage of load arched off the structure. To substantiate this explanation, note that the sides of the depressions are a series of steps and slopes, Figures 42, 43, and 46. These deformation patterns indicate that load was shifted away from the center of the depression in steps. The greater differential movement occurred in the center portion which was of course unloaded the most. As the load propagated outward from the centerline, less and less load remained on the structure and the larger the area involved at the level of the top of the device became. This can be seen clearly by the growth of the pressure profiles in Figures 26 through 28b.

Underneath the device, the soil deformed in a manner which resembled the classical elastic, plastic, and radial shear zones (Terzaghi and Peck) associated with bearing capacity.

The active arching patterns depicted in Figure 89 are similar to the deformations in sand reported by Ahlers, Havers, Kallstenius, Kvapil, and Selig. A detailed explanation of these findings is given in Chapter 2. The arches envisioned by Engesser and Caquot (1934) do not appear to be present in the static tests on clay. The arch or vault directly over the device conforms generally with the thoughts of writers on silos and grain bins such as Jenike (1958), Richmond, Gardner, and Walker. Watkins (1957) studied deformation patterns in sand by the use of X-ray techniques and lead balls. He

found depression patterns of much larger extent but similar in shape to those in Figure 89.

Clear-cut shear planes similar to those discussed by Terzaghi (1943), but which he admitted probably did not exist, were not found. The distortion patterns which did exist did not appear to propagate out on the slope hypothesized by Terzaghi in several of his articles (1936b). These distortions and arch patterns tended to follow a path almost directly above the device similar to the vertical planes used by Terzaghi, Newmark, Marston, Spangler, and several others discussed in Chapter 2.

The zone of tensile stresses explained by Terzaghi (1919) appeared to be present in the active tests of this program. The dome-shaped soil formation directly above the device generally could be separated from the remaining soil above the device after the active arching tests. Occasionally when the top of the device was lowered rapidly, the pressure on the top would suddenly drop to 0 and then build up with time as the soil appeared to flow down onto the device.

Figure 90, which is a compilation of the information in Figures 28d, 37, 39, 47, 48, and 49, shows typical soil deformations for passive arching under static conditions. The static passive tests were limited to surface pressures of 37.5 and 75 psi and a scaled depth of burial of $H/B = 1$. Scaled deformations of the top of the device were approximately $+72.9 \times 10^{-3}$ and $+82.67 \times 10^{-3}$, respectively.

Conclusions are limited to these test conditions and are not necessarily applicable to other conditions.

The deformations and extent of passive arching under these conditions were limited both horizontally and vertically. The major portion of the deformations appears to have occurred within one structure diameter above and beside the device. Some data were available from the cycling in Tests 2 and 3. They confirm the results observed in Tests 4 and 5.

The dome above the top of the device was slightly higher than the one shown for active arching, Figures 47 and 48. For the passive tests this dome tended to be more hemispherical than like the flat parabola seen in the active arching tests. The soil was also denser in this dome than in the one shown for active arching. The densification obviously came from the effect of the dome being forced into the surrounding soil. Although not discussed in this report, two static plate bearing tests were made with 2 and 18 inches of surcharge. Domes developed which were very similar to those seen above the device under passive arching conditions. The domes were inverted, in that the base of the device was tangent to the arc. The sides of the dome sloped out from the plate at angles varying from 26 to 32 degrees, Figure 91.

The soil seemed to deform around stiff test devices. The soil formed a natural dome as a shield in front of the blunt device. As

the stiff structure was loaded more than the surrounding soil, the soil underneath it was loaded. Pressures beneath the structure higher than the free field pressures caused larger deformations under the structure than the free field deformation and a tendency to decrease the load on the structure. This is a continuous process which accounts for the fact that the structural stiffness alone is not a good measure of the overall stiffness of the structure-soil system under passive arching conditions.

The passive arching patterns observed in this program were similar to those observed by Abbott in his layered-sand tests with small rigid-base structures. The three cases explained by Abbott appear consistent with the results obtained in this program. The deformation and pressure profiles below the device did not appear to conform to the zone of influence postulated by Mason (1965). The soil pattern above the device is similar to that postulated by Marston, Spangler, and associates at Iowa State University and later used by Van Horn in his development of loads on underground structures (1963a) as the "incomplete projection condition."

5.1.2 Test Configuration. Some of the significant work in the study of soil structure interaction has been accomplished with the use of the so-called "trapdoor," Terzaghi (1936c), McNulty, and Hendron (1968). Other studies have used structures located at the base of the test chamber, for example Abbott, Whitman et al. (1962),

Selig et al. (1961), Mosborg and Talda, to name a few. Chapter 2 contains a more detailed explanation of these experiments. One of the objectives of the static test program was to determine what effect the boundary has on arching. A knowledge of these effects could make the less expensive trapdoor studies of more use. Obviously, arching curves constructed using the trapdoor should form an upper limit to the amount of arching. Hendron's trapdoor study using buckshot clay was available and has been used as a basis for comparison.

Comparable active arching curves are plotted in Figure 92. The arching curves from the trapdoor study plot well under the idealized structure curves produced by the hydraulically controlled device, Tests 1 through 4. The same information is presented in terms of differential pressure in Figure 94. This method of plotting arching becomes more meaningful at surface pressures high enough to mobilize the maximum strength of clay soil. The differential pressure curves should collapse at high pressures, because the strength of buckshot clay, a material whose ϕ is near 0, should be practically insensitive to changes in surface pressure (Appendix A).

The curves from the two different configurations appear to have approximately the same shape. Deflections as small as 0.01 inch in all tests at P_S = 37.5 and 75 psi created large amounts of arching, Figure 92 and 94. In the trapdoor studies the amount of arching is considerably greater than the arching with the idealized structures

for a given amount of deflection throughout the curves.

Ultimate arching values for the spring-ring device, Tests 6 through 8, also are plotted in Figures 92 and 94. The object was to determine what effects, if any, could be attributed to the manner in which the top of the device was lowered. In Tests 6 through 8, the top of the device was pushed down by externally applied pressures rather than being lowered by reducing the internal structure pressure as was the case in Tests 1 through 4.

Tests 6 and 7 were performed at 37-39 psi and therefore should be comparable with the arching curves plotted in Figures 92 and 94.

It can be seen that the pressure on the spring-ring device was not the same as that experienced by the hydraulic device for the same differential deflection at the same depth of burial. This difference is hard to understand because the deflection of the structure is a function of stiffness, and the load the soil dissipates or attracts is some function of the strain it experiences over a particular area. There appear to be several elements involved in this apparent discrepancy.

First it is connected with the manner in which the structure is loaded. Considerable time (10-15 minutes) elapsed between each lowering of the hydraulic device in Tests 1-4 to allow the internal pressure to stabilize. Stabilization times were not required or used in Tests 6-8. On several occasions the top of the hydraulic

device was lowered at a rate which separated it from the soil. At this point, the test was stopped and the soil was allowed to regain contact. Observations of this nature were made by watching the device pressure-time curves. The soil never lost contact with the top of the spring-ring device, because the outside pressure of the soil was continually pushing against the spring in the device and vice versa.

Another element of the problem involved the method by which differential deflection was measured. The so-called "free-field deflection gage" was located 14 to 16 inches from the centerline of the test chamber. Differential deflection was measured in reference to this "free-field" gage. But in the previous section, it was shown that the area involved in the arching generally extended no further than 1 structure diameter outside the device and many times only 1 structure radius. Both the structure and the soil reacted to pressure within the affected area. In active arching the structure unloaded to the soil in its immediate vicinity and the soil reacted to the differential deflections directly above and beside the device. It was the deflection differences between the structure and the soil at the level of the top of the device which affected the soil above it. Once the structure started to load the soil, then the deflection of the soil adjacent to the structure increased. There was some time-dependent interaction between the soil and structure, similar to that observed by R. B. Peck in his analysis of observed deformations in the

Chicago subways, as the load was shifted back and forth seeking an equilibrium condition. But the soil, being a viscous material, reacted much more slowly than the device which reacted almost instantly.

The device for Test 6 was designed to be approximately one-half as stiff as the soil. The Test 6 data are plotted when ultimate arching was first reached and at two values during the long creep period, Table 5. The initial arching value for this spring-ring device plotted considerably above the arching curve for the hydraulic device at a comparable deflection. As time progressed and the differential deflection decreased, the arching values for Test 6 appeared to approach the comparable arching curves. This was a manifestation of the time effects explained above.

The data for the spring-ring device in Test 6 are shown in Table 5 and Figure 24b. Note that the scaled differential deflection reached a value of -6.67×10^{-3} during the initial pressurization. Then the differential deflection began to decrease, because the free-field soil was deflecting faster than the structure. This is logical as the structure began to experience less load than the free-field soil and the soil under the device slowed down its rate of deflection. The differential deflection was sufficient to develop a differential pressure of 14 psi after 2 hours and 20 minutes. Yet the differential deflection as measured in reference to the free field had been decreasing since a time 47 minutes after the test began. At time 3 hours and

8 minutes, the differential pressure had decreased to 12.5 psi and the differential deflection had decreased to -0.008 inch.

During the second pressurization of Test 6, scaled positions of pressure and deflection almost identical with the initial pressurization were attained. During the 63-hour creep period, the soil and structure attained an equilibrium position at ΔD = 0.0008-0.009 inches and ΔP = 11.2-12.9 psi . Thus the structure experienced a load which varied from 0.66 to 0.69 times the surface pressure. The structure's relative stiffness as compared to the soil was 0.60.

The arching results using the spring-ring device in Test 7 also are plotted in Figures 92 and 94. When the data for Test 7 are compared with those of Test 6, a much more flexible device, the differential pressures reflect their flexibility difference. One immediately questions why the differential deflection in Test 7 was larger at minimum arching. Close examination of the data in Table 5 shows that the deflections under the device were considerably larger in Test 7 and more than compensated for the difference in the deflection of the tops of the devices which was a result of their relative flexibilities.

Figure 39 can be used to examine the deflections more closely. Up until the pressure container broke, the deflection at a 5.5-inch radius, 2.5 inches outside the device, at the level of the top of the device was less than the deflection at the 16-inch radius. This

indicates passive arching action. This passive arching condition near the device was confirmed by the corresponding pressure profile in Figure 28c. Yet, the total deflection of the top of the device was greater than that measured in the soil at the same level and should have produced active arching, Figure 39. The majority of the device deflection consisted of soil deflection under the device. This deflection was considerably higher than that in the free field at the same level. Thus the structure experienced some passive arching action during the course of the test, relative to the deflections and pressures in its immediate vicinity, but at a test pressure of 37.5 psi, the device reacted to its deflection relative to the free field. Therefore, the total effect was active arching, Table 1.

Three points at P_S = 40 , 75 , and 100 psi have been plotted in Figure 92 for the spring-ring device of Test 8. The points are above the arching curves for Configurations I and II. The interrelation between differential deflection and the arching ratio at these surface pressures appears to have no relation to the arching curves produced at P_S = 37.5 and 75 psi by Configuration II.

Comparison of the differential pressures shown in Table 5 for Tests 6 and 8, both spring-ring device tests, at $\Delta D \approx$ -0.006, -0.034, and -0.040 during the pressurization process shows that the differential pressures between surface and structure are within 1 psi of each other in spite of the differences in H/B , 1 versus 3, and

surface pressures at these various deflections. When P_S exceeded 75 psi in Test 8, the differential pressures for this test were no longer identical with those in Test 6 at the same differential deflections.

From an examination of the static arching data produced in this test program and that produced by Hendron, it must be concluded that the amount of active arching is dependent upon the location of the structure relative to the fixed boundary underneath it. In addition, the manner of inducing arching is important. The amount of active arching produced by lowering the top of the device by decreasing the internal pressure was higher than that produced by a comparable spring-ring device whose deflection was caused by external pressures acting on the device. Thus, both the location of the test structure with reference to a fixed boundary and the path of loading are important in studying active arching. The differential pressure experienced by the structure is not simply a function of the differential deflection between the structure and the soil at some particular point. Both the free field and immediately adjacent soil deflections appear to affect the amount of active arching which the structure can induce.

In Figure 93 the passive arching curve produced in Test 5 using the hydraulically controlled test device is shown along with a comparable trapdoor test by Hendron. Until the scaled deflection reached approximately 15×10^{-3}, the curves are very similar. This appears

to be reasonable since the lower boundary of the test chamber should not be as important as in active arching, i.e. no unloading to a fixed base. In passive arching, it is the strength of the soil above the device which is involved. After a scaled differential deflection of 15×10^{-3} was exceeded and the arching factor approached 2, the effects of the soil over and under the device began to be seen in Figure 93. The hydraulic structure in Test 5 could never be as rigid as the trapdoor because of its location within the medium. The structure-soil system acts like a compound spring system. The higher the load on the structure, the more the soil under the device governs the actions of the system.

Figure 37 shows a comparison of the relative deflections during pressurization and the creep period while the top of the device used in Test 5 was held rigid. Note that the base deflection significantly exceeded the deflection of the soil at the same level. This behavior was observed throughout the test. The interaction between the device and the soil under it is not present in a perfectly rigid trapdoor and partially accounts for the fact that larger passive pressure differences were observed on the trapdoor than on the top of the floating structure used in this study.

Based on the very limited data available at $P_S = 37.5$ psi and $H/B = 1$, the lower boundary of the test chamber appears to have no effect on the passive arching phenomenon itself. The presence of the

soil under the device does limit the stiffness and thus the actual differential deflection possible with the floating device as compared with the rigid trapdoor.

5.1.3 Pressure Effects. Because of the pressure leakage observed in Test 2, it is difficult to determine pressure effects in the static test series. A plot of differential pressure versus differential deflection for both the trapdoor and hydraulically controlled device is shown in Figure 94.

At a scaled depth of $H/B = 1$, Hendron's data show that the differential pressure increased at a constant differential deflection when the surface pressure was increased from 37.5 to 75 psi. The pressure difference increased with increasing differential deflection. This action appeared to result from the change in modulus of the soil with surface pressure. Data from the present test series show similar effects within the range of deflections available.

The differential pressures attained in both this study and Hendron's show that a surface pressure of 37.5 psi was insufficient to develop the full strength of the clay, Table 1 and Figure 94. The slopes of the curves for $P_S = 75$ psi and $H/B = 1$ plus the differential pressures of approximately 45 psi ultimately attained in both sets of experiments show that the full strength of the soil was developed at large differential deflections, -9.14×10^{-3} for the trapdoor configuration and -77.17×10^{-3} for the floating device.

The large difference between the differential deflections required to develop a particular differential pressure is attributable to the lower boundary effects in the trapdoor experiments.

The effects of surface pressure also were studied by comparing the results obtained in Tests 3 and 8 at $H/B = 3$ and $P_S = 37.5$ and 240 psi , respectively. Early in the pressurization of Test 8 at differential deflections of -0.006 and -0.012 when the surface pressure was 30 and 60 psi, respectively, the differential pressures attained at comparable differential deflections were almost identical, Table 5. Once P_S exceeded 65 psi in Test 8, the results were no longer comparable with Test 6 in which the maximum P_S was equal to 37.5 psi. These results appear to show that at low surface pressures soil modulus is important, but at high surface pressures the soil strength determines the differential pressures attainable at a constant depth of burial.

It is of interest to compare the pressure profiles in Figures 26 through 28 with the theoretical pressure profiles shown in Figures 3 through 5. In Figure 3a Monfore shows a distribution determined by elastic analysis. Although the distribution was devised to determine the effects of geometry and relative compressibility on the registration of a pressure gage, it is just as applicable to the device used in this test series. No attempt was made in the present experiments to determine the distribution of pressure on the top of the device.

The distribution very near the gage resembles that seen in the active tests, for example Figure 26a. Note that the extent of the high-pressure region is dependent upon the ratio of the gage thickness to the gage diameter. According to Monfore's two-dimensional elastic solution, effects should have been observed to a radius of approximately 12 inches. This was not found to be true in the three-dimensional tests performed in this study. The majority of the redistribution of the arching effects occurred within one structure radius of the outside of the device. None occurred outside of a radius equal to one structure diameter. As discussed in Chapter 4 and Section 5.2.1 and as illustrated by comparing Figures 26b and 27c, an increase in surface pressure from 37.5 to 75 psi at a constant depth of burial of 6 inches does enlarge the area adjacent to the top of the structure affected by active arching.

Finn also presented an elastic solution to a similar problem. His distribution of arching stresses resulting from the lowering of a trapdoor is shown in Figure 4 and is similar to that shown by Monfore. The shape of the distribution also is similar to that observed at the level of the top of the device during the low-pressure (37.5 psi), static, active arching tests in the present program.

Finn's solution shows that the effects of active arching are dissipated at a height of 2-1/2B or 15 inches, in our case, above the

trapdoor. Compare this with the effects shown in Figure 32. Except during long-term creep at P_S = 240 psi , the results of the static tests confirm Finn's results. In fact, the effects appear to dissipate at a height of less than 2-1/2B. Examination and comparison of Figures 31b with 31d and 32a with 32b indicate that the height above the device to which arching effects extend is affected by pressure. At P_S = 37.5 psi the effects appear to extend one structure radius as compared to one structure diameter at 50 psi. Some of these effects may have been due to creep. When the 37.5-psi results at $H/B = 3$ are compared with those of P_S = 240 psi at $H/B = 3$, the height affected appears to extend less than two structure diameters at the higher pressure as compared to less than one structure diameter at the lower pressure. This appears to be the result of the three-dimensional effects and the total amount of energy dissipated within a given volume of soil under plastic and elastic deformation conditions.

The tension discussed by Finn, Terzaghi (1919) and Richart appeared to be present in the experimental program. Although the tensile forces transmitted within the medium could not have been large, examination of the deformation patterns within the soil, especially within one structure radius above the device, showed that tension stresses had existed.

Section 2.6.2 of Chapter 2 discusses the work of several authors

in more detail. One of the more interesting is an elastoplastic solution for the stress around a tunnel located in rock by Sirieys, Figure 5. Although the distribution cannot be applied directly to the test results in this report, it can be of assistance in interpreting the distributions observed. The distribution developed by the elastic solution, Figure 5d, is similar to those shown in Figures 3 and 4 but was changed considerably by the plastic region, Figures 5b and 5c. The latter distributions appear very similar to those in Figures 26 through 28. An elastoplastic solution certainly seems to be more reasonable based on the properties of the material and the observed test results.

During the passive arching phase of Test 4 with a hydraulically controlled device at a scaled depth of 1 and a surface pressure of 75 psi, the maximum differential pressure was +36.1 psi. This pressure was only 2.7 psi less than that developed during the initial passive arching phase of Test 5. Within the 37.5- to 75-psi range of surface pressures, there were virtually no surface pressure effects at a scaled depth of 1. This lack of significant pressure effects also was observed by Hendron (1968) as shown in Figure 97.

In summary, the volume of soil affected by active arching appears to increase with an increase in the surface pressure from 37.5 to 240 psi at a constant depth of burial. The amount of active arching at $H/B = 1$ is increased by increasing P_S from 37.5

to 75 psi. At P_S = 37.5 and H/B = 1 , all of the surface pressure was dissipated by active arching. At P_S = 75 psi and H/B = 1 , the maximum differential pressure developed was 3.3 times the unconfined shear strength of the clay as determined by both the trapdoor and the hydraulically controlled floating structure.

5.1.4 Depth of Burial. Figure 95a is a plot of the limited static data which shows the effects of depth of burial. The plot could just as easily have been made with straight lines. A similar plot was used by Mason (1965) to present the effects of burial depth in sand.

The important finding is that at a scaled burial depth of 1 the soil was able to absorb the full surface pressure of 37.5 psi under active arching conditions. A scaled depth of 3 was not required to take full advantage of active arching at this surface pressure and with water contents of approximately 26 percent. Similar results were found when Tests 2, 3, and 5 were recycled through the active arching phase.

When the surface pressure was raised to 75 psi, a scaled depth of 1 was not sufficient to completely dissipate the surface pressure. The arching curve for this test in Figure 23 shows that further device deflection would not have changed the differential pressure significantly. The maximum differential pressure attained was approximately 3.3 times the unconfined shear strength of the clay.

In Test 3 at $H/B = 3$, the last active cycle was at a surface pressure of 50 psi. Even after remolding, a scaled depth of 3 was sufficient to dissipate the full surface pressure and a scaled differential pressure, $2\Delta P/q_u$, of -2.73 was developed.

When the surface pressure was raised to 240 psi with the spring-ring device at $H/B = 3$, the maximum scaled differential pressure reached -5.2, Table 1. From the appearance of the arching curve in Figure 25b, it can be seen that this differential pressure was probably the maximum active arching available at this depth of burial and soil strength.

Figure 95b was prepared at a reasonable and constant $\Delta D/B \times 1{,}000$ of -2.5. In this manner, it is easier to see the effects of depth of burial at $P_S = 37.5$ psi. Figure 95a shows that the structure was fully buried at $H/B = 1$ and $P_S = 37.5$ psi. This condition is also apparent at the deflection used in Figure 95b. At $P_S = 37.5$ psi and small structure deflections such as those illustrated in Figure 95b, the soil and structure appear to be responding chiefly to modulus considerations. This is further illustrated by the effects of raising the surface pressure to 75 psi at $H/B = 1$.

Figure 94 also indicates the effects of depth of burial at various scaled deflections. Within the 37.5- to 75-psi surface pressure range, a given deflection dissipates more load at deeper depths of burial until the entire surface pressure has been dissipated. Take, for

example, P_S = 37.5 psi at scaled depths of burial of 1 and 3. At these depths of burial, the structure is "fully buried." This does not mean that the maximum arching possible at these depths of burial has been developed. But if the arching curve becomes parallel to the deflection axis and the differential pressure is less than the surface pressure, then the maximum arching for this depth of burial has been developed. The curves for $H/B = 1/3$ at P_S = 37.5 psi in Figure 94 are an example of this.

Figure 94 shows that active arching is very sensitive to depth of burial at a surface pressure of 37.5 psi and shallow depths of burial. Ultimate arching at P_S = 37.5 psi was developed at both $H/B = 1$ and $H/B = 3$ when a large range of differential deflections was available.

The number of static, passive arching tests was insufficient to draw any conclusions concerning the effects of depth of burial. The one data point available is shown in Figure 95.

As structure burial increases at a constant surface pressure and differential deflection, the amount of active arching will increase until the structure becomes fully buried. At this depth, all the surface pressure has been dissipated by the arching and further burial is not necessary. At 37.5 psi, further burial, increasing H/B from 1 to 3 , does increase the differential pressure more rapidly, i.e., at a constant differential deflection and surface pressure, more load

is arched away at the deeper depth.

5.1.5 Arching Curves. The static arching curves in Figures 21 through 25, 92, and 94 show that as a structure pushes into the soil around it the arching curve follows a different path from that which it follows when it pulls away from the soil around it. The load-deformation curve does not follow along the same path in the loading and unloading cycles. This is an important consideration for those formulating interaction and/or design codes. The form of the arching curves, their slopes, their range of values, and their change from active to passive or vice versa should be considered in the design of a soil-structure interaction code.

Examination of the active arching portions of Figures 21 through 24a shows that as the top of the hydraulically controlled device pulled away from the soil, a decrease in the load was experienced by the structure. Initially, the load decrease was very large for small deflections. If it were possible to scale these curves to a practical structure size, according to the results for Test 1, the top of a structure 20 feet in diameter, with less than 7 feet of earth cover, should only have to experience a total deflection of approximately 2.1 inches, of which 1.1 inch would be punching of the base into the soil, to lose approximately 27 percent of the incident load, at a surface pressure of 38 psi. If the total deflection of the structure was increased to 5.3 inches with its top deflecting 3.8 inches with respect

to the base, approximately 1.5 percent of the structure span, 43 percent of the load would be arched away from the structure.

If this same structure had 20 feet of clay cover (H/B = 1), the test results indicate that a total structure deflection, base plus top relative to the base, of approximately 0.4 inch would be sufficient to arch away 27 percent of the load. Over 92 percent of the load could be relieved with a total structure deflection slightly over 3.5 inches.

By increasing the surface pressure to 75 psi at this 20-foot burial, and at a total structure deflection of less than 0.5 inch, the load arched off the structure, approximately 10 psi, did not change. Obviously the percentage of load lost decreased, but the amount of soil shear strength mobilized for this differential deflection at this depth changed very little with the doubling of the surface pressure.

At the 75-psi surface pressure, Figure 23 shows that it was not possible to arch away 90 percent of the load with only 20 feet of cover. The maximum differential pressure was approximately 60 percent of the surface pressure.

Comparing ultimate arching in Tests 2 and 4, Table 1, it can be seen that the full shear strength of the soil was not being utilized in Test 2 even though the arching curve was parallel to the deflection axis. A larger differential pressure, -45.2 psi versus -37.0 psi, was

developed in Test 4 with P_S = 75 psi . In Test 2, the ΔP was approximately equal to the surface pressure, so no more load was available for arching. The mere fact that an arching curve is parallel to the deflection axis or the arching ratio is near zero is not sufficient evidence to state that ultimate arching exists. In order to prove maximum arching at a particular depth, the differential pressure must not increase with increasing deflection and it must be less than the surface pressure.

The arching curves for the spring-ring device in Figures 24b and 25b show that load was not arched away from the structure as rapidly with deflection as when the top of the structure was pulled away from the soil. The initial slope of the arching curves is considerably less than the slope in a comparable test using the hydraulic device, Figure 21b. Apparently considerable deflection is required to induce significant arching. For example, it took over 3 times as much differential deflection to lose approximately 10 psi in Test 6 as it took to lose the same ΔP in Test 2. The total structure deflection in this case was over 17 times as much and the deflection of the top alone was over 5 times as much as required to lose the same pressure in Test 2.

Figure 24b shows that the ultimate differential deflection of Test 6 was very close to that in Test 2 because the soil under the device reacted sharply to the unloading of the structure. At a differential pressure of 14.1 psi, the scaled differential deflections

were 2.17 and 2.50 in Tests 2 and 6, respectively, and the deflections of the top of the device with respect to the base were 0.14 and 0.12.

Comparing Figures 24b, 25a, and 25b with Figures 21 through 24a reveals that the shape of the active arching curves was changed by the change in test methods. The pressure-induced curves (spring-ring device) have a flatter initial slope. The shape of the passive portions of the curves was not affected to the same degree as there was only a slight decrease in the slope of the pressure-induced curves.

Figures 92, 93, and 94 show that the form of the active and passive arching curves produced by using the trapdoor configuration is very similar to those produced by the structure-induced arching in Tests 1 through 5 of this program. In addition, most of the recycled passive arching curves are similar to the structure-induced curve in the initial cycle of Test 5.

The active and passive curves produced using the hydraulic test device have a similar shape, Figures 21 through 24a. This is especially true for Figures 21a, 23, and 24a. In Figures 24b and 25b, the active and passive arching curves produced using the spring-ring device are not similar; the passive curves resemble the passive curves in Figures 21 through 24b and the active curves are not similar to the curves produced by any other test method. Thus, the form of passive arching curves does not appear to be affected by the method of inducing arching but that of the active arching curves is.

The larger deflection needed to induce active arching when the structure is loaded externally could be very important in buried structure design and shows that the use of arching curves produced by the reduction of internal pressures at a constant surface pressure to simulate active arching conditions on a real structure is questionable.

5.1.6 Active and Passive Arching. From an analysis of the test results, it can be seen that active arching is dependent upon at least the following variables: surface pressure, depth of structure burial, relative deflection between soil and structure, soil strength, and structure flexibility. The test results also showed that active arching is sensitive to the test configuration used and the method of inducing arching, i.e., decreasing the pressure on the inside of the structure or increasing the pressure of the soil surface.

At a particular surface pressure, it is possible to develop full arching if the structure is buried deep enough and has sufficient flexibility. Thus, flexibility and depth of burial both contribute to the reduction of the design load. The flexibility aspects of Tests 6, 7, and 8 are discussed with the dynamic tests in Section 5.3.

Several methods of design which take into consideration soil arching have been proposed. Some of the more important contributions are discussed in Chapter 2. In general, these methods may be divided into two classes: those which consider the equilibrium of horizontal differential soil elements between two sliding surfaces, and those

which consider that actual arches form in the soil. In the first case the sliding surfaces are usually vertical, but some authors have considered surfaces which propagate at an angle to the vertical.

As discussed in Section 5.1.1 there were no clearly defined shear planes under active arching conditions. There appeared to be a zone of deformation which extended both inside and outside of the volume of soil directly above the device. The zone was most clearly seen in Test 1 since the deformation pattern intersected the soil surface, Figures 41 and 42. The deformations seemed to indicate failure in the soil. The strain measured at the top of the device ranged from 16 to 25 percent and that at the surface ranged from 9 to 16 percent. With strains of this magnitude, the strength of buckshot clay is normally developed, Appendix A.

Based on the deformation patterns and the soil characteristics, an attempt was made to analyze Test 1 and later Tests 3 and 4 using a shear plane analysis.

Terzaghi's (1943) solution to the static soil arching problem, as modified by Mason (1965), was tried initially:

$$P_T = \frac{B}{4K \tan \phi}\left(\gamma - \frac{4C}{B}\right)\left[1 - e^{-2K(\tan \phi)\frac{2H}{B}}\right] + P_s e^{-2K \tan \phi \frac{2H}{B}} \quad (13)$$

(Equation has been modified to incorporate notation used in this report.)

γ = the unit weight of the soil. Assumed to be zero since its effects are so small as compared to those of P_S

C = soil cohesion

ϕ = angle of internal friction or shearing resistance

(It is recognized that both C and ϕ may not actually describe the phenomena alleged in the definitions. They are used as the parameters which describe the intercept of the rupture line with the vertical axis and the slope of the rupture line with reference to the horizontal axis in a Mohr's diagram.)

Values of ϕ and C were determined by UU or Q triaxial tests, Appendix A.

Values for K , the ratio of horizontal to vertical stress, were estimated using Figures 29 and 32. Four values of K , 0.8, 0.9, 1.0, and 1.1, were tried. Actually this solution is not sensitive to changes in the value of K for values of ϕ nearly equal to zero. The stress acting on the structure which was calculated using this approach, and assuming full development of shear planes to the surface, was approximately 10 psi higher than the stress measured in Test 1. For Test 4 at P_S = 75 psi and H/B = 1 , the calculated stress acting on the structure was approximately 26 psi lower than that measured when 6 inches of cover were considered and approximately 8 psi higher than that measured when only 3 inches of cover were considered. If the Terzaghi approach, as modified by Mason, was

going to be applicable to the static tests in this program, it should have worked for Test 1 at $H/B = 1/3$. The soil deformations observed and the arching curves indicate that the shear strength of the clay above the device was fully developed. A check of all static, active arching tests showed that this approach was overly conservative when $H/B = 1/3$ was considered and that it severely underestimated the loads on the structure at $H/B = 1$ or more.

The design procedure in the Air Force Design Manual by Newmark and Haltiwanger also was tried. (This procedure in several forms appears in many publications.) Case 1, which assumes the development of maximum shearing stress along the entire slip plane, was used.

$$\frac{4C}{B} + \frac{4P_s \tan \phi}{B} = \left(\frac{4C}{B} + \frac{4P_T \tan \phi}{B}\right) e^{\frac{4KH \tan \phi}{B}} \qquad (14)$$

(Equation has been modified to use notation used in this report.)

For Test 1 at $H/B = 1/3$ and $P_S = 37.5$ psi , the calculated solution for the stress acting on the structure was approximately 8 psi higher than the measured stress. In Test 4 at $H/B = 1$ and $P_S = 75$ psi , the calculated value of P_T was conservative by approximately 20 psi when compared with its measured value.

Although shear deformations were found in the soil, this does not prove that something similar to soil arches does not form in the soil. It would seem to be natural for the soil to tend toward an arch formation in order to transfer stress around a cavity, Richart. Soil

radiographs and examination of the actual soil indicate that there may be such a phenomenon, for example, the deformation patterns in Figure 41b. A tension crack can be seen in the soil at the upper right corner of the structure. This shows that the structure and soil dome partially pulled away from the soil above. Notice the change in the texture of the soil above and below this crack. Above the crack, the soil appears to be deforming in an arch pattern. The support of the arch would be adjacent to the top of the device in the heavily deformed material. Figure 26a shows that pressure was concentrated in this deformed area.

An analysis of Test 1 was attempted using an arch theory similar to that hypothesized by Engesser and later alluded to by Tschebotarioff (1951). A parabolic arch with supports in the area delineated by Figures 26a and 41b was used. A uniform vertical loading was assumed so that tensile and bending stresses were avoided. The maximum support reaction was assumed to be the surface pressure multiplied by the coefficient of passive earth pressure. The use of this coefficient would appear to conform to the stress conditions hypothesized by Terzaghi (1943).

Using $\phi = 6$ degrees and $C = 9.0$ psi, as determined by UU triaxial tests, in the following equation

$$K_p = \tan^2 45 + \frac{\phi}{2} + \frac{2C}{\sigma_3} \left(\tan 45^\circ + \frac{\phi}{2}\right) \qquad (15)$$

the value for K_p was determined to be 1.86 using an overpressure, σ_3, of 37.5 psi. The maximum pressure which the soil could support with P_S = 37.5 psi would be approximately 70 psi, assuming that the coefficient of passive earth pressure governed the support capacity of the soil. Examination of Figure 41b shows that the arch reaction should be inclined at an angle of approximately 45 degrees from the vertical. This is reasonable when compared with the 37.2 degrees measured in Test 8 at H/B = 3, Figure 34. Using 45 degrees as the inclination of the reaction and a maximum reaction of 70 psi, the vertical component of the reaction is 49 psi. Figure 26a shows that active arching affected the soil at the level of the device to a radius of 6 to 6-1/2 inches. The peak pressure measured in this area at ultimate arching was 47.5 psi. When a load balance was made within an area surrounding the centerline of the test chamber at a radius of 6 inches, using a surface pressure of 37.5 psi and a vertical reaction of 49 psi in the annular area surrounding the device, no load should have been measured on the device. The actual load on the top of the device at maximum arching was 13.3 psi.

Although Figure 34 was constructed using Test 8 data, it should be an indicator of the directions and changes in direction of the principal stress. In hypothesizing arches within the soil, one might assume that the direction of the principal stress would be vertical above the arch and horizontal below the arch under active arching

conditions. Figure 34 shows that 6 inches above the device the principal stress was essentially vertical at the beginning of the test and rotated toward a horizontal direction as the arching action progressed. The stress circle at the 4.5-inch radius 6 inches above the device shows the principal stress acting in a direction which would appear to coincide with the direction of the compressive stress within a "soil arch." The principal stress is directed away from the soil above the device at an angle of 40 degrees to the vertical. The stress circle approximately 2 structure diameters directly above the device and at a 4.5-inch radius shows the load being directed away from the soil above the device. The direction of the principal stress at this level also changed from a vertical position to a position which might correspond to the axis of an arch if one existed.

The planes of maximum shear shown at the level of the top of the device at a radius of 4.5 inches are more vertical than those hypothesized in Figure 42 for Test 1.

The hypothesized planes of maximum shear were drawn by using the extent of the deformed area above the device. The area involved would correspond to the zone of radial shear if one existed. The 37.5-psi surface pressure and the extent of the vertical deformation were sufficient to cause soil failure to occur under triaxial conditions. The specimen in the triaxial tests for Test 1 failed by bulging, not by the development of cracks or slip planes.

The deformation phenomenon which occurred at some depth in most of the static, active arching tests raises questions concerning both the slip plane and the arching theories. Neither theory explains the soil bulging around the depression which occurred at the surface for Test 1, Figure 41b, and at various depths for other tests, Figures 45 and 89. This hump sometimes progressed to a radius of 9 to 12 inches or one structure diameter outside the depression. The appearance of the soil under the ridge or hump was similar to that seen in a triaxial test when the soil failed by bulging rather than along a shear plane. In the radiograph for Test 1, Figure 41b, what appear to be fissures in the soil can be seen under the ridge. With the soil depressing under a compressive stress as its support was removed the horizontal stress increased under the active arching conditions until the surface pressure became the minor principal stress. As the soil failed under compression, there was no place for the displaced soil to move but up and away from the top of the device.

It is difficult to make a rigorous analysis of the active arching problem although some have been proposed. Most solutions are two dimensional. When the three-dimensional aspects of the problem are attacked, then attempted solutions become extremely complicated and require assumptions concerning the properties of the soil which are only approximate and certainly not as exact as the analysis might lead one to believe. In spite of the simplifying assumptions, a solution

to the static arching problem which agrees with test results has not been produced and the prospects are remote.

The soil deformations discussed above, especially the zone of plastic flow, are one indication of the difficulties inherent in this problem. Another indication is the fact that the principal stresses directly above the device were not vertical for passive arching or horizontal for active arching as most attempts at solution assume, Figure 34. Terzaghi (1943) assumed that the stress acting on top of his trapdoor was the minor principal stress under active arching conditions. This was not generally true during these tests until the soil actually separated, and then all the soil plug was under minimum stress. The soil directly above the device adhered to its top. The angles which the radials limiting the so-called zone of radial shear made with the horizontal plane did not correspond to reasonable ϕ angles for this material.

The passive arching problem received only a cursory examination during this study. The soil deformation patterns shown in Figures 47, 48, and 49 were clearly depicted. One or more domes formed above the device as it was forced into the soil. The soil deformed around this dome and the slickenside appearance of the dome is evidence of this movement, Figure 47a. Underneath the device, the soil deformations did not appear to correspond to those observed above the device. The device punched into the soil somewhat. The soil sloped toward the

center of the test chamber, Figure 47b. The pressure profiles and a radiograph made of the Test 7 soil specimen indicate that the soil deformation pattern was consistent with classic bearing capacity theory.

The deformation pattern observed above the device conformed generally with that hypothesized by Mason (1965) and that observed by Abbott and others in sand. The deformation pattern under the device did not conform to any other previous theory or hypothesis.

Mason's proposed solution for the passive case is a modification of the Terzaghi approach. A comparison of the results from Test 5, at $P_S = 37.5$ psi and $H/B = 1$, with the solution to Mason's equation,

$$P_T = \frac{B}{4K \tan \phi} \left(\gamma + \frac{2C}{B}\right) \left[e^{2K(\tan \phi)\frac{2H}{B}} - 1\right] + P_s e^{2K(\tan \phi)\frac{2H}{B}} \quad (16)$$

using soil parameters determined by triaxial test, $C = 11$ psi and $\phi = 3$ degrees, was made. This comparison showed that ΔP was 57.6 psi using the equation while a ΔP of 38.8 psi was measured in Test 5.

5.2 DYNAMIC TESTS

The dynamic test program consisted of 20 tests using the spring-ring device. Tests 11 through 14 were used to study surface pressure effects. Tests 11, 13, 15, 16, 18, and 19 were used to study the effects of structure burial. Tests 11, 17, 24, 25, and 27A, B, C were used to study the effects of repeated loadings on the same soil specimen. Tests 20 through 28 were used to study the effects of structure

flexibility. It was not possible to conduct a number of similar tests in order to obtain a statistical average, and results and conclusions must be evaluated with this fact in mind.

5.2.1 Soil Profiles. As with the static tests, the deformation patterns observed were more distinct at the higher pressures, Figures 79, 82, and 84. In addition to being more distinct, the deformations propagated farther vertically and horizontally. Compare Figure 79 with Figures 82 and 84. Only one distinct depression was observed in Test 12, while two were found in Test 14 and three in Test 18.

Although Test 18 had a somewhat higher pressure than Test 14, 310 versus 245 psi, the Test 18 structure was also buried 2-1/3 times as deep, 42 versus 18 inches. The spreading of the deformation pattern, which can be seen in Figure 84, evidently is a manifestation of both depth and pressure. Figure 87 seems to confirm this conclusion.

In addition to the increase in the number of depressions with pressure, the hump surrounding the depression pattern, previously discussed in Section 5.1.1, increased in size with increased pressure.

At P_S = 37.5 psi, the depression-hump pattern was not observed. Fracture patterns similar to those in Figures 79 and 87 were seen. Evidently the pressure was not sufficient to create large distinct

soil deformations. It is assumed that the soil phenomenon was the same at the low pressures, but of lesser extent. With proper techniques and sufficient time, it might have been possible to discern the soil deformations using X-rays.

A composite drawing of the soil deformations is presented in Figure 96. The triple depression within the 46- to 48-inch layer was not found in soil specimens with $H/B = 3$. It was seen only in Test 18 at $H/B = 7$, Figure 84. The fracture patterns are typical of all dynamic active arching tests. The center depression did not propagate to the surface even with a scaled burial depth of 1/3. The center depression appeared to become smaller in diameter as it propagated above the device. The fracture patterns above and below this depression seemed to be almost a mirror image of each other. The soil in the depressions surrounding ridges was very compressed and dense. Although the soil in the layer above a depression would deform into the depression, the deformation did not appear to be continuous through a layer of soil. For example, it was not possible to follow the central depression from the device to the surface through each layer of soil. The depression was found only at the artificial surfaces within the soil created by the compaction process. The soil hump around the depression generally became larger in diameter as it propagated toward the surface. The surface of the hump was slick and livery in appearance. Soil movement had taken place between the layers. Outside

the raised hump, the soil was normally tightly bonded and difficult to remove.

The ridges and depressions in the soil were very distinct when found. Figures 80 and 81 are good examples of the deformations observed.

At the level of the top of the device, the principal effects of active arching extended to a region 9 inches or less from the centerline of the test chamber or within one structure diameter outside the device. The majority of the unloading effects appear to extend no farther than one structure radius outside the device. The pressure profiles in Figures 60 through 62, 82, and 84 illustrate this point. Consideration of equilibrium at the level of the top of the device confirmed the pressure profiles.

A second loaded region at approximately the 10- to 14-inch radii can be seen in Figure 63a. This area was the principal loaded area for Test 23, which used a very flexible device. This makes sense when the large deflection of the structure is considered.

The soil layer adjacent to the device was very deformed in the areas loaded by the active arching, Figure 83. The soil deformations corresponded very closely with the vertical pressure profiles at the level of the top of the device.

The pressure profiles showing variation of soil stress with depth, such as those in Figures 64 through 66, showed that the effects

of arching extended at least 12 to 15 inches above the device depending upon surface pressure and depth of cover. This was confirmed by the deformations observed. The pressure profiles also showed that the arching effects progressed upward with time, but much more rapidly than under static conditions. As the arching moved up, the region approximately 3 inches above the device appeared to become free of arching effects. For example, a region between 3 and 12 inches above the device was affected in Test 13. The major portion of the arching appeared to be taking place within the soil one structure diameter above the device. All tests showed that the majority of all active arching took place within 3 to 6 inches above the device, except for Test 15.

In all the active arching tests there was a region 1 to 3 inches thick at the soil surface which appeared to be completely unaffected by the arching.

The height and width of the arching effects were confirmed by pressure ratio checks such as those illustrated in Figure 68. Figure 68b shows strong arching action one structure diameter above the Test 14 device, and Figure 68c shows strong arching action extending horizontally approximately one structure radius outside of the device. The more flexible devices in Tests 20 and 23 caused major arching action to progress higher in the soil. This can be seen in Figure 68e.

A comparison of the soil deformations under dynamic loads with those in static tests discloses that the deformations are usually not as distinct under low pressure, dynamic loading conditions. This is reasonable when the viscous nature of the clay is considered. The large, long-term movements associated with the static tests are not possible under dynamic loading conditions. The dome-shaped soil formations found within the small depressions in the dynamic tests were not always present under static conditions. The fracture patterns shown in Figure 96 were not prevalent in the static tests, Figure 89, but the more or less continuous, folded and distorted soil formations found in the static tests were not prevalent in the dynamic tests.

Active arching under dynamic conditions involved more than one type of soil deformation. Apparently no continuous slip planes developed but the soil did deform in a way that indicates that shearing stresses were involved. The soil was forced down by the surface pressure. The device moved down faster and farther than the soil; therefore, the soil moved inward in a set of steps as the device moved down. These depressions appeared to be a manifestation of shear. The soil's shear load was transferred in concentric circles away from the center of the test chamber just as explained for the static tests. The load was dissipated as it was transferred outward and upward through the soil. When the load was sufficient to fail the soil, a distorted zone developed as the soil moved downward.

In the low pressure tests, the soil deformed but did not distort or fail. There was some rebound but only minor permanent differential deformation.

The deformations which took place during passive arching Tests 24 through 28 were insufficient to permit detail study. A higher surface pressure was required to cause discernible distortions. Figure 88 shows the soil disturbance in Test 26. In general, the soil was massive in appearance with very little fracturing. The depression found one structure radius above the device was not similar to one found under active arching conditions. The appearance of the deformation pattern was somewhat similar to that seen approximately 3 inches under the plate in a plate bearing test, Figure 91. Figure 90 is rather typical of the deformations observed in the soil and radiographs of the passive tests.

Figure 63b is typical of the pressure profiles obtained in the passive tests, and shows that the effects of passive arching extended to a region approximately one structure radius from the device at the level of the top of the device. The pressure profiles with depth, similar to those in Figures 66c and 68e, showed that the major passive arching took place within the region approximately 3 to 6 inches above the device. Because there were no passive arching tests at depths greater than $H/B = 1$ or surface pressures greater than 64 psi, the extent of the soil deformations must be judged accordingly. At higher

surface pressures and deeper depths of burial, the extent of the soil deformations above the device due to passive arching probably would have been much larger.

5.2.2 Arching Curves. The arching curves for the dynamic tests are shown in Figures 51 through 59. Ultimate scaled arching values are given in Table 2. The active arching curves in Figures 51 through 56 are in a completely different form than those constructed for the static tests. The reason for this is the manner in which the loads built up at the level of the device and the means of measuring differential pressure. Although the critical portion of the test was measured in terms of a few milliseconds, there was a time lag in the buildup of pressure at the level of the device. Compare columns 2 and 3 of Table 6. Differential pressure is measured in terms of the surface pressure. Thus, there were some large differential pressures (ΔP) early in each test. This means that ΔP is meaningless until the pressures at the level of the device begin to stabilize near their peak value. The pressure wave has to overcome the inertia of the soil above the device before the pressure can have appreciable effects on the structure.

The only arching curves which do not begin at a high artificial value of arching are those for Tests 18 and 23, Figures 54b and 56b, respectively. In Test 23, the loads on the structure were so small that the inertia term in the equation of motion was able to cause

the load on the device to decrease instead of increase as was normally the case.

In Test 18, the inertia was again large with respect to the spring load. In this case, both values were large, but the inertia was very large because of high surface pressures involved, Table 6. The large load of 245 psi with 151 psi contributed by the inertia at 8 msec exceeded all other loads experienced by the structure. In the design of a structure under similar conditions, should this large load be considered? The question cannot be answered without determining the amount of time this load is exerted on the structure and thus the total energy the structure must absorb. If this happened to be an isolated, sharp acceleration spike, it might not be considered. Section 5.4 contains a discussion of the relation between structure stiffness and structure acceleration.

In addition to the peculiar shape of the early portions of the active arching curves, reflections from the base of the test chamber and the decrease of surface pressure cause the latter portions of these curves to exhibit some peculiar shapes. The majority of these latter points (Table 6) have been deleted from the curves, but enough were plotted to assist in pinpointing the time of arrival of the major reflected waves and to show what happens to the structure because of the reflections.

It is difficult, if not impossible, to determine whether maximum

arching has occurred by just examining the arching curves. The majority of the active curves have portions which are parallel to the deflection axis. This indicates no increase in the differential pressure with increasing deflection. The arching curves in Figure 51b are an example. The differential pressure at P_S = 70 psi was -11.0 psi. The results of Tests 13 and 14 at P_S = 151 and 245 psi, respectively, Table 6, clearly show that maximum arching did not exist in Test 12 since the differential pressures were -32.0 and -35.0 psi, respectively. The fact that ΔP only increased 3 psi when the surface pressure was increased from 151 to 245 psi along with the appearance of the arching curves in Figure 52 does show that maximum arching at $H/B = 3$ was developed in Tests 13 and 14.

One other caution in the use of these curves is the possible inaccuracies in the ΔD and q_u terms. The problem of measuring soil deflection and especially determining which soil deflection is important to the arching phenomenon has already been discussed. As explained in Appendix A, the unconfined soil strength used to scale pressures was determined using the Hvorslev miniature sampler and unconfined compression machine. Although a large number of tests were made and correlated with laboratory tests (see Appendix A), there is still considerable variation in the shear strengths for a particular water content, Figure A-7.

The arching curves in their present format appear to be difficult

to use in a design code at first glance. But deflection and load are increasing with time and there does not seem to be visible interplay between the soil and the structure. With the exception of Test 18, any loading and unloading iterations that may have existed are disguised by the overall gross loading and deflection of the structure and soil. This should be important to the designer because it can make the construction of a soil-structure interaction subroutine much simpler.

Table 2 contains a summary of the dynamic tests. The values for maximum and minimum arching were extracted from Table 6 using the arching curves. The points came from the portion of the arching curve which was generally parallel to the deflection axis. The points were selected in most cases at a time when the peak soil pressure had arrived at the level of the top of the device, but before the reflections affected the structure response to a noticeable degree. Both maximum and minimum arching are shown in the table when there is considerable difference between their values. The important point for the designer is minimum arching because this is when the maximum load is being exerted on the structure.

In the use of these curves, the reader also must be careful to look for the high loads that can be caused by the high accelerations early in the loading process.

The passive arching curves are contained in Figures 57 through

59. The form of the $\frac{\Delta D}{B} \times 1{,}000$ curves is different from the static, passive tests and also the active, dynamic tests. The decrease in the differential deflection at maximum arching was caused by the increased deflection of the base of the device as it was overloaded by the passive arching process. The $\frac{D_T}{B} \times 100$ curves do not display this peculiarity. These curves are somewhat similar to the passive curves seen under static conditions except for the lower initial slope and the effects of the pressure reflections and the decrease in the surface pressure.

The differential pressure attained under passive arching conditions in the static tests ranged from approximately +2.7 to +2.8 times the shear strength of the clay at a scaled depth of 1 with P_S = 37.5 psi. In the dynamic tests at $H/B = 1$, the maximum scaled differential pressure ranged from +0.4 to +0.8 times the shear strength of the clay except for the +1.08 in Test 25, a repeat test at 53.5 psi on the Test 24 soil specimen. The Test 25 ΔP appears high when compared with the remaining passive arching tests, especially Test 27C which was a repeat test at a surface pressure of 64 psi on a device 75 times as stiff as that used in Test 25.

The differential deflections under static arching conditions were much larger than those experienced by the structure under dynamic conditions. Both the dynamic and static data indicate

that passive arching is sensitive to only large changes in the differential deflections or absolute deflection of the structure.

For both active and passive arching, the design values given in Table 2 were selected as the maximum load acting on the device within the range of deflections which the arching curves indicated as good data. The active arching data in Table 6 show that the actual load on the device generally increased with increasing deflections for the reasons outlined above. Conversely, the static data in Table 5 show that the load on the device decreased with increasing deflection. This makes comparison of the dynamic data with the static arching curves somewhat difficult.

With the passive data, the load increased with increasing deflection for both the static and dynamic data as discussed above.

5.2.3 Depth of Burial. At a surface pressure of 37.5 psi, the depth of structure burial was critical to the amount of active arching only when the device was buried at a depth less than the structure diameter, Figure 97. Thus the device was "fully buried" at $H/B = 1$. This is consistent with the findings in Section 5.2.1 which disclosed that the major portion of active and passive arching took place within one structure diameter above the device.

Increasing the surface pressure by a factor of 4 to approximately 150 psi increased the differential pressure to 25 psi at $H/B = 1$ and 32 psi at $H/B = 3$. The structure was not still

"fully buried" at $H/B = 1$ when P_S was increased because more load was arched away from the structure at $H/B = 3$.

The maximum strength of the soil was not developed at $H/B = 1$ with $P_S = 37.5$ psi , because the higher surface pressure developed a higher ΔP . It is not possible to state whether the maximum strength of the soil was developed at $H/B = 1$ with the 157-psi surface pressure because no higher dynamic pressure test was performed at this depth of burial. There were no comparable static tests at $H/B = 1$. The lower pressure static tests at this depth of burial in which the hydraulic test device was used also were fully buried.

At $H/B = 3$ in Figure 97, it can be seen that maximum arching was probably developed in Test 13 at $P_S = 151$ psi. In Test 14 at the same depth of burial, a surface pressure of 245 psi was used yet the differential pressure only increased by 3 psi, which is within the accuracy of the measurement techniques. Thus, under dynamic loading conditions at $H/B = 3$, the soil was able to unload the structure by approximately 2.5 times its unconfined shear strength.

Measured with reference to static Test 8, at $H/B = 3$ and $P_S = 240$ psi , the high pressure dynamic tests did not appear to develop the full strength of the soil. The large amount of time and deflection allowed in the static tests prevent realistic comparison and should not be used as a basis of maximum arching. During the

15-hour creep period of Test 8, the ΔP decreased to -35 psi, exactly the same as the ultimate ΔP developed in the dynamic test at $P_S = 245$ psi .

By comparing the amount of arching at each depth of burial it can be seen that the device was not fully buried at $H/B = 1$ and $P_S \approx 150$ psi or at $H/B = 3$ and $P_S \approx 245$ psi. Since the shear strength of the soil is apparently determining the amount of arching experienced in the tests with $P_S \geq 150$ psi , the active arching will increase with an increase in the depth of burial until the amount of surface pressure available at the level of the device is insufficient to develop deflections which will develop the shear strength of the soil. At this point, the relative stiffness of the device determines the amount of arching. At the depths of burial used in this test program, it was not possible to develop a fully buried condition for P_S values between 150 and 300 psi.

One peculiarity in Figure 97 is the fact that Hendron's (1968) trapdoor data did not show a higher differential pressure than the data from this study. This apparent discrepancy or conflict with the arching curves in Figures 92 and 94 is due to the larger deflections developed at ultimate arching in the present study. Figure 98 in which all points in a particular set of curves are plotted at the same differential deflection shows the data in its proper perspective.

It is difficult to compare arching at various depths over the

wide range of relative deflections which induced ultimate arching for a particular test. For example, in comparing the $\Delta D/B \times 1{,}000$ values in Table 2 for Tests 15, 16, and 11 at scaled structure burial depths, H/B, of 1/3, 1, and 3, respectively, it can be seen that the scaled deflection at ultimate arching, $\Delta D/B \times 1{,}000$, increased from -0.33 to -8.50 to -11.67, respectively.

The amount of scaled deflection required to develop a constant scaled differential pressure increases with an increase in the depth of structure burial if surface pressure and the stiffness of the structure relative to the soil are held constant. There appears to be some relation between the $\Delta D/B \times 1{,}000$ required to develop a particular ΔP at a particular H/B, but no consistent relation could be developed. For example if $2\Delta P/q_u = -0.83$ is selected in Tests 15, 16, and 11, the respective values of $\Delta D/B \times 1{,}000$ are -1.33, -4.83, and -7.98. There is a difference of 3.50 between the $H/B = 1/3$ and $H/B = 1$ values, and a difference of 3.15 between the $H/B = 1$ and the $H/B = 3$ values.

In order to study the effects of structure burial depth in more detail, Figure 98a was prepared in terms of the load acting on the structure divided by the surface pressure. This relation is generally called the arching factor. The dynamic data were plotted at the deflection at which ultimate arching developed, but the static data points were plotted by selecting the arching factor at the same scaled differential deflection as the comparable dynamic test. The dynamic data at

P_S = 37.5 psi again show that the structure was fully buried at H/B = 1 because there was no decrease in the load on the structure when H/B was increased to 3. The full surface pressure was not arched away under dynamic conditions as was the case when the hydraulically controlled device was used under static conditions. The load experienced by the spring-ring device at P_S = 37.5 psi , whether statically or dynamically applied, is determined by the stiffness of the structure relative to that of the surrounding soil. This effect will be discussed in more detail in Section 5.2.5.

At P_S = 150-157 psi, it can be seen in Figure 98a that the structure was not fully buried at H/B = 1 . The various data points at H/B = 3 also are discussed in Section 5.2.5.

To get a better feel for the data under realistic scaled deflections, Figures 98b and c were prepared. A scaled differential deflection of $\Delta D/B$ = 2/1,000 in a 20-foot-wide structure would be less than 0.5 inch and a scaled differential deflection of $\Delta D/B$ = 5/1,000 would be approximately 1.2 inches. Scaled differential deflections of 10 to 15 might be reasonable for a large flexible structure.

In Figure 98b, the trend for the dynamic active arching data to plot inside the static data is reversed at this small differential deflection, except at H/B = 1/3 . The reason for this change seemed to be rate of pressure rise at the level of the device, inertia

effects, and the increase in the soil strength under rapid loading. The effects of burial depth on both the dynamic and static data can be seen. It is interesting to note that the 37.5-psi static and dynamic data from this program appeared to be fully buried at $\Delta D/B = 2/1{,}000$ and $H/B \geq 1$. Hendron's (1968) 37.5-psi data displayed a fully buried condition at $H/B \geq 2$. Maximum active arching had not been produced at $\Delta D/B \times 1{,}000 = 2$ by any of the tests, but the amount of arching was approximately 20 psi at $H/B = 1$ and 3 with $P_S = 37.5$ psi under dynamic conditions. In Hendron's (1968) static tests, the ΔP was approximately 26 psi at $H/B = 2$ and 3 and 17 psi at $H/B = 1$.

In Figure 98c, the high pressure tests have been added and ΔP has been scaled by the shear strength of the clay as determined by unconfined compression tests. At $P_S = 37.5$ psi, neither the static nor dynamic tests exhibit the fully buried condition which seemed to be present at the lower scaled deflection. The reason for this apparent anomaly was the fact that the differential pressures had not been scaled by the shear strength of the soil. Tables 5 and 6 show that a fully buried condition did not exist for the static or dynamic tests in Figure 98b. When possible, the differential pressure has been scaled by the soil strength.

The higher pressure dynamic data at $P_S = 150$-157 psi in Figure 98c show an increase of 1.4 and 2.7 in the amount of scaled

differential pressure at $H/B = 1$ and 3 , respectively, over that developed by the 37.5-psi tests. Test 14 at $P_S = 245$ psi could not be plotted because of the very large deflections experienced by the structure as soon as it was hit by the pressure wave.

Some of the effects of depth of burial on active arching can be seen by examining the pressure profiles for Tests 11, 15, and 16 in Figures 60a, 61a, and 61b. As the scaled depth of burial increased from 1/3 to 1 to 3, the area affected by the unloading appeared to enlarge from inside the 6-inch radius, to the 10-inch radius, to outside the 10-inch radius, respectively. As previously discussed in Section 5.2.1, the soil profiles also showed that the height of deformation propagation was sensitive to burial depth. This was clearly indicated by plots similar to those shown in Figures 68a, b, and d.

When ultimate arching was considered, depth of burial was important to the amount of active arching at $P_S = 37.5$ psi up to the point at which the structure appeared to be fully buried at $H/B = 1$. At higher pressures, $P_S > 150$ psi , a fully buried condition was not attained at $H/B = 3$. Maximum arching at $H/B = 1$ and 3 was attained by surface pressures of 150 psi or higher. The dynamic test at $H/B = 7$ may have produced maximum active arching but there was no way to substantiate this conclusion. The amount of active arching at higher pressures where the shear strength of the material was

important also was related to the depth of burial. In the low pressure tests, $P_S < 70$ psi , the amount of active arching appears to be more dependent on the relative stiffness of the device since the amount of soil shear strength mobilized at $H/B = 1$ or greater appears to be minimal.

5.2.4 Pressure Effects. Most of the pressure tests were made at a scaled deflection of $H/B = 3$. Tests 16 and 19 at $H/B = 1$ were also used to examine pressure effects.

Figure 97 shows the variation of the differential pressure at $H/B = 3$. Figure 98c shows the same data scaled by the unconfined strength of the clay. As explained in the previous section, these figures indicate that there was insufficient pressure to mobilize the strength of the soil at $P_S \leq 70$ psi . The load experienced by the structure is merely a function of its relative stiffness. Static Test 6, which also utilized the spring-ring device at $P_S = 37.5$ psi , appears to substantiate this conclusion, Figures 97 and 98a.

In Figure 97 it can be seen that part of the soil above the structure yielded at $P_S \geq 150$ psi , Tests 13 and 14. This was confirmed by the soil profiles discussed in Section 5.2.1.

In Section 5.2.3, fully buried and maximum arching conditions for the high pressure tests were discussed. It could not be definitely determined whether the surface pressures and device deflections were sufficient to develop the maximum arching available at

$H/B = 3$, but the fact that there was such a small increase in the ΔP between Tests 13 and 14, 3 psi, for such a large increase in P_S , 94 psi, indicates that the maximum strength of the soil had been developed, Figure 97. In Tests 13 and 14 at $\Delta D/B \times 1{,}000 = -19.2$ and -23.2 or $d_t/B \times 1{,}000 = -40.5$ and -51.5 , the scaled differential pressures $2\Delta P/q_u$ were equal to -2.53 and -2.29, respectively. Thus, the soil strength developed at $H/B = 3$ was approximately 2.3 to 2.5 times the shear strength of the soil.

There is some question whether more deformation or a higher surface pressure would have developed more arching at this depth of burial. Within the area where the soil experienced large yields, the shear strength of the soil had been mobilized. The differential strains at the level of the device, Table 2, more than exceeded the strains necessary to mobilize the maximum shear strength of the soil under triaxial conditions, Figures A-13 and A-24.

Figure A-23 shows that the strains experienced within the SBLG for all tests except Test 14 at $P_S = 245$ psi were comparable to the triaxial strains at failure in Figures A-13 and A-24. The shape of the stress-strain curves of the SBLG tests at $P_S \geq 240$ psi were more comparable to those produced by the data from the one-dimensional compression tests made with the impact loader, Figures A-21 and A-22. The maximum strain at $P_S \approx 240$ psi coincided with that found using Schindler's compression device at a comparable pressure, Figure A-23b.

The active arching produced above a critical threshold pressure under the test conditions reported appeared to develop the triaxial shear strength of the soil in a zone around the structure. The soil profiles and observations discussed in Section 5.2.1 appear to confirm this conclusion. The amount of active arching depends on the extent of this zone, the height and width above the device to which the strains propagate, and the magnitude of these strains. The process of shear development discussed by Newmark and Haltiwanger in the Air Force Design Manual appears to coincide qualitatively with the results found in this study and discussed in the preceding paragraphs.

Associated with the stress-strain curves was the soil modulus used as a measure of the flexibility of the soil. The soil modulus increased with an increase in surface pressure, Tables A-1 and A-2. This means that the soil modulus and consequently the relative stiffness of the structure were changing throughout most of the dynamic tests. In some cases a plateau was reached where the change was not rapid, Appendix A. This change in soil modulus partially accounts for the high loads early in some of the dynamic tests as disclosed by the arching curves, Sections 4.3.2 and 5.2.2.

The pressure profiles showing variation of soil stress with depth and time similar to those shown in Figures 64, 65, and 68 indicate that the depth of soil involved in arching increased from approximately 6 inches to 12 inches as the surface pressure was

increased from 37.5 to 240 psi. Except for Test 18 at $H/B = 7$ and $P_S = 310$ psi , the major portion of the active arching appeared to occur within 6 inches of the top of the device. In Test 18, active arching effects were observed 3 structure diameters above the test device. The large volume of soil involved in Test 18 was a manifestation of its high pressure and the depth of burial of the device.

Because of the small number of tests, it was not possible to determine a transition zone between the high pressure and low pressure tests. This transition zone should be sensitive to the shear strength of the soil at a constant depth of burial. Examination of the high pressure data in Table 6 indicates that the transition may be rather abrupt. When sufficient deflection is developed in the soil to mobilize its shear strength, there is a rapid increase in differential pressure.

If a small, constant differential deflection is selected and the change in the differential pressure with change of surface pressure is examined, it can be seen that ΔP increases with P_S in the active arching data in Figure 98c. It is difficult to determine any transition zone between the type of arching experienced in the low pressure tests and the arching action which appeared to take place in the higher pressure tests. This problem is complicated by vast disparity between the available $\Delta D/B \times 1{,}000$ values created by the large surface pressure differences. If $\Delta D/B \times 1{,}000 = 10$ at

$H/B = 3$ and $K_T/K_S \approx 0.7$ is selected, $2\Delta P/q_u$ increases from -0.74 to -0.93 to -3.51 at $P_S = 37.5$, 70, and 150 psi , respectively. It was not possible to use Test 14, with $P_S = 245$ psi , at this ΔD because the soil pressure at the level of the top of the device was so low at this scaled deflection. When $\Delta D/B \times 1{,}000$ was increased to 20, it was not possible to select a value for Test 11 because of the small deflections developed by a surface pressure of 37.5 psi, but $2\Delta P/q_u$ was equal to -0.75, -2.53, and -8.1 to -10.7 at $P_S = 70$, 150, and 245 psi , respectively. Note the very large changes in scaled ΔP as P_S was increased.

Thus, at a constant depth of burial, relative stiffness, and differential deflection, the amount of arching increases with surface pressure until a fully buried condition is attained or the maximum strength of the soil is mobilized. These two conditions are difficult to predict. In the case of the fully buried condition, the amount of arching which constitutes this condition changes with surface pressure until a state is reached in which all surface pressure is dissipated at the particular depth in question.

It was previously shown that the area involved in active arching seemed to enlarge up to a limiting point of 2B with an increase in pressure at $H/B = 3$. The maximum size of the area appears to depend upon the depth of burial and size of the structure. Thus, the amount of arching is not appreciably increased with an increase

in pressure once the maximum strength of the soil is developed at a particular depth of burial.

Once the limiting strength of the soil at a particular depth is reached, practically all of an increase in the surface pressure is applied directly to the structure if the deformed area does not or cannot enlarge. Some small change in the ΔP should result from the increases in soil strength with the increase in confining pressure, but this effect was minor in the pressure range used in this program, Figure A-14.

Repetitive testing of the soil sample was tried in three tests, 11, 24, and 27, Table 1. In all cases the repeated tests were at higher surface pressures. The compressive strength of the clay, as determined by the Hvorslev unconfined tests discussed in Appendix A, was somewhat higher after each test, Table 4 and Figure A-7. The effect on the differential pressure is difficult to ascertain just by examining Table 2. Figure 99b shows the points from the repeated tests with an X over the symbol. Logically, the relative stiffness and the differential pressure in the repeated test were different from that found in the original tests. In all repeated tests but Test 27B, ΔP was larger, and in all but Test 27C, the relative stiffness of the structure was smaller. Repeated tests at the same or higher pressure appear to be feasible to examine gross arching effects. It would

be difficult to examine the effects of relative stiffness with repeated tests, but examination of the effects of large changes in the surface pressure should be feasible, if the gains on the instrumentation can be properly adjusted.

Based on the very limited amount of data developed in this test program, $P_S < 65$ psi and $H/B = 1$, passive arching does not appear to be pressure sensitive under dynamic conditions, Figure 98c. Hendron's (1968) static test results in Figure 98b also show that at P_S less than 75 psi the passive arching at $H/B = 1$ or more is not pressure sensitive.

5.2.5 Stiffness. One of the principal parameters studied in this test program was the effects of the relative stiffness of the structure on the amount of soil arching induced. The structure stiffness was obtained and measured as explained in Chapter 3 and Appendix B. The structure was an elastic system throughout its deflection with only minor exceptions. The modulus data for all structures are shown in Table 3. The modulus data for the particular test device in a particular test are repeated in Tables 1 and 2.

The modulus of the soil used to design the experiments was established in the preliminary test program by use of confined compression and SBIG tests, Appendix A. During the test program, the modulus of the soil was determined from soil deflection and peak pressure wave velocity data generated during the actual tests,

Appendix A. Soil modulus data for each test are listed in Tables 1 and 2; the data from the preliminary design program are shown in Tables A-1 and A-2.

Three static tests (6, 7, and 8) were made with the spring-ring device, Table 1. Tests 6 and 7 were made with the device buried at $H/B = 1$, and Test 8 with the device buried at $H/B = 3$.

In Test 6, P_S was equal to 37.5 and the stiffness of the device relative to the soil was 0.6. It can be seen in Figures 92 and 98a, that the load developed on the device was approximately 0.62 times the surface pressure when full active arching was initially developed. After approximately 62 hours of creep, the load increased to 0.69 times the surface pressure. Thus at $P_S = 37.5$ it appears that the amount of initial active arching is dependent on the relative flexibility of the device. With time and continued soil deformation, the stress gradient decreased and the load increased on the structure.

The device used in Test 7 had approximately the same stiffness as the soil, $K_T/K_S = 1.25$. But, as shown in Figure 92, the resultant load indicated that the structure did not attain the load expected. Because of the high loading and resulting high deflections of the soil underneath the device when it was in a passive arching mode, it was not possible to attain an overall passive arching condition with reference to the surface pressure with this device. This phenomenon is explained in more detail in a later paragraph of this section.

Test 8 was conducted using a test device which was designed to be 0.7 times as stiff as the soil but was calculated to be 0.42 times as stiff in the posttest analysis. It can be seen in Figure 92, that as P_S was increased from 40 to 75 to 100 psi, the relative load on the device decreased. This was because the soil was not as stiff at the lower static pressures. As the surface pressure increased, the soil became stiffer and the relative stiffness of the structure decreased. When the surface pressure increased from 100 psi to 175 and 240 psi, it can be seen in Figure 94 and Table 5 that there was a large increase in the differential pressure from -19 to -54 to -58 psi, but a larger increase in the pressure acting on the device, from 81 to 129 to 182 psi. Thus, the structure stiffness did not determine the final load experienced by the structure, but stiffness did play a role, especially at the lower pressures. Based on the deformations and differential pressures observed, it appears that soil strength and depth of burial were the most important factors in determining the amount of arching experienced in this high pressure test, but the relative stiffness of the structure also played a role. The strength mobilized was $5.2 \times q_u/2$ psi .

Considerably more data concerning structure stiffness were collected during the dynamic test program. The spring-ring device was used in all dynamic tests. The tests particularly designed to study the effects of structure stiffness on arching were made with the

device buried at a scaled depth of $H/B = 1$ and with a surface pressure of approximately 37 psi.

In Figure 92, several of the dynamic tests have been plotted with the static arching data. The points shown are generally the arching factor and relative deflection at ultimate arching. This was determined to be the arching which existed when the load on the device was a maximum after peak soil pressure had arrived at the level of the top of the device but before the reflections appeared to be appreciable. Because of the very large deflections experienced in Test 23, a comparable deflection was chosen. Examination of the data in Figure 92 and Table 2 shows that the load experienced by the structure in Tests 16, 20, and 23 at $H/B = 1$ and $P_S \approx 37$ psi was determined by their stiffness relative to that of the soil. This also was the case for Test 11 at $H/B = 3$ and $P_S = 37.0$ psi . Note that the arching factors have no relation to those of the device-induced arching curves at the same deflections. Points fall on both sides of the comparable curves. The points of maximum arching in Tests 16 and 20 also are shown.

In order to present the flexibility data in a usable form, Figure 99 was prepared. This figure shows the variation of the load on the structure with changes in the relative stiffness of the structure. The basis of this figure is the data generated in Tests 16 and 20 through 28 at a constant value of $H/B = 1$ and $P_S \approx 37.0$ psi . The

curves were drawn using the data from these tests. Points from other tests were added to show their position relative to the basic data.

It was at the relatively low pressures, in this case less than 40 psi, that structure flexibility was the dominant factor in determining the loads on the structure (Section 5.2.4). As shown in Figure 99, it was possible to relieve almost all of the overpressure by the use of a very flexible structure because the surface pressure was not sufficient to overcome the strength of the soil at a scaled depth of $H/B = 1$.

When the scaled depth was decreased to 1/3, dynamic amplification of the load was experienced. But in Figures 99a and b, it can be seen that increasing or decreasing the depth of cover by a factor of 3 was not an overriding consideration at $P_S \approx 37$ psi. The data for Tests 15 and 11 fall within the scatter band of the basic data in Figure 99b and plot very close to the basic data curve in Figure 99a.

When the dynamic surface pressure increased to 70 and 157 psi, the data for Tests 12 and 19 at $H/B = 3$ and 1 , respectively, fall within the scatter band of the basic data in Figure 99b, but the data for Tests 13, 14, and 18, at $H/B = 3$ and 7 and $P_S = 151$, 245, and 310 psi, plot completely out of the range of the other data. There is no reason why these data should plot within the scatter band of the low pressure data since the amount of arching appears to be

governed largely by soil strength and their depth of burial was 3 times that of the basic data.

In Figure 99a, the high pressure data have been corrected for dynamic amplification using the average of the amplification factors (AF) shown in Table 7. This is explained in Section 5.3. The corrected data were not used in Figure 99b.

With the exception of Test 8, the static data also plot on or very close to the basic curve in Figure 99a. This tends to confirm the conclusion that dynamic effects were not important in the low pressure tests at a scaled depth of burial of 1 or larger. In addition, it shows that at high pressures where large soil deformations are involved, pressure effects are large and begin to override the flexibility effects.

The data point shown for Test 23 appears to plot out of the band of data. The very low stiffness used for this test device is not within a practical range for real structures. The entire surface pressure of 33.3 psi was dissipated by the active arching; therefore, the value of the surface pressure determined the ordinate of the data point shown. Whether a higher surface pressure would have developed higher differential pressures cannot be determined without additional tests.

For the structures stiffer than the soil, structure stiffness was not an important parameter once relative stiffness exceeded a

value between 4 and 5, Figure 99. Above these values the loads on the structure became more dependent upon the combined stiffness of the structure and the soil underneath it. With the very stiff structures, it was the soil stiffness which dominated the overall stiffness of the soil-structure system at $P_S \leq 60$ psi and $H/B = 1$. The device appeared to punch into the supporting soil. Therefore, variations in the stiffness of the stiff structure over a wide range from $K_T/K_S = 4.14$ to $K_T/K_S = 461.0$ were insignificant to the differential pressures developed. Soil strength also must have an effect on the magnitude of the passive arching, but its role could not be determined because of the small number of tests and their limited, low pressure range. The data plotted in Figure 99b also show that relative structure stiffnesses above approximately 4 had only minor, if any, effect on the amount of passive arching.

The findings from this test program relative to passive arching are very similar to those found by investigators working on the development of pressure cells. Taylor, Monfore, Whiffin and Morris, and others have shown that a stiff gage is a very accurate gage because it will overregister by a known amount over a wide range of flexibilities in the surrounding medium. The gage reported on by Whiffin and Morris overregistered from 1.1 to 1.2, depending on the size of the sensitive area on the gage face. This error became

almost constant at a relative stiffness of 10 or more. Similar results can be derived from the reports by Taylor and Monfore.

Investigation of the vertical soil stress profiles in Figures 62 and 63 shows that the area involved in the unloading at the level of the top of the device under active arching conditions tended to move away from the device with a decrease in the stiffness of the structure. The extreme case, Test 23, is shown in Figure 63a. The profiles indicate that as the structure less stiff than the soil began to unload, it loaded the soil in its immediate vicinity initially. This soil began to deflect at a more rapid rate than the soil farther out, as shown in Figure 73b, because of the increased load it was trying to support. Posttest investigation showed that this soil also seemed to have squeezed toward the area vacated by the structure. As the near soil deflected, it loaded the soil outside of it by the shearing actions developed in the differential deformations. The load-deformation action progressed upward and outward from the structure until the load gradients created had dissipated to a value which the soil could support. A structure with a very low relative stiffness can deflect a large amount and thus most of its load will be arched off. There appears to be a relation between the zone of influence of the arching and the amount of differential deflection in Figures 62 and 63. The scaled radius of influence, r/B , should be directly proportional to $\Delta D/B$ but insufficient soil deflection and

pressure data points were available at the level of the top of the device to make such a determination.

Although it was difficult to clearly determine its extent, the progressive failure or deformation mechanism described above apparently takes place in the soil above a device less stiff than the soil. Thus, the more flexible the structure, the larger its absolute deflection, and therefore the differential deflections. Larger deflections mean larger strains immediately above the device and thus, the development of strain at a greater height above the structure up to some limiting height which appears to be limited by the size of the structure and the depth of burial. The higher the soil deforms and thus loads adjacent soil, the wider the load distribution at the level of the top of the structure becomes. Figures 63a, 66b, and 68e seem to confirm the deformations described above.

For passive arching, the soil at the level of the top of the device appeared to be disturbed to a radius between 6 and 8 inches from the centerline of the device or between one structure radius and one structure diameter outside the device, Figure 63b. The soil above the device was disturbed approximately 3 to 4 inches or one structure radius above the device. These conclusions must be judged in light of the very limited number and variety of passive arching tests.

5.3 STATIC VERSUS DYNAMIC ARCHING

The relation between static and dynamic test data could be important if such a relation exists. This would permit the testing of structures under less expensive conditions and might allow the use of equivalent static loads in the design of protective structures.

As discussed in Appendix A, the compressive strength and thus the shear strength of buckshot clay are sensitive to the rate at which the material is loaded, Figures A-14 and A-24. In fact, this $\phi = 0$ material at the water contents tested is much more sensitive to strain rate than it is to confining pressures. In addition, the rate of rise to peak pressure was found to be sensitive to water content and incident pressure, Figure A-20.

In Figures 92, 93, and 94, the arching developed in individual static and dynamic tests is plotted so that it can be compared to the static arching curves. Figure 92 shows that the data produced in Tests 11 and 16 plotted above the comparable static arching curves. Two points are shown for Test 16, one at maximum arching and the other at minimum arching, or design conditions. In both cases, the data show considerably less arching than the static curves developed using either the trapdoor or hydraulically controlled device. When these same tests are compared with static Test 6, in which the spring-ring device was used, and the difference in relative flexibility is considered, it can be seen that there was very little, if any,

difference in the amount of final active arching which could be attributed to dynamic effects. The larger amount of arching in Test 16, as shown by the point depicting maximum arching, was probably due to the higher strength of the soil under rapid loading conditions, but the later design value at minimum arching for Test 16 indicates that the soil acted similarly to the static conditions once the load front had passed the device.

The arching value shown for Test 15 at $H/B = 1/3$ and $P_S = 39$ psi in Figure 92 is an exception. It plotted on the $H/B = 1/3$ and $P_S = 37.5$-psi curve developed by Hendron (1968), but below the curve produced by the hydraulic device used in this program. Similar results for this test are shown in Figure 94. When the test results were compared with the relative stiffness of the device, $K_T/K_S = 0.80$, it appeared that some dynamic load amplification occurred in Test 15.

When very flexible devices were used in the dynamic tests, as in Tests 20 and 23, the data approach the static arching curves. For Test 20, the points depicting maximum and minimum active arching straddle the comparable static arching curve in Figure 92. The amount of arching in Test 23 exceeded that of the comparable arching curve. The same sort of data in terms of ΔP are shown in Figure 94. To this figure have been added data from the high pressure static and dynamic tests.

The close comparison of the amount of arching in Tests 6 and 16 can be readily seen in Figure 94. In addition, the data points for dynamic tests at $P_S \approx 37$ psi, such as Tests 22 and 23, do not disclose any dynamic effects on the structure load when compared with the static data.

Comparison of the static Test 8 data points in Figure 94 with the results of dynamic Test 14 at comparable surface pressures ($P_S \approx 240$ psi), depth of burial ($H/B = 3$), and calculated relative stiffnesses of 0.42 and 0.66, respectively, shows that more arching was initially developed in Test 8, $2\Delta P/q_u = -5.2$ versus -2.29.

With time, the differential pressure developed in Test 8 decreased to a value of -3.2 which corresponded to an unscaled differential pressure identically equal to that developed in Test 14, -35 psi. Two conclusions which have been discussed previously are evident from this examination. First, trapdoor- and structure-induced active arching curves cannot be used to estimate the amount of arching under dynamic conditions, whether dynamic load amplification is present or not. These methods of inducing arching override all other considerations, but do not necessarily produce maximum arching when compared with very flexible structures, $K_T/K_S < 0.20$. Second, it is difficult to compare arching in tests with comparable surface pressures, depths of burial, and stiffnesses unless a particular differential deflection or differential pressure at which to

make the comparison is chosen.

When comparable static and dynamic active arching data are examined at a particular depth of burial in Figure 97, it is difficult to determine any trends because the data have not been normalized to a particular differential deflection. The ultimate differential pressure developed at $P_S = 37.5$ psi under static conditions with the trapdoor and hydraulic device exceeds that developed under comparable dynamic conditions at all depths of burial used. The difference is approximately 19 psi at $H/B = 1/3$ and 27 psi at $H/B = 1$ and 3 . This difference does not exist when the dynamic data are compared with data from Test 6 in which a spring-ring device was used. The small difference between the amounts of arching developed in Test 6 and Test 16 can be attributed to differences in the stiffness of the test device used. No dynamic effects were evident.

The same type of information in a different form is shown in Figure 98a. In this figure, the static deflections were equal to the deflections in the comparable dynamic tests. This eliminated some of the problems of comparing static and dynamic data. The effects of dynamic amplification can be seen within the high pressure data at $H/B = 1$ and 3 . The loads on the structure as depicted by the arching factor, P_T/P_S , are larger than the relative stiffness ratio, K_T/K_S , and larger than the comparable static test made with the spring-ring device. Dynamic amplification of the load appears

to override the increased soil strength due to the rapid loading, particularly when large deflections are considered.

When the differential pressures for comparable static and dynamic tests are compared at small identical deflections, $\Delta D/B \times 1{,}000 = 2$ and 5 , in Figures 98b and c, a clearer picture of the dynamic effects emerges. In Figure 98b the differential pressures developed in the dynamic tests at $P_S \approx 37$ psi exceeded those of the comparable static tests at $H/B = 1$ and 3 , but not at $H/B = 1/3$. The latter phenomenon was the result of the amplification of the load at the shallow depth under dynamic conditions. At the deeper positions, the strength of the soil under rapid loading conditions appeared to play a role in determining the amount of differential pressure. Dynamic Test 16 also developed a larger ΔP than static Test 6 under the conditions depicted in Figure 98b. Because of the lower boundary condition previously discussed, Hendron's (1968) trapdoor data developed higher differential pressures than any other test configuration, static or dynamic, at comparable conditions of depth and surface pressure.

When the differential deflection, $\Delta D/B \times 1{,}000$, was increased to -5.0 in Figure 98c, all data, static or dynamic, at $P_S \approx 37$ psi plotted very close to a scaled differential pressure, $2\Delta P/q_u$, of -1.0 at $H/B = 1$ and 3 . The static spring-ring device in Test 6 produced virtually the same differential pressure as that

developed under comparable dynamic conditions. Thus, there were no appreciable dynamic effects on the structure load or soil strength after the surface pressure reached a steady state.

When P_S was increased to 150 psi and higher, the differential pressures at an equal low differential deflection exceeded the static data at $H/B = 1$ and 3 by a large margin. Test 8 at $H/B = 3$ and $P_S = 240$ psi was a comparable static test, but as shown in Figure 98c, its differential pressure developed at $\Delta D/B \times 1{,}000 = -5$ was considerably smaller than that developed under dynamic conditions.

The test results discussed above are logical when time effects are considered. The viscous clay material is time sensitive even when two relatively slow times, Figures A-12 and A-24, are compared. It was not possible for the large deformations experienced in the static tests to take place in the dynamic tests. Therefore, ultimate arching under static conditions without regard to deflections was higher in all the static tests. But, the soil was stronger under faster loading conditions as shown in Figures A-12 and A-24, and when the equal, reasonable small deflections were used, then more arching was produced under dynamic arching conditions.

At the later times when minimum arching developed during the low pressure dynamic tests, the surface pressure had reached a steady condition. Any dynamic effects on the structure load or the soil strength appeared to have diminished. This was not true during the

dynamic tests at $P_S > 40$ to 70 psi . The fact that the dynamic amplification of the load appeared to play a large role in these tests, and the increase in the shear strength of the material were both clearly evident, Figure 98c.

A comparison of the modulus data in Tables A-1 and A-2 shows that the soil modulus was invariably higher when equal pressures were applied under very rapid loading conditions. The design of the stiffness of the device took this difference into consideration. A more detail explanation of the calculation of soil modulus is given in Appendix A.

This test program revealed that dynamic pressures involve high structure accelerations, just as with aboveground structures. At $P_S \geq 70$ psi, the load applied to the structure at all depths used was amplified. Calculation of the dynamic amplification factor for each test was performed as described in Section 4.3.6. The results of the calculations and a comparison with the relative structure stiffness are shown in Table 7. The average of the amplification factors calculated using two different rise times, time to maximum pressure and time to first peak pressure, was used to plot the high pressure data in Figure 99a. This brought the data closer to the curve drawn using the low pressure data, $P_S \approx 37$ psi, but the higher loads developed during the high pressure tests are still evident.

Considering the effects of the structure configuration, the large

deflections under static conditions, the dynamic amplification of the load, and the changes in the soil strength and modulus with high pressure dynamic loads, it would be unconservative to use static active arching data to compute the design loads on flexible structures expected to be subjected to surface pressures higher than approximately 40 psi. Even when used for lower pressure design, the test results indicate that depth of burial, H/B , should be equal to 1 or more and the static data should be determined with a model structure which produces active arching by the exertion of external pressures rather than some device which induces arching by lowering the top of the structure artificially.

Selig (1960) and Van Horn (1963a) in their approaches to dynamic design of underground structures have recommended the use of equivalent static loads which are less than that produced by the actual dynamic pressure. The results from this test program indicate that this practice could be unconservative at comparable structure deflections. When time and deflections are disregarded, this approach may be more accurate.

Two other time effects were noted in examining the test data. First, very early in the loading cycle, the loads applied to the soil surface had to overcome the inertia of the mass of the soil above the device. This effect partially accounted for the unusual shape of the dynamic arching curves and is discussed in detail in Section 4.3.2.

Second, the actual arching experienced by the structure lagged the soil deflection which induced the arching. In addition, the deflection of the soil did not react immediately to the load transferred to it by the arching action. In examining the detail data in Tables 5 and 6, these phenomena should be recognized. Although the arching curves were plotted at particular time intervals, the actual differential deflection which caused the amount of arching measured occurred at an earlier time and the soil deformations measured were caused by a load transfer that occurred at an earlier time. Thus, there was a time sequence of events. Arching is not an instantaneous phenomenon. The structure-induced arching, which is not realistic in terms of actual structures, caused the load on the structure to react almost instantaneously with the structure deflection. In this case, the soil deformations still lagged the loading.

A comparison of the static and dynamic passive arching data is presented in Figures 93 and 98 in various forms. In all cases the amount of passive arching produced under static pressure conditions with the trapdoor or hydraulically controlled device exceeded that produced under dynamic conditions at the same depth of burial and surface pressure. The dynamic surface pressure varied from 31.0 to 64.0 psi, while the static surface pressure was 37.5 psi. At these pressures, no dynamic effects were observed. Evidently, the method of producing arching under static conditions was an overriding

consideration. No static data were produced using the spring-ring device to compare with the dynamic test data.

5.4 SUMMARY OF EXPERIMENTAL RESULTS

In this section some of the more pertinent findings of the experimental program are summarized. The findings are a guide to the effects which can be expected during active and passive arching under static and dynamic loading conditions. Throughout Chapters 4 and 5, items of possible interest to the designer or investigator have been discussed. Any use of the information developed in this test program must be guided by the test conditions and assumptions described throughout the main text and the appendices.

Soil deformation patterns above and beside the test device were studied in detail to discover the extent of the redistribution of stress caused by the arching action in the cohesive material. The active arching zone directly above the device consisted of a 4- to 5.5-inch-diameter, circular depression whose diameter grew smaller with height above the device. Surrounding the depression was a raised portion of soil which varied in diameter from approximately 2 to 10 inches outside the depression. The hump or ridge pattern was more distinct in the static and dynamic tests in which P_S exceeded 50 psi. In the higher pressure dynamic tests, more than one depression usually was found; as many as three concentric depressions were

found inside the hump at P_S = 310 psi , and two were found at P_S = 245 psi .

The soil deformation pattern extended upward from the top of the device and outward from the centerline of the test chamber with increase in test time, surface pressure, and structure flexibility.

This depression-hump formation appeared at the soil surface in only two static tests: at $H/B = 1/3$ and P_S = 37.5 psi ; and at $H/B = 1$ when a surface pressure of 37.5 psi did not create a surface deformation, but a repeated test on the same soil specimen at P_S = 50 psi did cause a surface depression. Both of these tests were made with the hydraulically controlled device in which the scaled deflection of the top of the device, $d_t/B \times 1{,}000$, reached approximately 80. The highest scaled deflection of the top reached with a spring-ring device was approximately 60 at a static pressure of 240 psi, and 56 at a dynamic pressure of 310 psi. In no case did the soil deformation pattern propagate to the soil surface in a dynamic test, even at $H/B = 1/3$. There was normally a soil layer 1 to 3 inches thick near the soil surface, depending on depth of burial, which was free of deformation.

The depression pattern was not seen in the dynamic tests at $P_S \approx 37.5$ psi , but it was observed in all dynamic tests at a higher pressure. In the low pressure dynamic tests, the soil generally rebounded after the test. There were only very minor differential

deflections between the test device and the soil at the completion of these tests.

The soil deformation patterns were more distinct in the static and higher pressure tests. At static and dynamic surface pressures of 240 psi, the depression pattern was observed 2 structure diameters above the test device. When the surface pressure was increased to 310 psi in a dynamic test, soil deformation was observed approximately 2.5 structure diameters above the structure.

In addition to the study of soil deformation, it was possible to detect active arching action in the soil by observing the horizontal and vertical soil pressures above the test device. In this manner it was determined that the majority of the arching action took place within the first 3 to 6 inches of soil directly above the device. At all static pressures used and at dynamic surface pressures above 40 psi, a hemispherical dome 1 to 3 inches in height formed on the top of the device. It appeared that the majority of the arching action occurred in the soil between this dome and the level approximately one structure diameter above the test device.

As the soil deformed above the device, the load arched off the structure was distributed to the soil at the level of the top of the device. This redistribution occurred within the region one structure diameter outside of the device with the majority occurring within one structure radius. At $P_S \approx 37.5$ psi , the loaded area extended to a

radius of 4.5 to 6.5 inches from the centerline under static conditions, and to a radius of 6 to 6.5 inches under dynamic conditions. When the surface pressure was raised to 75 psi, the loaded region extended to approximately 9 inches from the centerline under static conditions and 6.5 to 7 inches under dynamic conditions. As the surface pressure was increased, the loaded area extended horizontally to a radius of 6 to 8 inches at $P_S \approx 150$ psi dynamic, 8 to 10 inches at $P_S \approx 245$ and 310 psi dynamic, and 9 inches at $P_S \approx 240$ psi static. All of these tests were made with structures designed to have the same stiffness.

The loading of the soil near the device caused it to deflect further than the soil farther out. The soil at the level of the device sloped down toward the device from a radius of 9 to 12 inches, depending on the surface pressure and flexibility of the device. The higher the pressure or the more flexible the device, the farther out the sloped region began. Thus the extent of this region was related to the amount of deflection the test device experienced.

The horizontal extension of the deformed area above the device, depressions and ridges, also was dependent upon the surface pressure. The higher the pressure, the larger the area involved at a particular level. The effects of flexibility on the horizontal extent of the deformed area above the device could not be determined.

The lateral and vertical extent of the active arching zone in

the soil was a manifestation of the stress gradients developed. The wet, viscous clay used in the experiments tolerated only small stress gradients. Thus for equilibrium to be satisfied, the load arched around the structure had to be distributed to an increasingly larger area.

The deformations above the device appeared to be similar to those developed during triaxial laboratory tests. The soil zone around the depressions experienced a combination of compression and shear bulging. The pressure profiles in the zone affected by active arching above the device showed that the direction of the major principal stress changed from near vertical to near horizontal as the structure deflected. The size of the deformed zone above the device appeared to depend upon the surface pressure, depth of burial, structure stiffness, soil strength, and the time within which the soil deformations took place.

The distorted zone in the soil beside the device occurred within the high pressure zone disclosed by the vertical pressure profiles. The soil deformations appeared to be nothing more than a manifestation of compression. The pressure profiles at low pressure, $P_s < 40$ psi , resembled the pressure profiles calculated by elastic analysis. At higher pressures, the pressure profiles resembled those predicted by an elastoplastic analysis.

Much less information was available for the study of soil action

under passive arching conditions. In general, the soil formed a hemispherical dome approximately one structure radius high and one structure diameter wide directly above the test device. The soil deformed around this dense, solid dome. Manifestations of this dome could be seen at the soil surface in the static test using the hydraulically controlled device at $P_S = 37.5$ psi and $H/B = 1$. Raised portions above the device were not observed at the soil surface in any of the dynamic tests made with the stiff spring-ring device at $P_S \leq 64$ psi and $H/B = 1$.

The soil at the level of the top of the device was unloaded by the passive arching action to a radius of approximately 6 to 7 inches or one structure radius outside the device.

In both the active and passive tests under static and dynamic test conditions, the soil deformations under the test device resembled those associated with normal bearing capacity deformations.

The static tests were made using two test device configurations: in one the top of the device could be lowered by externally reducing the hydraulic pressure within the device; in the other, a spring-ring device, the extent of deflection of the top was determined by the amount of pressure exerted on the device and the spring constant built into it. In addition, data were available from a previous investigator, Hendron (1968), who used a trapdoor configuration with the same soil at comparable water contents. All dynamic tests were

made with the spring-ring device.

It was found that the amount of active arching produced using the trapdoor device exceeded that developed by the hydraulically controlled device whose base was located 5 structure diameters above the bottom of the test chamber. The arching induced by the hydraulic device exceeded that developed by the spring-ring device placed in the same location in the soil. Thus, the manner of inducing arching, i.e. whether induced by external or internal pressures, affected the amount of arching.

The fixed boundary surrounding the trapdoor logically supported higher loads and thus supported higher active arching at a given deflection of the trapdoor and a given depth of burial.

The amount of differential deflection developed between the structure and the soil was limited by the actions of the soil underneath the device. The amount of soil deflection depended on the load the structure was experiencing at any particular time, although there was a delay between the loading of the structure and the resulting soil deflection under it.

Thus the test configurations used affected the amount of active arching and the way this arching developed. This latter point was evident from examining the arching curves produced by various configurations. The general forms of the arching curves produced using the trapdoor and hydraulic device configurations were very similar, i.e.,

a very high initial slope which gradually lessened with an increase in the differential deflection. The curves became parallel to the deflection axis when the surface pressure had been dissipated or the maximum strength of the soil had been developed. The form of the active arching curves produced by the spring-ring device under comparable static conditions was considerably different. These curves had much less initial slope. There was very little change in the slope until a particular deflection (pressure) was reached at which the soil appeared to begin to fail because the slope changed abruptly to a steeper angle. This change occurred at $P_S \approx 75$ to 100 psi with $H/B = 3$. With each increment of increased pressure and resulting increased differential deflection, the slope became steeper until there was an abrupt change to no slope, and the arching curve became parallel to the deflection axis. This occurred at $P_S \approx 175$ psi with $H/B = 3$. At $P_S \approx 37.5$ psi the steep slopes were not experienced and the deflection of the soil under the device had a large influence on the arching curves.

The dynamic active arching curves, with minor exceptions, were not the same form as those produced by any configuration under static surface pressure conditions. The dynamic test curves were affected by the inertia of the soil above the structure and the structure itself. Maximum arching, as measured with reference to the surface pressure, normally occurred early in the test at the lower

differential deflections. A plateau was normally reached in every test at some minimum arching value at which the amount of arching did not change with increasing deflection. This plateau did not necessarily depict a condition of maximum arching or complete dissipation of the surface pressure. It was necessary to study several tests at several pressure levels at a particular depth of burial before determining the major factor involved in loading the structure.

In general, the active arching curves were continuous until they were disturbed by reflections from the base of the test chamber. The curves did not disclose any load-unload interaction between soil and structure. The curves appeared to be a manifestation of the overall gross loading and deflection of the structure.

The passive arching curves produced under all static conditions were very similar in form. They showed a high initial slope depicting a large amount of passive arching with a small amount of deflection. The slope of the curves changed rapidly to a position parallel to the deflection axis. This indicated a condition in which the amount of arching was not changing with further deflection.

The lower boundary associated with the trapdoor data appeared to have no effect on the amount of passive arching when compared with the hydraulic device located in the medium until a scaled deflection $\Delta D/B \times 1{,}000 = 15$ was reached. At this point the bearing capacity of the soil under the device limited the amount of arching which

could be developed at large deflections. Thus, the test device located in the medium could never develop as much passive arching as the trapdoor configuration.

The passive arching curves produced under dynamic test conditions were similar to the static curves. Their initial slope was not as steep but their overall form was closely comparable. At $P_S \approx 37$ psi with the spring-ring device, the soil under the device had a marked effect on the curves plotted using scaled differential deflection.

Thus, both the location of the fixed boundary and the path of loading are important to the amount of active arching. They are not nearly so important to passive arching. During any loading and unloading cycle, the structure goes through active and passive arching conditions. These curves do not follow the same trace. As soon as the arching condition changes, the form and the path of the resulting arching curve change.

At $H/B = 1/3$, a condition of maximum arching at $P_S = 37.8$ psi was approached using the hydraulic device under static conditions. The scaled differential pressure was $2\Delta P/q_u = -1.67$. All indicators showed that the maximum strength of the clay at this depth was being utilized to produce the differential pressure of -24.5 psi. At the same surface pressure and depth under dynamic conditions, a scaled differential pressure of $2\Delta P/q_u = -0.53$ was developed. The arching

curves were parallel to the deflection axis throughout most of their length. Dynamic amplification of the load was experienced in the dynamic test. When the effects of this amplification were taken into consideration, the differential pressure increased from -5.7 psi to approximately -20 psi. Considering the comparative unconfined soil strength in the two tests, 10.8 psi for the dynamic versus 14.7 psi for the static, the soil arching in the two tests was similar.

At $H/B = 1$, in the low pressure tests ($P_S < 40$ psi), the test device was fully buried. Under both the static and dynamic conditions, the amount of arching did not change with an increase in the depth of burial, but it did change with the stiffness of the structure. With the extremely flexible structure, $K_T/K_S = 0.03$, under dynamic conditions, the surface pressure was completely dissipated. Under static conditions, the same result was attained with both the trapdoor and the hydraulic device. When the stiffness of the device was increased to $K_T/K_S \approx 0.7$, the load on the device increased a comparable amount at $H/B = 1$ and $H/B = 3$. Thus the structure remained fully buried, but the amount of arching depended on its stiffness relative to that of the soil. This also appeared to be true under static conditions.

When the surface pressure was increased at $H/B = 1$ to 75 psi static and 157 psi dynamic, there was a sharp increase in the amount of arching. The scaled differential pressure increased under static

conditions to $2\Delta P/q_u = -3.3$ and under dynamic conditions to $2\Delta P/q_u = -1.4$. The static test was made with the hydraulic device, so there was no way to check the arching factor against the relative stiffness; but in the dynamic test, the arching factor was 0.84 versus a relative stiffness of 0.54. If the effects of dynamic amplification of the load are subtracted, then the arching factor was between 0.52 and 0.55.

When the surface pressure was increased to the 70- to 245-psi range at $H/B = 3$, it was more feasible to study the effects of depth of burial and pressure because of the larger number of tests. The scaled differential pressure increased to $2\Delta P/q_u \approx -5.2$ with static surface pressure ranging from 175 to 240 psi and $2\Delta P/q_u \approx -2.5$ with a dynamic pressure ranging from 150 to 245 psi. The ranges are given because practically no change occurred in the differential pressures and thus in the amount of arching developed within the stated pressure ranges. The ΔP ranged from -54 to -58 psi in the static tests and from -32 to -35 psi in the dynamic tests. These results indicate that the amount of active arching developed at these pressures and this depth of burial was mainly dependent upon the shear strength of the soil. This shear strength did not vary much with the confining pressure since ϕ was near 0 for buckshot clay at a water content of approximately 26 percent. When the effects of dynamic amplification are taken into consideration in the 70-psi

dynamic test, it appears that this test was governed more by the relative stiffness of the structure. Therefore, at $P_S > 70$-100 psi there appears to have been a transition zone in which the relative stiffness of the structure was as important as soil strength in determining the amount of arching. Below this pressure range, soil and structure modulus played the predominant role.

Once the effects of dynamic load amplification, as determined by the rise time of the pressure pulse and the period of the structure, were considered, there was still evidence of the effects of the relative stiffness of the structure on the load it experienced at high pressures, $P_S \approx 150$ to 245 psi . The load amplification experienced in the dynamic tests was not observed at $H/B \geq 1$ when the surface pressure was 40 psi or less. At higher pressures and shallower depths of burial, the load experienced by the structure was amplified.

The accelerations imparted to the structure also varied with its stiffness. At $P_S \approx 32$ to 38 psi and $H/B = 1$, the acceleration of the top of the very flexible structures was approximately twice that found in the free field at the same depth of burial, 74 g's versus 37 g's. The acceleration of the structure base was only about one-half that of the soil at the same level, 18 g's versus 33 g's. The acceleration of the top of the structure was over twice that of the base with the very flexible structure. As the stiffness of the

device was increased, the accelerations of its top and bottom approached one another and the acceleration of the soil.

When the structure became stiffer than the soil, $K_T/K_S \approx 4.5$, the acceleration of the base tended to exceed that of the top, 38 g's versus 35 g's, and both exceeded that of the soil at the same level by approximately 15 g's and 7 g's, respectively. As the stiffness of the test device was increased further to $K_T/K_S \approx 340$, the acceleration of both the top and base of the device increased to approximately 45 g's. As the stiffness of the structure increased, the contribution of the inertia of the structure to the load it received became less and less.

The amount of structure acceleration also was dependent upon surface pressure and depth of burial. Doubling the surface pressure more than doubled structure acceleration at each test pressure, but increasing the depth of burial from $H/B = 1/3$ to $H/B = 1$ decreased the structure accelerations by a factor of 3. Increasing the depth of burial to $H/B = 3$ decreased structure acceleration by another factor of 3.

As the stiffness of the device relative to that of the soil increased to the $K_T/K_S \approx 0.9$ to 3 range in the dynamic tests, estimation of the load on the structure at $P_S \approx 37.5$ psi became difficult. In this range, relative stiffness became very sensitive to small changes in the soil stiffness, and the soil stiffness was

changing throughout the test as the rise time and the amount of pressure changed. Once the relative stiffness of the device exceeded a value of $K_T/K_S \approx 4$, the load on the device became independent of its stiffness.

Within the surface pressure range used, $P_S \approx 31$ to 64 psi at $H/B = 1$, no effects of pressure on the amount of passive arching were observed.

In general, the test program showed that structure stiffness was important for what it did and did not contribute to the amount of arching the device experienced. Under active arching conditions, at the lower end of the spectrum of test pressures used, relative structure stiffness largely determined the structure load. Even in the higher pressure range when dynamic amplification was taken into consideration, a combination of relative stiffness and soil strength determined the structure loads. Under passive arching conditions, the structure stiffness made no contribution to the structure load when $K_T/K_S > 4$. The amount of passive arching never exceeded a value equal to 1.1 times the shear strength of the soil as determined by unconfined compression tests.

CHAPTER 6

SUMMARY, CONCLUSIONS, AND RECOMMENDATIONS

6.1 SUMMARY

Twenty-eight tests (8 static and 20 dynamic) were conducted on two types of test devices, described in Chapter 3, buried in a cohesive soil (buckshot clay) described in Appendix A. The following measurements, summarized in Tables 1 and 2, were made when applicable: overpressure applied to the soil surface, horizontal and vertical soil pressure at various depths above and below the test device, vertical soil pressure at various radii from the top of the test device, load applied to the top of the test device, acceleration of the top and base of the test device, deflection of the top of the device relative to its base, deflection of the base of the device referenced to the base of the test chamber, deflection of the soil at various levels and radii referenced to the structure, and soil acceleration at various levels in the test chamber, Figure 15. In addition, infrequent measurements were made of the strain in the top and base of the structure, the pressure acting on the inside of the test device, the strain in the soil deflection rods, and the accelerations experienced by the sides and base of the test chamber.

The test devices were buried at depths ranging from 1/3 to 7 times their outside diameter. Three surface pressure ranges were

used: low (31 to 40 psi), medium (50 to 75 psi), and high (150 to 310 psi).

By the use of the deflection and acceleration of the top and the damping and spring constants of the test device, the load acting on the top of the device was calculated at various times during the test. In the static tests, the load was calculated using the internal pressure of the hydraulic device and the top deflection and spring constant of the spring-ring device. Differential pressure was calculated by subtracting the average pressure acting on the top of the device from the surface pressure at the same time interval. The differential deflection of the device referenced to the soil was measured by adding the deflection of the top of the device to that of its base and subtracting the deflection of the soil measured in the free field at the level of the top of the device.

The relations between differential pressure and both the differential and total deflection of the device (normally termed arching curves) were plotted and analyzed with respect to the device configuration used, its relative stiffness, its depth of burial, and the surface pressure. In addition, the relation between soil pressure at the level of the device versus time and location were plotted. Curves were developed showing the relation between the amount of arching and depth of burial and the amount of arching and structure stiffness.

Several theoretical solutions and the amounts of arching measured were compared.

6.2 CONCLUSIONS

Active and passive soil arching can be induced in a cohesive soil, Figures 21 through 25 and 51 through 59. Although the amount of active soil arching decreases when creep occurs under static loading conditions, it does remain substantial within the time frame investigated (20 to 70 hours), Figures 24b and 25b.

The soil deformation pattern above the device during both static and dynamic, active arching tests consisted of a depression surrounded by a ridge, as shown in Figures 41 and 80. The depression grew smaller and the ridge grew larger with height above the device. Their maximum extent depended upon the magnitude of the surface pressure, the structure's depth of burial, the structure's stiffness, and the duration of the test.

A hemispherical dome of soil formed on the top of the device in the active tests and appeared to separate from the remaining soil above the device, Figures 41b, 50a, and 82. In addition, a series of what appeared to be arch formations formed above the depression-ridge patterns, Figures 50b, 81a, 85, and 86.

A hemispherical dome also formed above the test device during the static, passive arching tests. The soil above this dome broke

around it in a fractured pattern, Figures 47 and 48. Similar soil deformations were not found in the dynamic tests, but it was assumed that this lack of a clear-cut pattern was due to the low surface pressures used.

The soil pressure profiles constructed at the level of the device depicted the extent of loading and unloading which took place during the active and passive arching conditions. The profiles for a particular condition were similar in the static and dynamic tests. The profiles at low dynamic pressures resembled those predicted by an elastic solution, Figures 3 and 5 versus Figures 60a, 61b, and 62a and b. The high pressure profiles resembled an elastoplastic solution of the circumferential stress distribution around a cavity, Figure 5 versus Figures 60b and c. The static pressure profiles resemble both distributions, Figures 26, 27, and 28. Both the static and dynamic, passive pressure profiles resembled the elastoplastic solution, Figure 5 versus Figures 26b and 28c.

As shown by the pressure profiles and the soil deformations, the major part of the load transfer in both active and passive arching under static and dynamic conditions occurred within one structure diameter above and beside the test device. With the low surface pressures, $P_S \leq 40$ psi, the major portion of the arching occurred within one structure radius above and beside the test device.

The test configuration used had a definite effect on the amount

of active arching, Figures 92 and 94. The nearness of the boundary in the trapdoor studies of Hendron (1968) increased considerably the amount of arching which could be accomplished at a particular deflection over that induced using the hydraulically controlled device which was located up in the medium.

When the spring-ring test device was used up in the medium, the amount of arching accomplished at a particular differential deflection under comparable test conditions was less than that induced by either of the other configurations. This decrease in the amount of arching was due to the method in which active arching was induced. With the trapdoor and hydraulically controlled device, support was removed from under the soil, allowing it to deform. This can be termed structure-induced arching. The surface pressure was held constant in these tests. With the spring-ring device, the top of the structure deflected as the surface pressure increased. There was continuous interaction between the soil and the structure as the soil forced the top of the structure down. This can be termed pressure-induced arching. The amount of arching developed under these two conditions was considerably different.

The results of the tests using the trapdoor or the hydraulically controlled device do not appear to be particularly useful except to place an upper limit on the amount of active arching possible at a particular depth of burial and surface pressure, and as a scientific

study of the pure arching mechanism in soil.

The lower boundary present in the trapdoor experiments apparently had no effect on the amount of passive arching, Figure 93. The location of the hydraulic device in the medium did have some effect at large deflections since it was not possible to duplicate the rigidity of the trapdoor device. As soon as the load on the structure reached a level above the surrounding soil, the soil under the device began to deflect faster than the free-field soil at the same level. Thus, the maximum passive arching possible with the trapdoor device at comparable test conditions always exceeded that developed by the test device located up in the medium.

The spring-ring device appeared to develop even less passive arching than either of the other configurations, although the amount of data available in this area is sparse. This was because the structure could not expand to a height greater than its original height, but always deflected some distance based on its spring constant and the amount of load. Differential deflections were never as large with the spring-ring device as those developed with the other two configurations. Thus, the data developed using the trapdoor and hydraulic device are of little use in the development of actual structures, but can be used to further our understanding of passive arching.

The change in the device configuration also had an effect on the

form of the active arching curves. The form of those curves resulting from the hydraulic device was very similar to that produced using the trapdoor, but different from those produced using the spring-ring device. Under static loading conditions, the spring-ring arching curves had much less initial slope. The amount of differential deflection required to develop a particular differential pressure was larger. This was true until a critical transition pressure was reached at which time the slope of the curves produced by the spring-ring device increased, Figures 23 and 25.

The active arching curves produced under dynamic loading conditions generally were of a different form than any static arching curves. Maximum arching occurred at smaller deflections and the differential pressure decreased with increased deflection and the passage of time until the curve became parallel to the deflection axis. All of the dynamic, active arching curves, except those produced with the very flexible devices, acted in this manner.

The arching curves were generally continuous and smooth, without any manifestations of interaction between the soil and structure until the reflections from the base of the test chamber hit the device.

In the low pressure region, $P_S < 40$ psi, it was possible for structures less stiff than the soil to attain a fully buried condition at $H/B = 1$ with both static and dynamic overpressures. This appeared to be true under dynamic conditions for $P_S \approx 70$ psi at

$H/B = 3$. At these pressures and depths, the stiffness of the device relative to that of the soil determined the load which the structure experienced under both static and dynamic conditions. Thus it was possible to accurately estimate the load that would be experienced by the device in the low and medium pressure ranges using curves similar to those shown in Figure 99.

As the dynamic surface pressure was increased from $P_S \approx 37.5$ psi to $P_S \approx 150$ psi, the amount of active arching at $H/B = 1$ increased from $2\Delta P/q_u = -0.65$ to $2\Delta P/q_u = -1.42$. An attempt was made to hold the relative stiffness of the device at a constant $K_T/K_S = 0.7$ throughout the investigation of the effects of surface pressure and depth of burial. When the depth of burial was increased to $H/B = 3$ at a dynamic surface pressure of $P_S \approx 150$ psi, the amount of active arching increased to $2\Delta P/q_u = -2.53$ as compared to $2\Delta P/q_u = -0.61$ at $P_S \approx 37.0$ psi and $2\Delta P/q_u = -0.75$ at $P_S = 70$ psi. Yet an increase in the dynamic surface pressure to $P_S \approx 245$ psi only increased the ΔP from 32 psi to 35 psi at $H/B = 3$. It can be seen that the amount of arching increased sharply when the surface pressure was increased above 70 psi. But an increase in the surface pressure above $P_S \approx 150$ psi had very little effect on the amount of arching. Thus, it was concluded that the full strength of the soil had been developed at the particular depth in question and was the main factor determining the amount of load which the structure was receiving.

Similar results were experienced in the limited number of static tests with the spring-ring device. At $P_S \approx 37$ psi, the stiffness of the structure relative to that of the soil determined the amount of arching and thus the load experienced by the structure at $H/B = 1$. When the surface pressure was increased to $P_S \approx 175$ to 240 psi, the soil strength largely determined the amount of arching at $H/B = 3$.

It was found that dynamic amplification of the load occurred at $H/B = 1$ and 3 with $P_S > 150$ psi and at $H/B = 7$ when $P_S = 310$ psi. The amount of load amplification was calculated using the rise time of the pressure pulse at the depth of burial in question and the period of the structure. The period of a structure increased with a decrease in its stiffness and thus increased the possibility of dynamic amplification of the load.

In order to develop the full shear strength of the soil, the device had to be flexible enough to produce sufficient soil deformations. Once the full strength of the soil was developed at a particular depth, the further deflections allowed by a very flexible device were of no value.

Comparison of the experimental results with design techniques which feature the development of shear planes in the soil and the equilibrium of forces on a differential soil element showed these techniques to be unconservative at $H/B \geq 1$.

Another aspect of the structure stiffness was the effect it had

on the accelerations experienced by the top and base of the structure. The top of the very flexible devices experienced accelerations much higher than the soil at the same level, while the base registered accelerations considerably lower than those measured in the soil at the same level. As the structure's stiffness increased, the accelerations of its top and base approached each other at a point near the acceleration experienced by the soil. When the device became stiffer than the soil, then its accelerations became larger than that of the soil but considerably less than that experienced by the top of a flexible structure.

Under passive arching conditions it was found that the stiffness of the structure relative to the soil had no effect once $K_T/K_S > 4.0$. At structure stiffnesses greater than that of the soil, the stiffness of the soil underneath the device dominated the overall stiffness of the structure-soil system. With dynamic surface pressures ranging from $P_S \approx 31.0$ to 64.0, the structure load never exceeded 1.5 times the surface pressure for a range of $K_T/K_S = 4.14$ to 461.0. The amount of passive arching was determined by the shear strength of the clay and never exceeded a scaled differential pressure, $2\Delta P/q_u$, larger than 1.1. At $H/B = 1$ and within the pressure range examined, the amount of passive arching did not appear to be affected by surface pressure.

The conclusions outlined above must be judged in light of the

test conditions plus the size and geometry of the test device. Structure geometry was not varied.

6.3 RECOMMENDATIONS FOR FUTURE STUDY

A series of dynamic tests at $H/B = 1/3$ with a flexible test device, $K_T/K_S \approx 0.2$, should be conducted. The surface pressure should begin at 45 psi and increase in 10-psi increments until the differential pressure becomes practically constant. The test device then should be moved to $H/B = 1$ and $H/B = 3$ in succession, and the same procedure repeated, starting at 50 psi. This procedure is necessary to firmly establish the transition zone between the stiffness-dominated active arching at relatively low surface pressures and the soil strength-dominated active arching in the high pressure range. In addition, the program envisioned should provide the data needed to fully develop the active arching mechanism and define the volume of soil involved. Using the developments and experimental data available from the present program, only a limited number of tests should be required.

Once the pressure range in which soil strength governs the amount of arching is clearly delineated at $H/B = 1$, the water content of the soil, and thus its strength, should be varied. This would ensure that the role of soil shear strength has been fully developed, and also should assist in confirming the soil failure

mechanism and area of soil involved in the active arching process. The three-gage array idea should be utilized to determine the direction of the principal stress in the area involved in the arching action. Radiographs are an excellent vehicle for determining the extent of soil arching, but the techniques for extracting the soil, constructing the mosaic, and using the densometer need to be perfected.

Once the area involved in the active arching process has been confirmed, then an attempt should be made to establish the relation between the soil strain at the top of the device, the height of soil involved in arching, the stress-strain curve for the soil determined by dynamic triaxial tests, and the differential pressure.

Passive arching tests with a very stiff structure, $K_T/K_S > 10$, should be made at higher pressures, $P_S > 70$ psi, at $H/B = 1$, and a separate series of tests at $H/B = 1/3$ and 3 with P_S increasing from 60 to 500 psi should be performed to confirm the findings of the present program relative to the role of structure stiffness and to determine the role of soil strength.

The data from the present test program should be used in an elastic analysis of active arching in the low pressure range. Soil modulus as determined by one-dimensional compression tests at the programmed test pressure should be used.

In addition, an attempt should be made to use the arching

curves, the relative structure stiffness, and the surface pressure data developed in this program as a basis for the formulation of a soil-structure interaction code.

A number of previous investigators have studied the effects of structure configuration. Most of the work is concerned with passive arching. The role of structure diameter and its relation to the loading and unloading areas of the soil under active arching conditions need to be developed. Considerable data also are available on the relation of the diameter-height ratio of the structure to the amount of arching in sand. Similar data are needed for a flexible device buried in a cohesive soil.

The device developed in the present program should be used in an experimental program with sand as the medium of burial. The arching mechanisms in sand and clay appear to be similar, but the role of the surface pressure will be very different. High surface pressures (350 to 1,000 psi) and very flexible structures (K_T/K_S = 0.2 to 0.5) should be included in the test program. The advantages of using flexible structures in sand will probably be much greater than for cohesive soils. The data available on actual and model structures buried in sand should form the basis of a comparative study and the development of relations between the idealized structure and real structures, if they can be established.